Optical manipulation of ultra cold gases and Dipolar BCS

Von dem Fachbereich Physik

der Universiät Hannover
zur Erlangung des Grades eines

Doktors der Naturwissenschaften

Dr. rer. nat.

genehmigte Dissertation von

Dipl.-Phys. Łukasz Dobrek

geboren am 10.11.1976 in Warszawa/Polen

2003

Referent: Prof. Dr. Maciej Lewenstein
Koreferent: Prof. Dr. Jan Artl
Tag der Promotion: 19 Juni 2003

Abstract

Physics of ultra cold atoms and molecules is one of the most rapidly developing areas of the modern atomic, molecular, optical physics and quantum optics. This area covers several sub-areas of diverse importance, but definitely two trends can be easily identifies: i) fundamental research on properties of ultra cold atoms and molecules, and in particular atomic and molecular condensates trapped and lattice gases; here the fundamental questions of nature and form of phase transitions in degenerate systems are being posed and studied; ii) more applications oriented research on ultracold atoms and molecules, involving in particular applications in precision measurements, atomic clocks, frequency standards, atom and molecule interferometry, quantum information, quantum engineering, "super" chemistry etc.

This thesis concerns both of these major trends. The applications, or more specifically quantum engineering aspect are discussed in the first four chapters of the thesis, which deal with optical manipulations of ultra cold gases, in particular optical generation of vortices in Bose condensates, quasi-solitons in Fermi gases, and retarded dipole-dipole interactions in Bose, or Fermi gases.

This thesis consists of four main chapters. Chapter 2, "Optical generation of vortices in Bose Einstein Condensates". In this chapter we study theoretically the generation of vortices by phase imprinting in trapped Bose-Einstein condensates. Phase imprinting is achieved by passing a short off-resonance laser pulse through an appropriately designed absorption plate, and impinging it on a condensate. We answer the fundamental question of how the circulation and the vortex are introduced into the system, and discuss the creation of vortex arrays. We discuss vortex dynamics and interactions in such configurations. Various methods of vortex detection based on interference combined with Bragg scattering are also analyzed.

In Chapter 3, "Fermionic 'Solitons'" we investigate in detail the concept of low energy excitations of ultra cold Fermi gases. This excitations are generated using the same idea of phase imprinting as that employed in the generation of vortices in BEC. We address in this chapter some questions concerning the generation (via phase imprinting) of soliton–like solutions in a single–component Fermi gas of neutral atoms at zero and finite temperatures. By using both numerical and analytical calculations, we find the conditions under which it is possible to find in non-interacting Fermi gases, quasisolitons which resemble the properties of solitons in non–linear integrable equations. We present the results for both spatially homogeneous and trapped cases, and emphasize the importance of Fermi statistics and the absence of interactions for the existence of such solutions.

In Chapter 4, "Generating Dipole Condensate" we keep studying the possibilities of optical manipulations of ultracold gases. In particular, we study two different ways to laser-induce dipole-dipole interactions in trapped Bose-Einstein condensates. The first one employs the fact that those atoms in high Rydberg states posses a large dipolar moment. We first analyze the idea of imposing the dipole moment as a time average over short stroboscopic pulses. These pulses are coherently transporting the atoms from the ground atomic state to some high Rydberg state and back. The second idea is based on the observation that in strong static or oscillatory electric fields, atoms polarize and acquire dipole moment. We analyze the possibilities and limitations of inducing such a high electric field using lasers of low frequency.

In Chapter 5, "Dipolar BCS", we continue our study of trapped fermionic gases, with the analysis of the BCS transition in trapped dipolar fermionic gases. We find that the critical strength of the dipole-dipole interaction to achieve BCS pairing, depends on the trap geometry. We find the particular form of this dependence, and present the solutions for the order parameter.

This first chapter is meant as a general introduction to the thesis. This introduction is by no means exhaustive, and should be rather treated as a collection of basic facts concerning ultra cold gases, without rigorous derivations. The last subsection of the introductory chapter, discusses very briefly the most important achievements and trends in the field and the current state of the art.

keywords: Bose Einstein condensation, ultra cold Fermi gas, BCS

Zusammenfassung

Die Physik ultrakalter Atome und Moleküle ist eines der am schnellsten entwickelnden Felder der modernen Atomphysik, Molekülphysik, Optik und der Quantenoptik. Im Gebiet der ultrakalten Gase kann man zwei Trends identifizieren. Eine eher den Fundamentalen Fragen im Gebiet der ultrakalten Gase gewandte Forschung, wobei hier die Eigenschaften, wie die Natur und Form der Phasenübergänge, von Bose-Einstein Kondensaten von Atomen und Molekülen in Fallen oder optischen Gittern von Interesse sind. Auŝerdem eine eher der Anwendung von physikalischen Effekten orientierten Forschung im Gebiet der ultrakalten Gase, wobei hier hochpräzise Messungen, atomare Uhren, ein Frequenzstandard, Atom- und Molekülinterferometer, Quanteninformation, ”quantum engineering”, ”super” Chemie und weitere Anwendungen interessieren.

Diese Doktorarbeit betrifft beide Trends. In den ersten vier Kapiteln ist das Thema ”quantum engineering”. Hier wird die optische Manipulation für das Anregen von Wirbeln in Bose-Einstein Kondensaten, das Anregen von Quasisolitonen in Fermigasen und die Erzeugung retardierter Dipol-Dipol Wechselwirkungen in Bose- oder Fermigasen diskutiert.

In Kapitel 2, ”Optical generation of vortices in BEC”, wird die Erzeugung von Wirbeln mittels der Phaseaufprägung auf ein Bose-Einstein Kondensat in der Falle theoretisch untersucht. Es wurde die fundamentale Frage beantwortet, wie dem System die Zirkulation und die Wirbel hinzugefügt werden. Auŝerdem wurde die Erzeugung, die Dynamik und die Wechselwirkung in Wirbelfelder untersucht. Verschiedene Methoden, Wirbel mit einer Kombination aus Interferenz und Braggstreuung zu detektieren, werden hier auch studiert.

In Kapitel 3, ”Fermionic ’Solitons’”, werden die Anregungen mit niedrigen Energien ultrakalter Fermigase untersucht. Die Erzeugung dieser Anregungen basieren auf der Phasenaufprägung, wie das schon von der Erzeugung von Wirbeln und Solitonen in Bose-Einstein Kondensaten bekannt ist. Solitonähnliche Lösungen in Einkomponentigen Fermigasen neutraler Atome bei endlicher Temperatur und Nullpunkt-Temperatur sind von Interesse gewesen. Mit Hilfe sowohl numerischer als auch analytischer Methoden, haben wir Bedingungen gefunden, unter den es bei nicht wechselwirkenden Fermigasen möglich ist, Quasisolitonen zu finden, die ähnliche Eigenschaften aufweisen, wie die von integrablen nichtlinearen Gleichungen bekannten Solitonen.

In Kapitel 4, ”Generating Dipole Condensate”, werden die laserinduzierten Wechselwirkungen eines Bose-Einstein Kondensates in der Falle analysiert. Zwei Methoden werden hier vorgeschlagen und untersucht.

Die erste Methode hat die groŝen Dipolmomente von Atomen im Rydbergzustand als Grundlage. Es wurde die Idee theoretisch untersucht, stroboskopisch kurze Laserpulse anzuwenden, die Atome vom Grundzustand in den Rydbergzustand anregen, um ein mittleres Dipolmoment einem Bose-Einstein Kondensat aufzuprägen.

Die zweite Methode basiert auf dem Effekt, dass Atome von starken, entweder statischen oder oszillierenden, elektrischen Feldern polarisiert werden und somit ein starkes Dipolmoment generieren. Es wurden die Möglichkeiten, aber auch die Grenzen, solche elektrische Felder mit Laserfeldern niedriger Frequenz zu erzeugen, untersucht.

In Kapitel 5, ”Dipolar BCS”, werden die Untersuchungen mit der Analyse von BCS-Übergängen dipolarer, gefangener Fermigase fortgesetzt. Es wurde die Abhängigkeit einer kritischen Stärke der Dipol-Dipol Wechselwirkung, um BCS-Paarung zu erhalten, von der Fallengeometrie identifiziert. Auŝerdem wurde eine spezielle Form dieser Abhängigkeit gefunden und die Lösung für den Ordnungsparameter dargestellt.

Schlüsselwörter: Bose Einstein Kondensation, Ultrakalte Fermigase, BCS

Table of Contents

General Introduction **1**
- Bose-Einstein Condensation 2
  - Bose Einstein Condensation in an ideal trapped gas 2
  - Bose-Einstein condensation in an interacting gas 4
- Phase Imprinting 5
- Ultracold Fermi gas 5
- Cooper Pairs 6
- Trends in ultra cold atom physics 8

Optical generation of vortices in BEC **9**
- Introduction 9
- “Phase imprinting” 10
  - Vortex formation 12
  - Multivortex formation 12
- “Phase imprinting” with multiple plates 15
  - Vortex arrays with single absorption plate 15
  - Vortex arrays with multiple absorbtion plates 16
- Detection of vortex arrays using interference 19

Fermionic ’Solitons’ **24**
- Introduction 24
- Solution of the many–body Schrödinger equation 25
  - Zero temperature 25
  - Finite temperatures 28
- Wigner function approach 29
- Density matrix formalism 34
  - Numerical results 39

Generating Dipole condensate **40**
- Stroboscopic method 41
  - Method 41
  - Analysis 42
- Dynamically induced dipole 44
- Results 45

Dipolar BCS **48**
- Numerical results 53

Conclusions **57**

Appendixes **58**
- Bibliography 58
- Wigner Function 64
- Gap Equation 65

1 General Introduction

Physics of ultra cold atoms and molecules is one of the most rapidly developing areas of the modern atomic, molecular, optical physics and quantum optics. Nobel Prize in physics in 1997 has been awarded to C. Cohen-Tannoudji, S. Chu and W. Phillips, as well as in 2001 to C. Wieman, W. Ketterle and E. Cornell for their achievement in physics of ultra cold atoms. This area covers several sub-areas of diverse importance, but definitely two trends can be easily identifies: i) fundamental research on properties of ultra cold atoms and molecules, and in particular atomic and molecular condensates trapped and lattice gases; here the fundamental questions of nature and form of phase transitions in degenerate systems are being posed and studied; ii) more applications oriented research on ultracold atoms and molecules, involving in particular applications in precision measurements, atomic clocks, frequency standards, atom and molecule interferometry, quantum information, quantum engineering, ”super” chemistry etc.

This thesis concerns both of these major trends. The applications, or more specifically quantum engineering aspect are discussed in the first four chapters of the thesis, which deal with optical manipulations of ultra cold gases, in particular optical generation of vortices in Bose condensates, quasi-solitons in Fermi gases, and retarded dipole-dipole interactions in Bose, or Fermi gases. The common root is provided here by the use of a laser to ”imprint a phase” on atomic wave functions, or to induce conservative interatomic forces The fundamental aspects concern our study of the existence and critical temperature for the superfluid Bardeen-Cooper-Schrieffer transition in ultracold Fermi gases with dipolar interactions.

This thesis consists of four main chapters. Chapter 2, ”Optical generation of vortices in Bose Einstein Condensates”, is based on two papers [1, 2] of the same title. This work was done in close collaboration with the experimental Quantum Optics group at Hanover University and theory groups from Center of theoretical physics in Warsaw and Białystok. In this chapter we study theoretically the generation of vortices by phase imprinting in trapped Bose-Einstein condensates. Phase imprinting is achieved by passing a short off-resonance laser pulse through an appropriately designed absorption plate, and impinging it on a condensate. We answer the fundamental question of how the circulation and the vortex are introduced into the system, and discuss the creation of vortex arrays. Using multiple absorption plates we show that genuine vortex arrays can be created in a controlled way. We discuss vortex dynamics and interactions in such configurations. Various methods of vortex detection based on interference combined with Bragg scattering are also analyzed.

In Chapter 3, ”Fermionic ’Solitons’” we investigate in detail the concept of low energy excitations of ultra cold Fermi gases. This excitations are generated using the same idea of phase imprinting as that employed in the generation of vortices in BEC. We address in this chapter some questions concerning the generation (via phase imprinting) of soliton–like solutions in a single–component Fermi gas of neutral atoms at zero and finite temperatures. By using both numerical and analytical calculations, we find the conditions under which it is possible to find in non-interacting Fermi gases, quasisolitons which resemble the properties of solitons in non–linear integrable equations. We present the results for both spatially homogeneous and trapped cases, and emphasize the importance of Fermi statistics and the absence of interactions for the existence of such solutions. This chapter is based on Ref. [3].

In Chapter 4, "Generating Dipole Condensate" we keep studying the possibilities of optical manipulations of ultracold gases. In particular, we study two different ways to laser-induce dipole-dipole interactions in trapped Bose-Einstein condensates. The first one (proposed in [4, 5]) employs the fact that those atoms in high Rydberg states posses a large dipolar moment. We first analyze the idea of imposing the dipole moment as a time average over short stroboscopic pulses. These pulses are coherently transporting the atoms from the ground atomic state to some high Rydberg state and back. The second idea (proposed in [6]) is based on the observation that in strong static or oscillatory electric fields, atoms polarize and acquire dipole moment. We analyze the possibilities and limitations of inducing such a high electric field using lasers of low frequency.

In Chapter 5, "Dipolar BCS", we continue our study of trapped fermionic gases, with the analysis of the BCS transition in trapped dipolar fermionic gases. We find that the critical strength of the dipole-dipole interaction to achieve BCS pairing, depends on the trap geometry. We find the particular form of this dependence, and present the solutions for the order parameter.

This first chapter is meant as a general introduction to the thesis. The first subsections explain the concept of Bose Einstein condensation, and the theoretical ways to describe it. Subsection "Phase Imprinting" briefly introduces the method employed in Chapter 2 and Chapter 3. The consecutive subsection is devoted to the theory of ultra cold fermionic gases. This introduction is by no means exhaustive, and should be rather treated as a collection of basic facts concerning ultra cold gases, without rigorous derivations. The last subsection of the introductory chapter, discusses very briefly the most important achievements and trends in the field and the current state of the art.

1.1 Bose-Einstein Condensation

In 1924 Satyendranath Bose [7] proposed a novel statistics for counting photons in a state of thermodynamical equilibrium. Using this statistics he was able to explain Planck's law for the black body radiation. Later on Albert Einstein extended Bose's method to massive particles [8], [9]. This counting method constitutes the basis of the Bose-Einstein statistics. Contrary to the case of fermions, which obbey the Pauli exclusion principle, bosons tend to accumulate in a single quantum state. This phenomenon is called Bose-Einstein condensation (BEC). In this section we briefly review some important concepts related to BEC in trapped gases. We shall first discuss the non-interacting case, and later on discuss the effects of the interatomic interactions.

1.1.1 Bose Einstein Condensation in an ideal trapped gas

Let us consider a system of non interacting bosons in thermal equilibrium in a harmonic trap, characterized by a chemical potential, μ, a total number of atoms, N, and a temperature, T. The occupation of the different energy levels is provided by the Bose-Einstein distribution

$$N_{\vec{n}} = \{\exp[\beta(E_{\vec{n}} - \mu)] - 1\}^{-1},$$

where $\beta = K_B T$, and $\vec{n} \equiv \{n_x, n_y, n_z\}$ are the quantum numbers describing the harmonic oscillator levels. Without loosing of generality we assume in the following a spherical harmonic trap of frequency ω, such that the energy spectrum is given by $E_{\vec{n}} = \hbar\omega(n_x + n_y + n_z + 3/2)$. The total number of atoms is

$$N(T, \mu) = \sum_{\vec{n}} N_{\vec{n}},$$

and the total energy

$$E(T, \mu) = \sum_{\vec{n}} E_{\vec{n}} N_{\vec{n}}.$$

As in the case of a Bose gas in absence of trapping potential [10], we separate the contribution of the lowest eigenvalue from that of the rest of eigenstates.

$$N(T,\mu) - N_0 = \sum_{\vec{n}} \frac{1}{\exp[\beta E_{\vec{n}}] - 1}.$$

Assuming that the level spacing becomes progressively smaller for $N \to \infty$, the energy spectrum can be considered as continuous, and the sum can be replaced by an integral. Knowing the density of states $\rho(\epsilon) = (1/2)(\hbar\omega)^{-3}\epsilon^2$ we can rewrite the above formula as an integral over the energy:

$$N - N_0 = \int_0^\infty d\epsilon \frac{\rho(\epsilon)}{\exp[\beta\epsilon] - 1} = \zeta(3)\left(\frac{K_B T}{\hbar\omega}\right)^2,$$

where ζ is the Riemann Zeta function. The limit $N_0 \to 0$ defines the critical temperature T_c for onset of the BEC,

$$K_B T_c = \hbar\omega\left(\frac{N}{\zeta(3)}\right)^{1/3}.$$

From the previous discussion, it is clear that at sufficiently low temperatures quantum statistics starts to play a dominant role. In order to fully understand this point, we should recall that to every particle one can assign a corresponding de Broglie wavelength λ, which constitutes a measure of the position uncertainty. The momentum of the particle is proportional to the inverse of the de Broglie wave length $p = h/\lambda$. The kinetic energy of the particle is then $E_{\text{kin}} = p^2/2m$. Using the expression $E_{\text{kin}} = 3K_B T/2$, coming from the equipartition of the energy, we can write the thermal wavelength as:

$$\lambda_T = \sqrt{\frac{4\pi^2\hbar^2}{3mk_{\text{B}}T}}. \tag{1}$$

At very low temperatures, λ_T can become larger than the interparticle distance. When this occurs, the wavepackets of two different particles overlap significantly, and the particles become undistingishable. From the previous discussion, this should occur when more than one particle is found within a volume λ_T^3. More exactly, and for the case of a trapped ideal gas, this occurs for $T < T_c$, where T_c is defined above.

Unfortunately, when cooling a gas down to T_c, the equilibrium state becomes a mixture of a gas and a solid. In order to achieve the condensate one has thus to carefully supercool the gas, and keep it in the metastable state preventing crystallization. Unfortunately, to prevent crystallization very low densities are required, which in turn implies a very low value for the critical temperature of the condensation.

The smallness of T_c introduces very stringent conditions for the observation of BEC, and as a consequence of that, until very recently only the case of ^{4}He was extensively investigated experimentally, since Helium does not crystalize. For a Helium density $\rho \approx 10^{22}\text{cm}^{-3}$ we get a critical temperature: $T_c \approx 3.14$K. This temperature, as observed by London [11], is very close to the temperature of the lambda transition to superfluidity in He, $T_\lambda = 2.17$K. Unfortunately, in the case of Helium the interparticle interactions play a very relevant role, and the physics departs very far from that a Bose-Einstein condensate in an ideal gas. In particular, for typical Helium experiments, the condensate fraction is of the order of less than 10%. It was not until the decade of 1990's that the developments in cooling and traping of neutral atoms lead to the achievement of BEC in dilute alkali gases, where almost ideal BEC can be achieved [12]. For these experiments, the atomic density lies typically within the range $10^{13} - 10^{14}\text{cm}^{-3}$, and the critical temperature for condensation is of the order of 100nK, or lower. These extremely low values explain why highly sophisticated cooling and trapping techniques are needed to confine and manipulate the atoms. Fortunately, these techniques have advanced dramatically during the last few years, which open fascinating perspectives for the manipulation and engineering of macroscopic quantum states, as throughly discussed in this Thesis.

1.1.2 Bose-Einstein condensation in an interacting gas

Although the current experiments deal with extremely dilute atomic gases, the role of interactions cannot be neglected. In particular the interactions are necessary to explain in detail the shape of the condensate ground-state wavefunction and excitations, and they are definitely crucial to explain the remarkable phenomenon of superfluidity, and also different nonlinear phenomena in BECs, such as for instance dark solitons.

In order to describe an interacting condensate, we write the full manybody Hamiltonian of the system, $\hat{H}$:

$$\hat{H} = \int \mathrm{d}r \hat{\Psi}^\dagger(\mathbf{r},t) \left[-\frac{\hbar^2}{2m}\Delta + V_t(\mathbf{r},t) \right] \hat{\Psi}(\mathbf{r},t) + \frac{1}{2} \iint \mathrm{d}r\mathrm{d}r' \hat{\Psi}^\dagger(\mathbf{r},t)\hat{\Psi}^\dagger(\mathbf{r}',t)\hat{V}(\mathbf{r}-\mathbf{r}')\hat{\Psi}(\mathbf{r},t)\hat{\Psi}(\mathbf{r}',t),$$

where $\hat{\Psi}(\mathbf{r},t)$ is a bosonic field operator, $V_{\mathrm{t}}(\mathbf{r})$ is a trap potential,

$$V_t(\mathbf{r}) = m\omega^2 r^2/2,$$

and $\hat{V}(\mathbf{r}-\mathbf{r}')$ is the two-body interaction potential. We shall consider in the following that the interaction potential is of the van der Waals form (other interaction potentials are possible, e.g. dipole-dipole interactions as discussed at the end of this Thesis). For the extremely low energies involved in condensate experiments, it is in general not necessary to know in detail the exact form of the interatomic potential. On the contrary, the atomic scattering is fully characterized by a single parameter, namely the s-wave scattering length, a_{sl}. In that case, it is possible to subsitute the actual potential by a pseudopotential with the same a_{sl}:

$$\hat{V}(\mathbf{r}-\mathbf{r}') \rightarrow \frac{4\pi a_{sl}\hbar^2}{m}\delta_3(\mathbf{r}-\mathbf{r}'),$$

where m is a mass of atoms. Note that if $a_{sl} > 0$ the interaction potential is repulsive, whereas if $a_{sl} < 0$ it is attractive. Note also, that our previous assumption concerning the binary character of the interactions relies on the diluteness of the gas. A gas is considered dilute if

$$\langle n \rangle |a_{sl}|^3 \ll 1,$$

where $\langle n \rangle$ is the average density of the gas. For typical densities ($10^{13} - 10^{15} cm^{-3}$) and typical values of a_{sl} ($1 - 100$nm), $\langle n \rangle |a_{sl}|^3 < 10^{-3}$, two-body collisions are dominant in comparison with three-body ones. In the following we shall always considered this regime.

The bosonic field operators $\hat{\Psi}$ and $\hat{\Psi}^\dagger$ fulfill the usual commutation relations:

$$\left[\hat{\Psi}(\mathbf{r},t), \hat{\Psi}(\mathbf{r}',t)\right] = \left[\hat{\Psi}^\dagger(\mathbf{r},t), \hat{\Psi}^\dagger(\mathbf{r}',t)\right] = 0,$$

$$\left[\hat{\Psi}(\mathbf{r},t), \hat{\Psi}^\dagger(\mathbf{r}',t)\right] = \delta_3(\mathbf{r}-\mathbf{r}').$$

The Heisenberg equation for $\hat{\Psi}(\mathbf{r},t)$ becomes:

$$\mathrm{i}\hbar\frac{\partial \Psi}{\partial t} = \left[\left(-\frac{\hbar^2\Delta}{2m} + V_t(\mathbf{r}) \right) + \frac{4\pi\hbar^2}{m}\hat{\Psi}^\dagger(\mathbf{r},t)\hat{\Psi}(\mathbf{r},t) \right] \hat{\Psi}(\mathbf{r},t). \tag{2}$$

This is basically an exact equation, but unfortunately, there exists no known method to solve it exactly. In the presence of a condensate, the previous equation is solved by means of the so-called Bogoliubov approximation, which is based on the assumption that below T_c the average value of $\langle \hat{\Psi} \rangle = \Phi$ is non zero. In this case one can write the bosonic operator as:

$$\hat{\Psi}(\mathbf{r},t) = \sqrt{N}\Phi(\mathbf{r},t) + \hat{\delta}(\mathbf{r},t) \ ,$$

where $\hat{\delta}(\mathbf{r},t)$ describes fluctuations around the average, and N is the particle number. The average $\Phi(\mathbf{r},t)$ receives the name of condensate wave function, and fulfills the normalization condition:

$$\int \mathrm{d}r|\Phi|^2 = 1.$$

At very low temperatures, in a system of very many particles ($N \gg 1$), when the ground state of the system is macroscopically occupied, the average value $\langle\hat{\Psi}(\mathbf{r},t)\rangle = \Phi(\mathbf{r},t)$ is much larger than the fluctuations $\hat{\delta}(\mathbf{r},t)$. In this case we can rewrite $\hat{\Psi}^\dagger\hat{\Psi}\hat{\Psi}$ as:

$$\hat{\Psi}^\dagger\hat{\Psi}\hat{\Psi} = N^{\frac{3}{2}}|\Phi|^2\Phi + 2N|\Phi|^2\hat{\delta} + 2\sqrt{N}\Phi\hat{\delta}^\dagger\hat{\delta} + N\Phi^2\hat{\delta}^\dagger + \sqrt{N}\Phi^\star\hat{\delta}\hat{\delta} + \hat{\delta}^\dagger\hat{\delta}\hat{\delta}\ .$$

Skipping all the terms proportional to fluctuations, we obtain an equation for $\Phi(\mathbf{r},t)$:

$$\mathrm{i}\hbar\frac{\partial\Phi(\mathbf{r},t)}{\partial t} = \left(-\frac{\hbar^2\Delta}{2m} + V_{\mathrm{t}}(\mathbf{r},t) + N\frac{4\pi a_{\mathrm{sl}}\hbar^2}{m}|\Phi(\mathbf{r},t)|^2\right)\Phi(\mathbf{r},t). \tag{3}$$

This nonlinear Schrödinger equation is known as of Gross-Pitaevskii equation (GPE). In addition to the external trap $V_t(\vec{r})$, the particles feel the mean-field potential provided by the other condensate particles. The ground-state solution is obtained from the time-independent GPE.

1.2 Phase Imprinting

In this section, we discuss the phase imprinting method proposed in Ref. [1]. A far off resonant laser pulse is directed onto an absorption plate, with a spatially varying absorption coefficient. This variation leads to a modulated intensity of the outgoing pulse, which in turn results, after properly focusing onto the condensate, in a Stark shift potential for the bosons, $V_l(\vec{r},t)$, proportional to the laser intensity. Consequently, the corresponding Schrödinger equation becomes:

$$\mathrm{i}\hbar\frac{\partial\Psi(\vec{r},t)}{\partial t} = \left(H_{orig} + V_l(\vec{r},t)\right)\Psi(\vec{r},t), \tag{4}$$

where H_{orig} is the non-perturbed original nonlinear Hamiltonian of the system.
When the characteristic time T_{orig} of the dynamics driven by H_{orig} is much larger than the pulse duration T_l, the solution of Eq. 4 can be easily written as:

$$\Psi(\vec{r},t+T_l) = e^{-\mathrm{i}V_l(\vec{r})T_l/\hbar}\Psi(\vec{r},t). \qquad (5).$$

From equation (5) we see that this method allows, in principle, to engineer in an arbitrary way the phase of the wavefunction. In this Thesis we study the use of the phase imprinting method to create vortices in BEC (Chapter 2), and solitons in an ultra cold fermionic gas (Chapter 3). This technique has been successfully employed by the two experimental groups [13], [14] to generate solitons in BEC.

1.3 Ultracold Fermi gas

Up to this point we have mainly considered the case of bosonic gases. Chapter 3 and Chapter 5 are devoted to the study of properties of ultra cold fermionic gases, which in contrary to the bosonic case, obey the Pauli exclusion principle, which arises from the standard anticommutation relations for the fermionic operators:

$$\{a_{\sigma_1}, a^\dagger_{\sigma_2}\} = a_{\sigma_1}a^\dagger_{\sigma_2} + a^\dagger_{\sigma_2}a_{\sigma_1} = \delta_{\sigma_1,\sigma_2}.$$

Here we will briefly present the theory of the quantum degenerate Fermi gas. Quantum degenerate Fermi gases are fundamentally different from Bose gases. Due to the Pauli exclusion principle, in the case of identical Fermions not more than one can occupy a single state. Therefore for the low temperatures the physics is determined by the presence of Fermi sea. For $T = 0$ all the fermion occupation numbers are equal to unity up to the Fermi energy E_{F}, and zero for higher energies. The presence of the finite temperature smoothes the step in occupation number distribution, and introduces a small transition region close to the Fermi energy. For such a distribution only particles near the surface of the Fermi sea can contribute to physical processes. There is simply no particles of much higher energies. The interaction of particles deep in the Fermi sea is forbidden due to the Pauli exclusion principle and energy conservation. One of the most interesting phenomena in degenerate Fermi gas is superfluidity, related to the creation of Cooper pairs [15]. This are pairs of correlated fermions which are corelated in the momentum space: if one of them occupies the motional state $\vec{k}$, the other one occupies the motional state $-\vec{k}$.

1.4 Cooper Pairs

First, let us introduce the function Φ_N which is the $N-$ particle wave function of $N/2$ pairs of fermions.

$$\Phi_N = \sum_{k_1} ... \sum_{k_{N/2}} g_{k_1} ... g_{k_{N/2}} a^{\dagger}_{k_1+} a^{\dagger}_{-k_1-} ... a^{\dagger}_{k_{N/2}+} a^{\dagger}_{-k_{N/2}-} \Phi_0,$$

where Φ_0 is the particle vacuum. This function is very difficult to work with; Instead we will consider the generating function of the one above:

$$\tilde{\Phi} = \prod_k \left(u_k + v_k a^{\dagger}_{k+} a^{\dagger}_{-k-} \right) \Phi_0,$$

where the product extends over all plane wave states. Normalization condition gives us $u_k^2 + v_k^2 = 1$. The above function was first introduces by Bardeen, Cooper and Schrieffer [16].

Now we can start our discussion of interacting Fermi system. Let $\mathcal{H}$ be the Hamiltonian of the interacting Fermi system, and $\mathcal{N}$ the total particle number operator. In order to find the ground state of the system we want to minimize the following expression:

$$\langle \tilde{\Phi} \mid \mathcal{H} - E_F \mathcal{N} \mid \tilde{\Phi} \rangle,$$

Here E_F is simply the Lagrange multiplier. We will see later that it plays a role of Fermi energy. and at the same time of a chemical potential.
The kinetic energy operator given by

$$\mathcal{K}_0 = \sum_{\mathbf{k},\alpha} \epsilon_k a^{\dagger}_{\mathbf{k}\alpha} a^{\dagger}_{-\mathbf{k}\beta},$$

wher the summation in the above formula extends over all possible momentum $\mathbf{k}$ and spin $\alpha = \{+,-\}$ states, while $\epsilon_{\mathbf{k}} = \hbar^2 (k^2)/2m - E_F$ is simply a kinetic energy minus E_F. In the state $\tilde{\Phi}$ the value of kinetic energy is given by:

$$\langle \tilde{\Phi} \mid \mathcal{K}_0 - E_F \mathcal{N} \mid \tilde{\Phi} \rangle = \sum_{\mathbf{k},\alpha} {v_{\mathbf{k}}}^2 \epsilon_{\mathbf{k}}.$$

Much more interesting is the interaction Hamiltonian:

$$\mathcal{K}_{\mathrm{int}} = \frac{1}{2} \sum_{\mathbf{k},\mathbf{k}'\mathbf{q}} V(\mathbf{k}+\mathbf{q}, \mathbf{k}'-\mathbf{q} \mid \mathbf{k}, \mathbf{k}') a^{\dagger}_{\mathbf{k}+\mathbf{q}\alpha} a^{\dagger}_{\mathbf{k}'-\mathbf{q}\beta} a_{\mathbf{k}'\beta} a_{\mathbf{k}\alpha},$$

This form of interaction takes into account the conservation of momentum and spin. Let consider the transition of a pair of fermions from the state $(\mathbf{k}+, -\mathbf{k}-)$ to $(\mathbf{l}+, -\mathbf{l}-)$, and let denote $V(\mathbf{l}, -\mathbf{l} \mid \mathbf{k}, -\mathbf{k}) = V_{kl}$. The function $\tilde{\Phi}$ can be split into 2 parts $\tilde{\Phi} = v_k\phi_{k1} + u_k\phi_{k0}$, where the function ϕ_{k1} describes the state, where the pair $(\mathbf{k}, -\mathbf{k})$ is occupied, the function ϕ_{k0} whereas describes the state, where this pair is not occupied. Similarly we can split $\tilde{\Phi}$ into 4 parts taking into account 2 pairs:

$$\tilde{\Phi} = v_{\mathbf{k}} v_{\mathbf{l}} \phi_{\mathbf{k}1}\phi_{\mathbf{l}1} + v_{\mathbf{k}} u_{\mathbf{l}} \phi_{\mathbf{k}1}\phi_{\mathbf{l}0} + v_{\mathbf{l}} u_{\mathbf{k}} \phi_{\mathbf{l}1}\phi_{\mathbf{k}0} + u_{\mathbf{k}} u_{\mathbf{l}} \phi_{\mathbf{k}0}\phi_{\mathbf{l}0}.$$

The transition element V_{kl} is given by the $\langle \phi_{\mathbf{k}1\mathbf{l}0} \mid \mathcal{H}_{\text{int}} \mid \phi_{\mathbf{k}0\mathbf{l}0} \rangle$ which can be trivially computed. Now, we can write the full expression for energy of the interaction Fermi system in the state $\tilde{\Phi}$:

$$\langle \tilde{\Phi} \mid \mathcal{H} - E_{\mathrm{F}}\mathcal{N} \mid \tilde{\Phi} \rangle = 2\sum_{\mathbf{k}} \epsilon_{\mathbf{k}} v_{\mathbf{k}}^2 + \sum_{\mathbf{kl}} V_{kl} u_{\mathbf{k}} u_{\mathbf{l}} v_{\mathbf{k}} v_{\mathbf{l}}.$$

We want to minimize this energy with respect to $v_{\mathbf{k}} u_{\mathbf{l}}$ taking into account the normalization condition. The best way to do that is to change variables let: $u_{\mathbf{k}} = \sin\theta_{\mathbf{k}}$ and $v_k = \cos\theta_{\mathbf{k}}$. In these new variables the equations for the minimum can be written as:

$$0 = \frac{\partial}{\partial\theta_{\mathbf{k}}} \langle \tilde{\Phi} \mid \mathcal{H} \mid \tilde{\Phi} \rangle = -2\epsilon_{\mathbf{k}} \sin 2\theta_{\mathbf{k}} + \sum_{\mathbf{l}} \cos 2\theta_{\mathbf{k}} \sin 2\theta_l V_{\mathbf{kl}}, \tag{6}$$

or

$$\epsilon_{\mathbf{k}} \tan 2\theta_{\mathbf{k}} = \frac{1}{2} \sum_{\mathbf{l}} V_{\mathbf{kl}} \sin 2\theta_l.$$

Now we define:

$$\Delta_{\mathbf{k}} = -\sum_{\mathbf{l}} V_{\mathbf{kl}} u_{\mathbf{l}} v_{\mathbf{l}},$$

$$\eta_{\mathbf{k}} = \sqrt{\epsilon_k^2 + \Delta_{\mathbf{k}}^2}.$$

Solving (6) for Δ we find finally the gap equation:

$$\Delta_{\mathbf{k}} = -\sum_{\mathbf{l}} V_{\mathbf{kl}} \frac{\Delta_l}{2(\eta_{\mathbf{l}}^2 + \Delta_{\mathbf{l}}^2)^{1/2}}. \tag{7}$$

This equation has always at least one solution, i.e. $\Delta_{\mathbf{k}} = 0$. This corresponds to $v_{\mathbf{k}}$ equal to unity for kinetic energy smaller than E_{F}, and vanishing otherwise. The wave function is given simply by a Slater determinant of all states of energy less than E_F. (7) can have, however, a different solution. Let us consider a simplified interaction of the form:

$$V_{\mathbf{kl}} = \begin{cases} -V & \text{if } |\epsilon_{\mathbf{k}}|, |\epsilon_{\mathbf{l}}| < \hbar\omega_D; \\ 0, & \text{otherwise.} \end{cases} \tag{8}$$

For this interaction Δ becomes independent of $\mathbf{k}$. Now, we can solve the equation (7). Let us first sum over the spin orientations; this will give an additional factor $N(\epsilon_{\mathbf{l}})$ which is the density of states per unit energy for a given spin direction. Since we are interested in energy interval close to the Fermi energy we will write $N(\epsilon_{\mathbf{l}}) = N(0)$ which is a value at the Fermi level. We change summation into integration and write:

$$\Delta = N(0)V \int_{-\hbar\omega_D}^{\hbar\omega_D} \Delta \frac{d\epsilon}{2\sqrt{\Delta^2 + \epsilon^2}} = N(0)V\Delta \sinh^{-1}\left(\frac{\hbar\omega_D}{\Delta}\right).$$

This equation has solutions only for positive V which means that pairing in Fermi system can occur only with attractive interactions (see (8)) and a solution in the week coupling regime is given by:

$$\Delta = 2\hbar\omega_D e^{-1/N(0)V}.$$

Solution with non zero Δ describe a superfluid (superconductor); Δ has than a meaning of the energy gap: elementary excitation that destroy or create a Cooper pair, have energy larger than Δ.

1.5 Trends in ultra cold atom physics

After the experimental observation of BEC in 1995 [12, 17, 18], the physics of ultracold bosonic and fermionic gases has attracted an enormous interest. It is impossible to review, even briefly, the large amount of significant contributions to this field, which have appeared during the last few years. In this section we intend to provide a necessarily rough overview of the main theoretical developments.

Right after the achievement of BEC in Rubidium the stability of BEC with attractive interactions was a subject of major interest [19, 20, 21, 22]. It was predicted that due to the presence of the trapping potential the condensate could be stabilized for sufficiently low number of particles. This effect was experimentally observed at the Rice University in 1997 [23]. The dynamics of BEC has been also carefully analyzed, particularly the low energy collective oscillations, which were studied by means of sum rules formalism [24]. An additional problem of major importance for experiments, is that of the condensate expansion after releasing the trapping potential. The expansion, the analysis of the excitations, and other physically relevant problems, have been intensively analyzed by means of the hydrodynamic approach, employing self-similar solutions [20, 21, 25]. Of course, the equilibrium properties, and dynamics has been additionally considered by numerically solving the GPE [26].

The interest in BEC can be partially explained by the double nature of the BEC as a quantum fluid, and as a coherent matter wave. As a quantum fluid, the BEC offers an extraordinary tool to study in detail different condensed-matter theories. In particular, different effects related with the key concept of superfluidity have been reported [24, 27]. Especially remarkable in this sense, have been the analysis of the physics of quantized vortices in BEC [28, 29, 30, 31]. As a coherent matter wave, the BEC presents phenomena which resemble with those appearing in nonlinear optics. Those phenomena have been discussed under the term "nonlinear atom optics" [32, 33, 34], and the theory of solitons in BEC [13, 14, 35, 36]. For the case of coupled BECs, the coherence of the condensates manifest itself in the appearance of Josephson currents [37, 38]. However, the coherence of the BEC is not an immediate property. In particular, for low-dimensional trapping geometries, it has been predicted the appearance of quasicondensates, i.e. equilibrium BEC with a spatially fluctuating phase [39, 40]. This quasicondensates should have a crucial role during the BEC kinetics [41]. Other relevant theoretical contributions during the last years are related to the analysis of multicomponent condensates [42, 43], the physics of dipolar gases [4, 44, 45, 46, 47], the physics of finite temperature effects [48], the creation of molecular condensates [49, 50], the shift of T_c due to interactions [51, 52, 53], or the reduction of 3body losses in He* [54]. Very recently, the development of the trapping techniques, together with the possibility of changing the scattering length via Feshbach resonances, has opened the way towards the achievement of strongly-correlated systems in atomic samples. Examples of these systems are provided by 1D Bose gases (Tonks-Giradeau gas) [55, 56], 1D Fermi gases (Tomonaga-Luttinger liquid) [57], 2D rapidly rotating Bose gases (which resemble the physics of Fractional Quantum Hall Effect) [58], and lattice gases [59, 60, 61]. Related with the latter, recently the superfluid to Mott Insulator transition was observed at MPQ Garching [62].

Experimental studies of trapped Fermi gas were initiated at JILA [63, 64] with ^{40}K. Theoretical work on degenerate trapped Fermi gases was mostly related to the collective excitations [65], and the role of Pauli exclusion principle on optical and collisional properties [66]. The possibility of increasing critical temperature, using resonance coupling thought a Feshbach resonances was studied in [67]. Fermi gases of polar molecules [68] attracted great interest after progress in trapping and cooling of such molecules [69]. Possibilities of identifying BCS using excitation spectrum [70, 71], and optical properties [72] has been studied.

2 Optical generation of vortices in BEC

2.1 Introduction

In the recent years the studies of ultracold atomic gases have concentrated to a great extend on investigations of various aspects of superfluidity in Bose-Einstein condensates (BEC). One aspect concerns the existence of critical velocity for the dissipationless flow, that has been demonstrated by MIT group ([73, 74], for theory see [75]). Perhaps more effort has been, however, devoted to study of generation and dynamics of vortices in BEC [76, 77, 78]. These studies are related to engineering of various collective excited states of BEC, such as directly related to superfluity "scissors modes" [79, 80], and non-topological textures such as dark solitons [13, 14].

There are two different physical situation in which vortices can be investigated. In rotating traps vortices appear in a natural way as thermodynamic ground states with quantized angular momentum [81]. Stability and other properties of vortices in rotating traps has been thoroughly discussed in Refs. [82, 83, 84]. In stationary trap the creation of vortices (or, related dark solitons) requires the use of dynamical means, and independent stability analysis.

So far, three laboratories have been able to generate and study vortex dynamics. In JILA experiment [78], atoms on a border of a single component Rubidium condensate ($F = 1, m_F = -1$) are excited using a Raman transition to the state ($F = 2, m_F = 1$) in such a way that the resulting condensate wave function of the created condensate has an "imprinted" phase that corresponds to a vortex state. This method, proposed in Ref. [85], is very much related to the "phase imprinting" method discussed in this thesis. It corresponds to creation of vortices in a nonrotating trap. In experiment of ENS group [76, 77], a Rubidium gas is evaporatively cooled while being "stirred" by a focused laser beam. "Stirring" can be kept on, or turned off after the nucleation of vortices, corresponding to a rotating, or nonrotating trap, respectively. In the ENS experiment not only a single vortices, but also vortex arrays have been observed. In MIT experiment [86] the huge vortex arrays have been observed.

Even though two successful experimental methods to create vortices have been demonstrated, it is in our opinion worth to study other possible vortex generation methods that might provide certain advantages over the two above mentioned ones. There exist several theoretical proposals, how to generate vortices in nonrotating traps: stirring of the condensate using a blue detuned laser [87, 88], or several laser beams [89], adiabatic passage [90], Raman transitions [91] in bicodensate systems, laser beam vortex guiding [92], or laser beam diffraction on a helical light grating [93]. In this thesis we concentrate on the method of "phase imprinting" using absorption plates, that we have proposed in the recent Rapid Communication [1]. This method has been very successfully applied to generate solitons [13, 14], and it offers specific kinds of control of the generation process, and thus the fascinating possibility of quantum state engineering. In the case of dark solitons, it allows for instance, not only for creation of a single soliton, but also for controlled engineering of multiple dark soliton textures [13].

2.2 "Phase imprinting"

The general idea of the "Phase Imprinting" method was already discussed in Paragraph 1.1, here we would like to use it for vortex creation. An intended wave function phase dependence is ϕ, i.e. we want the phase of wave function to be proportional to azimuthal angle. This can be easily achieve using laser pulse imaged through an absorption plate with the same absorption coefficient dependence as the one intended on the wave function phase Figure 1.

Before we turn to details, we should stress that the dynamical generation of vortices differs from the case of rotating traps, in which a *pure vortex* state with angular momentum $L_z = 1$ (in units of $\hbar$) is selected in the process of reaching the thermal equilibrium. In our case, generation of *pure* vortices requires tuning of parameters which is hard, but not impossible to achieve in experiments. Our method is suitable for creation of generic states with *vorticity* [94]. The scenario of vortex creation is such that the state without any topological defects during or right after the phase imprinting is dynamically unstable and develops typically into a state with several vortex lines, around which the circulation of velocity does not vanish. Some of this vortices are pushed away from the center of the trap to the regions of low density where they remain hardly observable. In effect, "ideal" single vortices, or vortex arrays can be created in the middle of the trap. This structures seem to be dynamically stable and their lifetime definitely is sufficiently long to allow for experimentally feasible detection. It is one of the main goals of this section to illustrate this scenario of topological defect creation (somewhat similar to Carman instability in nonlinear optics [95]) with numerical simulations.

Dynamics of BEC, and thus the process of creation and evolution of vorticity at zero temperature is well described by the time-dependent Gross-Pitaevskii(9) equation for the wave function $\psi(\mathbf{r}, t)$:

$$\mathrm{i}\hbar\partial_t\psi = \left(\frac{-\hbar^2\nabla^2}{2M} + V_{NL}(\mathbf{r}, t) + V_t(\mathbf{r}) + V_l(\mathbf{r}, t)\right)\psi, \tag{9}$$

where $V_t(\mathbf{r}) = M(\omega_x^2 x^2 + \omega_y^2 y^2 + \omega_z^2 z^2)/2$ is the external trap potential which we assume to be harmonic, M is the mass of the atom, and $\omega_x, \omega_y, \omega_z$ are the trap frequencies. The nonlinear term $V_{NL}(\mathbf{r}, t) = g|\psi(\mathbf{r}, t)|^2$ describes the mean field two-body repulsive interaction whose strength g is related to the scattering length a by $g = 4\pi N\hbar^2 a/M$, where N is the total number of condensed particles. The term $V_l(\mathbf{r}, t)$ describes an effective potential created by an external laser beam impinging on the condensate after passing through a plate with appropriately modulated absorption coefficient. In the following we will study the two dimensional version of the (9), in which we replace g by g/D, where D is the characteristic depth chosen such that the ground state chemical potentials of the 3D and 2D systems are equal.

We consider a short pulse of light with a typical duration of the order of fractions of microseconds with properly modulated intensity profile. If the incident light is detuned far from the atomic transition frequency its main effect on the atoms is to induce a Stark shift of the internal energy levels. As the intensity of light depends on the position, the Stark shift will also be position dependent as will be the phase of the condensate. As a result, the laser pulse creates vorticity in a Bose-Einstein condensate initially in its ground state.

This method is very efficient and robust, it allows for engineering of a variety of excited states of BEC containing vortices. In the ideal case the method allows to generate genuine vortices with integer angular momenta. In the presence of imperfections, typically more complex vortex patterns are generated.

The topological defect introduced by a vortex is related to the behavior of the phase of the wave-function at the vortex line: the phase "winds up" around this line i.e. it changes by an integer multiple m of 2π on a path surrounding the vortex. Index m is the vortex charge. The light beam, before impinging on the atomic system, is shaped by an absorption plate whose absorption coefficients varies linearly with rotation angle φ around the plate axis see Figure 1. As a result, $V_l(\mathbf{r}, t)$ depends on the distance from the propagation axis ρ, and the azimuthal angle φ.

In the ideal case this absorption plate causes a real jump of the potential at, say $\varphi = 0$. In this case we can model the potential for $0 \le t \le T$ by

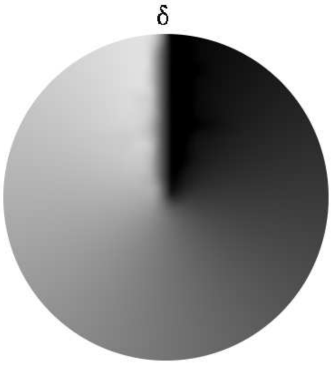

Figure 1:
Absorption plate. L is the radial extension on which the absorption profile was smoothed in our simulations, whereas δ is the angular extension of the smoothing.

$$V_l(\rho,\varphi) = \begin{cases} \hbar A I \varphi \sin^2(\pi\rho/2L) & \text{for } \rho \leq L; \\ \hbar I \varphi & \text{for } \rho > L \end{cases},$$

being zero for other times. Here T is the (square) pulse duration, whereas I denotes the characteristic Stark shift (proportional to the laser intensity); L is the characteristic length scale, on which the absorption profile is smoothed in our calculations in the vicinity of the propagation–rotation axis. As has been discussed in Ref. [1] the use of more realistic temporal pulse shapes does not change the results significantly. In the following we will use square pulses, since it allows to control the pulse area in a simpler manner.
The characteristic time and length scales for the BEC that we consider are ms, and μm, respectively. Note, that for this parameter range T is short ($\simeq \mu$s), and $\hbar I$ much larger then other energy scales. Thus, using the results of Paragraph 1.1 the dynamical effect of $V_l(\rho,\varphi)$ corresponds approximately to a "phase imprinting"(5). Since during the interaction with the laser, all other terms in Eq. ((9)) can be neglected, the wave function after switching off the pulse becomes

$$\psi(\mathbf{r},T) = \exp(-iTV_l(\rho,\varphi)/\hbar)\psi(\mathbf{r},0). \tag{10}$$

For the ideal case, choosing $IT = m$, we get the desired phase dependence characteristic for a pure vortex state. Unfortunately, the above picture is oversimplified, because the wave function ((10)) in general does not vanish at the vortex line ($\rho = 0$), which means that it has an infinite kinetic energy and unphysical character. Correct and precise description requires that one has to solve the full dynamics of the system for $0 \leq t \leq T$, taking especially into account the kinetic energy term. Moreover, experimentally realistic absorption plates cannot generate the singularity in the φ–dependence of V_l. For this reason we smooth the φ–dependence of the intensity I on the scale of δ radians (see Fig. 1). "Phase imprinting" with this smoothed intensity distribution cannot generate pure vortex states — it can, however, as we shall see below, generate in a controlled way states with predetermined vorticity.

In this thesis we have used essentially the same numerical method as in Ref. [1]. The Gross-Pitaevskii equation was solved using the split operator method in 2D (x and y plane). The simulations were divided into two stages: the initial excitation stage of duration $T \simeq 0.16\mu$s, with about 1000 time steps, and the second stage with a characteristic time scale of ms, and about 1000 steps/ms. We have assumed that initially a condensate containing $N = 10^5$ Rubidium atoms (with

$a = 5.8$nm) was trapped in a disc-shaped trap of frequencies $\omega_x = \omega_y = 2\pi \times 30$Hz, $\omega_z = 2\pi \times 300$Hz. In this case the condensate radius was about 15μm. We have used $I = 6 \times 10^6$Hz, and adjusted T to obtain the desired values of the pulse area ($IT/\pi \simeq 1, 2, \ldots$). The ρ–dependence of the potential V_l was smoothed with $L \simeq 1.7\mu$m, and the φ–dependence with $\delta \simeq 0.04 - 0.15$ radians. The smallest possible value of $\delta \simeq 0.04$ radians was determined by the spatial grid size which typically was 512×512 points in a 40μm $\times$ 40μm box. During the dynamics, after switching off the laser, the following quantities are conserved: wave function norm, mean energy, and mean z-component of the angular momentum. They were monitored in order to control the accuracy of numerics. The first two quantities were constant within the accuracy of the method, the third one in some cases has exhibited slow variations of the order of a percent.

The summary of the results of [1] is as follows: the "ideal absorbtion" plate (with $\delta = 0.04$) allows for perfect single vortex generation. Conditions remain valid for the case, when focusing of the laser is slightly off center, or $\delta = 0.15$. Of course, graduate degradation of the vortex pattern is expected as both of this imperfections increase.

2.2.1 Vortex formation

One of the major fundamental questions is how the nonzero circulation, i.e. a topological defect is introduced into the system during the phase imprinting. The scenario of vortex creation can be at best illustrated in conditions in which the pulse area is not integer. This is shown in Fig. 2 where we present a "movie" showing the condensate density during the imprinting of a phase $2.5(2\pi)$, and at later times until 1ms.

Here, the case of "ideal" absorption plate with $\delta = 0.04$ radians, and a sharp jump in the optical potential on the scale of the grid is considered. During the imprinting or a little later, i.e. for the times of the order of μs a characteristic valley develops in the density profile along the phase jump line. The density adjusts here to the imprinted phase. The valley is, however, dynamically unstable, and within a time scale of fractions of ms breaks down into a certain number of vortices. The vortices created in the middle of the trap seem to be dynamically stable. In Fig. 2 these are two vortices represent by the thick black dot in the middle of the trap (the resolution of the figure does not allow to see the vortices separation). This vortex pair is surrounded by several single vortices which flow away along spiral trajectories towards the outer regions of the condensate.

The valley in the density profile reaches within a fraction of ms a size corresponding to the condensate healing length. The time scale of the density adjustment corresponds to the inverse of the characteristic frequency, determined by the mean field energy in the condensate, $g/\hbar V$, where V is the volume of the condensate ($V \simeq \pi 15 \times 15 \times 4\mu\mathrm{m}^3$). It is the time required by the second sound to travel over a distance of the order of the healing length.

The scenario of introducing the topological defects into the system is similar to the Carman instability in nonlinear optics [95]. Dynamical instabilities play here an essential role. Basically, the mechanism of vortex creation is the same in the case of laser pulses with the area being an integer multiple of 2π. In this case, however, the width of the valley is much smaller, i.e. its the valley is much steeper. It follows from our simulation that dynamical instability in such situation appears much faster, and therefore the time scale for vortex formation is much shorter. This is illustrated in Fig. 3.

2.2.2 Multivortex formation

By adjusting the area of the pulse it is possible (using a single absorption plate) to create multivortex arrays, similarly as in experiments of ENS [76]. We have performed detailed analysis of the final vortex configuration as a function of the pulse area. We present these results obtained for a Rb condnesate and the same trap parameters as above in Table 1. As expected, increasing area leads to formation of regular arrays of more and more vortices. Such configurations (which are stationary in rotating traps [83, 96]) undergo slow rotation in the nonrotating trap, but seem to be nevertheless dynamically stable over the time scales of at least 100 ms, but most probably much longer.

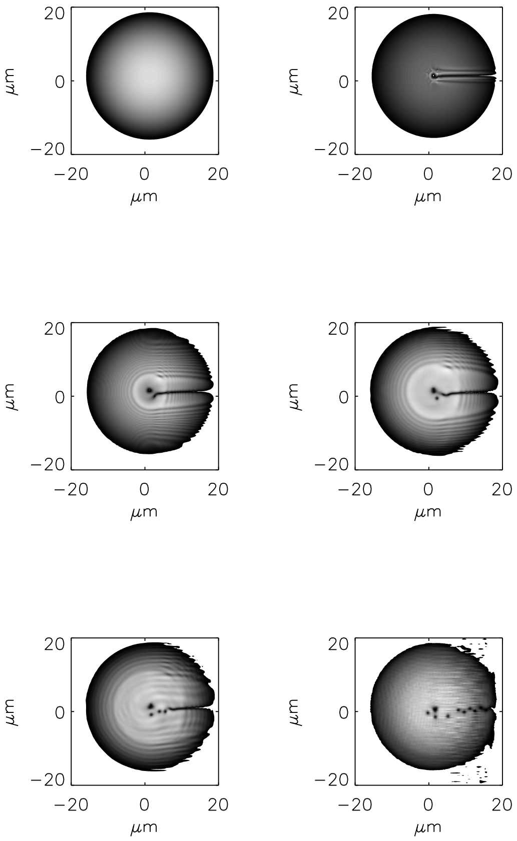

Figure 2:
BEC density during and right after the “phase imprinting” for the case of ”ideal” absorption plate with $\delta = 0.04$ *radians, and a sharp jump in the optical potential on the scale of the grid. The time of impinging was equal* $2.5/I$*. One observes the characteristic valley in density along the phase jump. The valley decays into vortices. The ”movie” present snapshots taken at times varying from* $t = 0$ *up to* $t = 1.6ms$

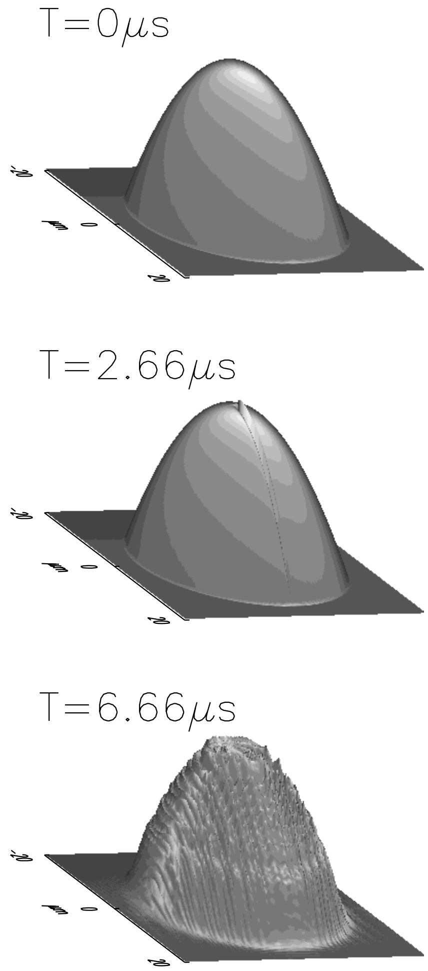

Figure 3:
BEC density during and right after the "phase imprinting" for the case of "ideal" absorption plate with $\delta = 0.04$ *radians, and a sharp jump in the optical potential on the scale of the grid. The time of impinging was equal* $2/I$*. One observes the characteristic valley in density along the phase jump. The valley decays into vortices. The "movie" present snapshots taken at times varying from* $t = 0$ *up to* $t = 6.66\mu s$*.*

Area $[2\pi]$	**Description**
$0 - 0.133$	No vortex
$0.133 - 0.5$	From 1 up to 8 vortices near the border of the condensate
$0.5 - 0.8$	1 vortex in the center of the trap and from 1 to 8 vortices near the border of the condensate
$0.8 - 1.2$	1 vortex in the trap center
$1.2 - 1.4$	1 vortex in the trap center and several vortices near the border of condensates
$1.4 - 1.533$	No vortex in the trap center but about 4 vortices near the trap center and $2 - 3$ near the border of the condensate
$1.533 - 1.733$	2 vortices in the trap center and $1 - 2$ vortices near the border
$1.733 - 2.2$	2 vortices in the trap center
$2.2 - 2.2466$	2 vortices in the trap center and from 3 up to 8 vortices near the border
$2.466 - 3.666$	3 vortices in the trap center and 2 near the border of the condensate
$3.666 - 4.2$	4 vortices in the trap center
$4.2 - 4.466$	4 vortices in the trap center and $3 - 5$ vortices out of trap center
$4.466 - 5.2$	5 vortices in the trap center
$5.2 - 5.533$	5 vortices in the trap center and from 1 to 5 near the border of the condensate
$5.33 - 6.2$	6 vortices in the trap center

Table: Generally, speaking the table shows that when the pulse area is close to $2\pi k$, with $k = 1, 2, \ldots$, then the corresponding k vortex array in the center of the trap is formed. For areas between the integer values it may happen that we have also some number of vortices, but this number is not a monotonic function of the pulse area.

2.3 “Phase imprinting” with multiple plates

The results above show that “phase imprintig” allows for controlled vortex generation. This fascinating possibility of macroscopic quantum state engineering can be realized even better if the multiple absorption plates are used. In order to understand the possibilities of coherent control better in the system considered, we will first discuss generation of the vortex arrays as a function of the absorption plate parameters in more details.

2.3.1 Vortex arrays with single absorption plate

To investigate the generation of multiple charged vortices we have first solved the Gross-Pitaevskii equation with the effective potential created by an external laser beam passing through a single absorption plate. Choosing $IT = 3$ (here $T \approx 0.84\,\mu$s) we get the desired phase for $\mathrm{m} = 3$ vortex state. In Figure 4 we plot the angular momentum acquired by the condensate being initially in the ground state as well as the energy of the condensate during the process of phase imprinting. The local minima which appear in the curve describing the condensate energy correspond to the imprinting of the phase for $\mathrm{m} = 1$ vortex state (pulse duration of $0.28\,\mu$s) and for $\mathrm{m} = 2$ vortex state (pulse duration of $0.56\,\mu$s).

It turns out that the extent of the region on which the absorption profile is smoothed plays an important role. It affects the position of the created vortex. For small diameter of smoothing area the vortex is generated near the center of the trap and rapidly decays into a few (for $\mathrm{m} > 1$) not “well developed” vortices. The descendent vortices become well separated only when the size of the smoothing region gets large enough. It is demonstrated in Figure 5 where the radius of the region smoothing the absorption profile equals 4.0 oscillatory lengths (osc. length $\approx 2.0\,\mu$m). However, in such a case the vortices are always shifted away from the center of the trap. Certainly, this is not the way of creating of multiple symmetric vortex configurations.

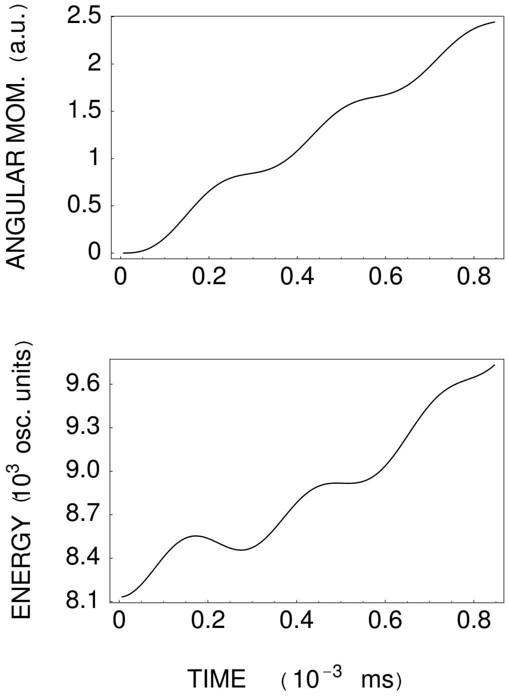

Figure 4:
Angular momentum per atom and the energy of the condensate in the first $0.84\,\mu$s *when the laser pulse acts on the condensate through the single absorption plate. The number of atoms* $\mathrm{N} = 50000$ *and the trap frequency* $\omega = 2\pi \times 30$Hz.

Instead of that, the vortices (black dots marked by the numbers) circulate both the trap center as a whole and individually the geometrical center of the vortex configuration. Closer inspection shows (Figure 6) that the geometrical center rotates the center of the trap at approximately constant radius, whereas the relative motion is a sum of oscillatory motion and rotation.

2.3.2 Vortex arrays with multiple absorbtion plates

To generate symmetric vortex configurations we propose the following extension of the "phase imprinting" method. Instead of a single absorption plate we use rather a several of them arranged one by one. The parameters of the laser pulse impinging on the condensate are taken in such a way that passing the pulse independently through any plate the phase characteristic for a pure single vortex state is imprinted just as it was done before. However, now the direction of the jump of the potential caused by each plate is arbitrary as well as the size of the area where the absorption profile is smoothed. The overall action of a chain of the absorption plates is roughly a sum of individual results. This method allows for engineering arbitrary configurations of vortices including also those with positive and negative vortex charge. Figure 7 illustrates the case of symmetric 3-vortex (all positive) configuration. We find that once generated this configuration appears to be quite robust except the circulation around the center of the trap.

Changing the diameter of the space over which the absorption profile is smoothed we are able to generate the vortex configurations of different size. It turns out that the frequency of the circulation of the vortex array depends on that size; the smaller radius of the configuration implies higher frequency. The overall behavior is visible in Figure 8. The frequency of the circulation is

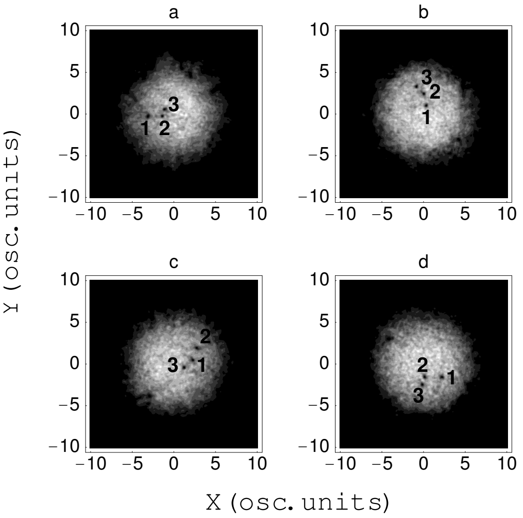

Figure 5:
Snapshots of the condensate density after illuminating through the single absorption plate (under the same conditions as for Figure 4). The successive frames describe moments: (a) 10.6 *ms, (b)* 15.9 *ms, (c)* 21.2 *ms, and (d)* 26.5 *ms. The vortices (black dots) are marked by the numbers.*

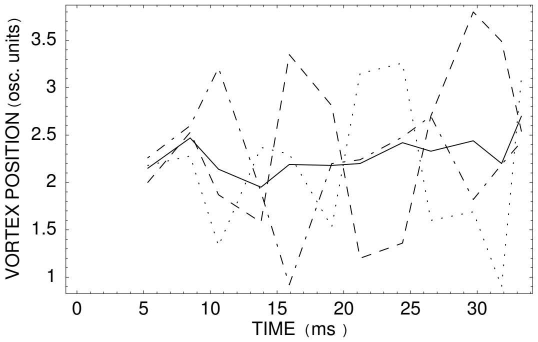

Figure 6:
Relative (with respect to the geometrical center) position of the vortex as a function of time. Parameters are the same as in Figure 5; particular lines correspond to: vortex nr. 1 (dashed-dotted line), vortex nr. 2 (dotted line), and vortex nr. 3 (dashed line). The solid line follows the distance of the geometrical center of the vortex configuration from the center of the trap.

always higher than the frequency of the trap and the question about the link of the vortices created in such a way and the vortices which appear in the rotating trap can be raised.

Since the frequency of a rotation of the vortex around the center of the trap depends on the distance between the vortex and the center, playing with this distance we can investigate the collisions between positive charged vortices. An example is presented in Figure 9. An array of three vortices was generated with the help of three absorption plates with slightly different radii of smoothing area (4.0, 3.5, and 3.0 oscillatory lengths, respectively). Frame (b) shows the instant when the vortex '1' maximally approaches the vortex '2' and partially passes its velocity to the

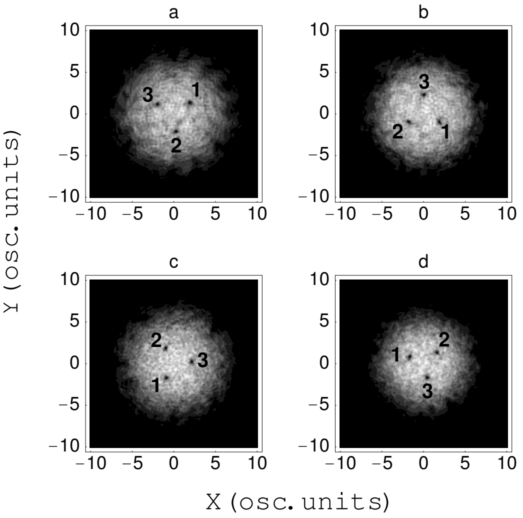

Figure 7:
Evolution of the symmetric 3-vortex configuration. The array of vortices circulates as a whole around the center of the trap. The frequency of this rotation is higher than the frequency of the trap and depends on the size of the configuration, i.e., the distance of the vortices from the center of the trap (see Figure 8). The consecutive snapshots correspond to instants at (a) 9.5 *ms, (b)* 12.7 *ms, (c)* 17.0 *ms, and (d)* 21.2 *ms after the imprinting of the phase. The absorption profile for every plate is smoothed over the region of the radius of* 4.0 *oscillatory lengths and the jumps of the potential caused by the plates are located every* 120^0.

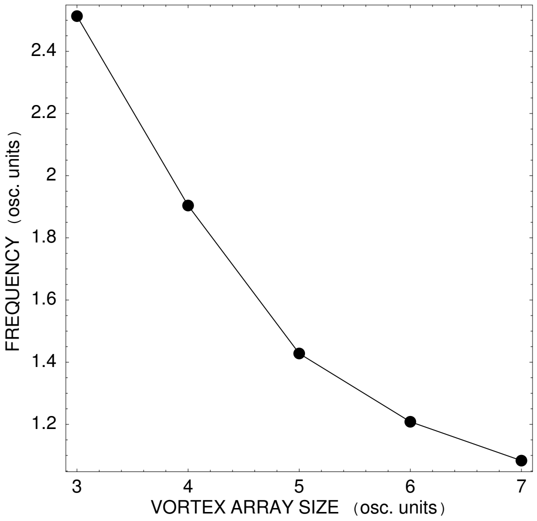

Figure 8:
Frequency of the rotation of 3-vortex array as a function of its size.

vortex '2'. Then the vortex '2' accelerates and after some time collides on the vortex '3' (Frame (c)). After next 6 ms the vortex '3' hits the vortex '1' and then the above scenario is repeated.

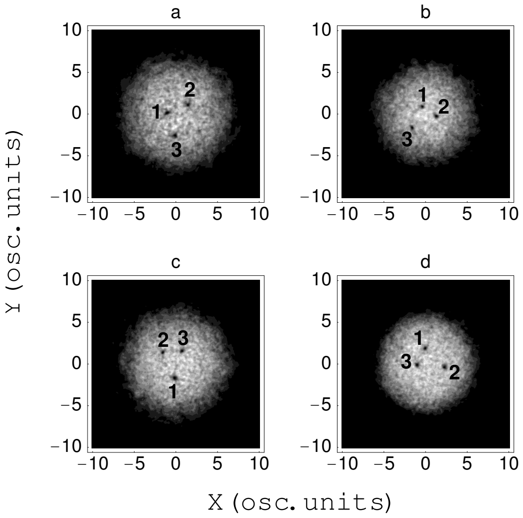

Figure 9:
Non–symmetric 3-vortex configuration at different times: (a) 14.8 *ms, (b)* 16.4 *ms, (c)* 23.3 *ms, and (d)* 29.7 *ms.*

Dynamics of the vortex motion gets more complex when the number of vortices increases. Figure 10 shows a qualitatively new behavior. It turns out that in such a complex system vortices "like" to group in pairs. Once the pair of vortices is created, it rotates around its geometrical center as well as the center of the trap. This motion continues until the collision with the other pair or a single vortex happens. Then the pair is broken and likely the exchange of vortices occurs; a new pair of vortices is built. In the case of Figure 10 the condensate was prepared with the help of six absorption plates. Frames (a)–(d) are examples of vortex pairs appearing in the condensate. From these frames it is also clear that there is a mechanism for vortex exchange.

Finally, we have investigated the simplest vortex configurations with positive and negative charged vortices. The "phase imprinting" method with multiple absorption plates seems to be an ideal tool for generating such configurations. The simplest case is a one positive charged vortex and one negative charged vortex. For that we need two plates with absorption coefficient modulated clockwise for one plate and counterclockwise for another one. The radius of the region over which the absorption profile is smoothed is slightly different for both plates (3.5 and 2.0 osc. units) and the jump of the potential is taken along $\phi = 0$. Figure analogous to Figure 4 shows that almost no angular momentum is transferred to the condensate in this case. Instead of that, a pair of opposite charged vortices with large momentum is created. The vortices repel each other as well as the "edge" of the condensate (Frames (a) and (b)), collide after 20.2 ms (Frame (c)), and then move together through the condensate over a few ms without an annihilation (Frame (d)).

2.4 Detection of vortex arrays using interference

Multiple vortices and vortex arrays can be detected using the same method of self-interference which we have proposed in [1]. This method is analogous to the ones used in nonlinear optics. In the context of matter waves similar methods were proposed in [94, 97]. Our idea is to combine this method with the recently developed techniques of Bragg diffraction for BEC manipulation [98].

Efficient detection is one of the most important aspect of the investigation of vortices. Experimentally monitoring density profiles with the necessary resolution is difficult, since the vortex core is very small. This can be circumstanced by opening the trap (see for instance [76, 78]). An

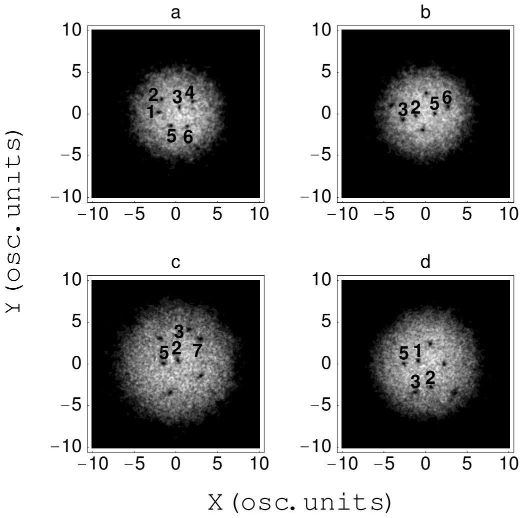

Figure 10:
Illustration of "pairing", a phenomenon which appears in multi–vortex configurations. Frames (a), (b), (c), and (d) correspond to evolutionary times: 24.4 *ms,* 42.9 *ms,* 47.1 *ms, and* 68.8 *ms, respectively.*

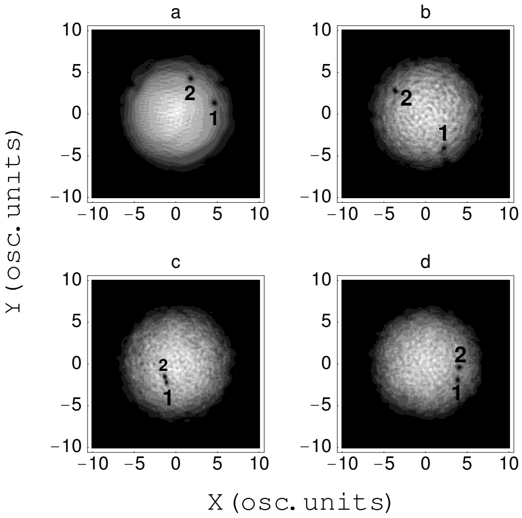

Figure 11:
Example of dynamics of the vortex configuration including both positive and negative charged vortices. The snapshots are taken at times of (a) 4.2 *ms, (b)* 11.7 *ms, (c)* 20.2 *ms, and (d)* 23.3 *ms. No annihilation of vortices occurs during the collision (Frame (c)).*

interesting way is to monitor the phase of the wave function in an interference measurement. Such interference measurements are routinely done in nonlinear optics. In the context of BEC, they were first proposed by Bolda and Walls [94], who considered the interference of two condensates moving towards each other. If both condensates are in the ground state (no vortices), one expects interference fringes as those observed by Ketterle et al. [99]. In the case of interference of one condensate in the ground state with the second one in the $m = 1$ vortex state, a fork–like dislocation in the interference pattern appears. The distance between the interference fringes is determined by the relative velocity of the condensates, which can be controlled experimentally. This is a very efficient and clear method of vorticity detection. It requires, however, the use of two independent condensates.

In Ref. [1] we have proposed to combine the interference method with the recently developed Bragg diffraction technique [98], which has been for instance successfully used in a four wave mixing experiment [100]. The idea is to transfer part of the atoms coherently to another momentum state using one, or several stimulated two-photon Raman scattering processes. The procedure is the following:

- first we create the vortex, or vorticity state in the trap;
- we open the trap and let the condensate expand;
- when the density is reduced to values for which nonlinear interactions are negligible, we apply the Bragg pulses. Part of the wave function attains a phase factor that signifies the fact that the corresponding momentum was transferred to part of the atomic sample.

If the resonant width of the Raman transition is narrower than the wave function spreading in the momentum space (in our case the velocity spread is typically about 0.12μm/ms) not all momentum components can experience the shift. In that case the contrast of interference fringes will be reduced. One can however correct for this by adiabatically opening the trap before applying Bragg pulses. The resulting wave function is the superposition of two vortex (or vorticity) states moving apart from each other, with a velocity that can be easily controlled by choice of the angle between the Bragg beams. In the following we will use velocities of the order of 1 mm/s, which allow for efficient detection after 4-5 ms when the vortices are about 5μm apart;

- detection consists of optical imaging that is accomplished within a few μs. The interference patterns have a characteristic length scale of a few μm.

Below we present the results of numerical simulation of this detection scheme. The corresponding interference patterns were obtained for the case $\delta \simeq 0.04$ radians, for 3 and 6 vortex arrays. The interference patterns show multifork dislocation, termed by us “quantum peacocks”, which are presented in Figure 12 and Figure 13. The shape of the interference pattern allows here unambiguously to detect the vortex number, array configuration, and provide the information about the phase of the wave function.

Interference method is also very useful to understand the scenario of topological defect creation in the condensate. We illustrate this point in the ”movie” in Figure 14. The presented interference pattern can hardly be measured experimentally (because of the short time scale of the process), but we present them in order to get more insight and understanding of the process of generation of an ”ideal” single vortex presented in Fig. 3. The sharp jump in the optical potential has very large gradients and introduces very strong force pushing the atoms transversally away from the region of the potential jump. The density valley is created already after 1.33 μs, but not topological defect is present (interference fringes are deformed but not broken). In the successive snapshots we see how dynamical instabilities lead to such a large shift and deformation of the fringes that finally brake and join smoothly with the corresponding nearest upper neighbor. This occurs for all, except the central fringe which builds after 6.66 μs a very clear fork pattern, corresponding to the topological defect.

It is worth stressing that the method of vortex detedtion based on interference patterns has been recently used in experiments by ENS group.

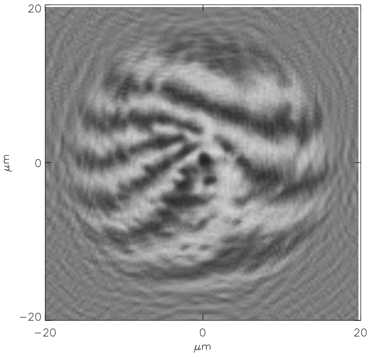

Figure 12:
Interference pattern of the 3 *vortex array* 1*ms after applying Bragg pulses transferring momentum to a part of the condesate (along "x" axis in the plane of the figure), which coherently pushed a part of the condensate with velocity* $0.01\, mm/s$*. The case of equal splitting of the whole condensate has been assumed. The incident pulse was focused at the trap center, had a sharp step in the intensity profile (*$\delta = 0.04$*), and had the area* $IT = 3(2\pi)$*.*

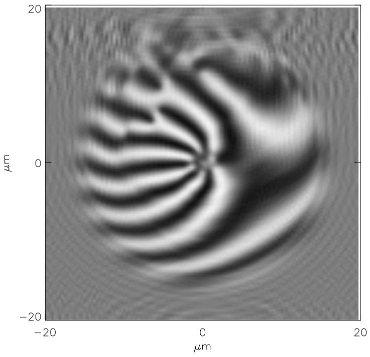

Figure 13:
Interference pattern of the 6 *vortex array* 1 *ms after applying Bragg pulses transferring momentum to a part of the condesate (along "x" axis in the plane of the figure). which coherently pushed a part of the condensate with velocity* 0.01*mm/s. The case of equal splitting of the whole condensate has been assumed. The incident pulse was focused at the trap center, had a sharp step in the intensity profile (*$\delta = 0.04$*), and had the area* $IT = 3(2\pi)$*.*

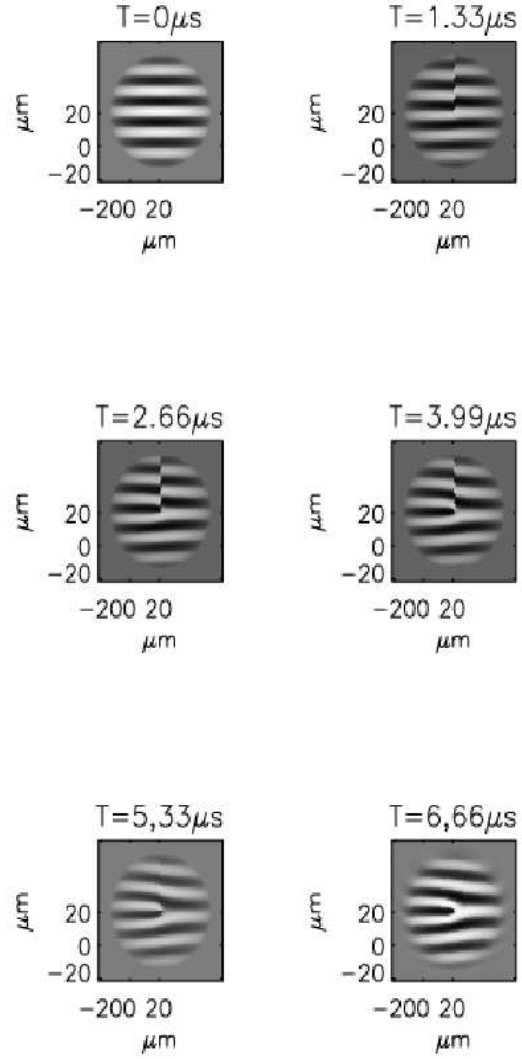
T=0μs

T=1.33μs

T=2.66μs

T=3.99μs

T=5,33μs

T=6,66μs

Figure 14:
The movie illustrating generation of the single vortex presented in Fig. 3 by using the interference patterns.

3 Fermionic 'Solitons'

3.1 Introduction

Recent pioneering work by DeMarco and Jin [63] on realization of quantum degeneracy in a trapped gas of fermionic ^{40}K atoms has triggered the interest in properties of cold fermions. As opposed to bosons, fermions cannot occupy the same quantum state, i.e., they obey the Pauli exclusion principle. Since at low temperatures only the s–wave scattering gets important, the spin–polarized fermions stop to collide at lower temperatures and rethermalization process necessary for evaporation breaks down. This difficulty has been overcome by trapping and cooling the fermions in two hyperfine states, enabling in this way the evaporation by collisions between atoms in a different spin states [63, 64]. Other groups have achieved quantum degeneracy in a gas of ^{6}Li atoms by sympathetic cooling of a mixture of bosonic (^{7}Li) and fermionic (^{6}Li) atoms reaching the temperatures down to $0.2T_F$ [101, 102]. Later group of J. E. Thomas achieved the degenerate Fermi gas by evaporative cooling in presence of strong magnetic field to induce strong resonant coupling [103]. Possibilities of cooling Bose-Fermi mixture of ^{40}K and ^{87}Rb were studied in [104].

Despite of experimental difficulties in achieving the strong quantum degeneracy in fermionic gases, some theoretical work on degenerate Fermi gases in the normal phase at zero and finite temperatures has already been done. The static properties of one– and two–component system were analysed in Refs. [105], [106] and [107]. Collective excitations in degenerate Fermi gases in the normal phase were discussed within the hydrodynamic approximation in Ref. [108] and on the basis of the sum rules in Ref. [65]. In the absence of s–wave collisions other forces, like for instance dipole–dipole interaction, start to play role. The fermionic dipoles have been investigated recently, including the analysis of stability conditions [109]. Another aspect of dynamic behavior of a degenerate Fermi gas is studied in Ref. [110] where the question about the possibility of generation of solitons and vortices in a normal state of non–interacting Fermi gas is asked. It is shown by solving the many–body Schrödinger equation that the phase imprinting method is capable of generating the solitons and vortices in such a system. An alternative method of generating such structures is discussed in Ref. [111].

So far, the phase imprinting method has been successfully applied to generate solitons in Bose–Einstein condensates [13, 14]. Although not realized experimentally yet, it offers also a rather rare opportunity of control of the generation of vortices [1, 2]. The method consists in passing an off–resonant laser pulse through the appropriately designed absorption plate followed by the impinging it on the atomic gas. The laser pulse is short and strong enough so that the atomic motion is negligible during the pulse and the basic effect of light is a generation of strong optical potential $V_{opt}(\vec{r},t)$ due to the ac–Stark effect. This potential acts for a short time τ_{dur}, and essentially imprints a desired phase of atomic wave functions $\varphi(\vec{r}) = \int_0^{\tau_{dur}} V_{opt}(\vec{r},t)dt/\hbar$. After this, the density and the phase try to adopt to each other, which results in generation of structures like solitons and vortices, depending on the pattern written in the absorption plate.

In this chapter we explore further the possibility of generating the quasisolitons in a gas of non–interacting Fermi atoms. According to the common knowledge regarding solitons, the nonlinearity of the problem plays essential role, since it cancels the dispersion and allows for a propagation of shape preserving pulses. So, at the first glance it is surprising that solitons can exist in a system of non–interacting particles described by the many–body Schrödinger equation, i.e., the linear equation. However, we show that, due to the Fermi statistics, there exists the regime of parameters where soliton–like solutions can exist in the non–interacting Fermi gas.

3.2 Solution of the many–body Schrödinger equation

3.2.1 Zero temperature

At zero temperature the many–body wave function of a system of non–interacting particles (fermions) is given by the Slater determinant with the lowest available one–particle orbitals occupied.

$$\Psi(\vec{r}_1, ..., \vec{r}_N) = \frac{1}{\sqrt{N!}} \begin{vmatrix} \varphi_1(\vec{r}_1) & . \ . \ . & \varphi_1(\vec{r}_N) \\ . & & . \\ . & & . \\ . & & . \\ \varphi_N(\vec{r}_1) & . \ . \ . & \varphi_N(\vec{r}_N) \end{vmatrix} . \tag{11}$$

The one–particle orbitals $(\varphi_1(\vec{r}), ..., \varphi_N(\vec{r}))$ are orthogonal and they undergo unitary evolution. Hence, their orthogonality is sustained, both during the phase imprinting and afterwords. Therefore, the one–particle density matrix is at any time given by the following formula

$$\rho_1(\vec{r}\,', \vec{r}\,'', t) = \frac{1}{N} \sum_{i=1}^{N} \varphi_i(\vec{r}\,', t)\, \varphi_i^*(\vec{r}\,'', t)\,,$$

and its diagonal part is just the particle density.
Evolution of each single–particle orbital is obtained from the one–particle Schrödinger equation and can be split into two stages. First, the phase imprinting technique is used to disturb the system in a way of writing a desired phase on it. Assuming fast enough phase imprinting, the resulting wave function has the form (this procedure can be also performed numerically within the finite duration of the imprinting process):

$$\varphi_k(\vec{r}) \longrightarrow \varphi_k'(\vec{r}) = \varphi_k(\vec{r})\, \exp(i\phi(x))\,,$$

for $k = 1, ..., N$, where $\phi(x)$ is the phase imprinted on each atom. Throughout this paper we deal with the generation of quasisolitons, we assume that the imprinted phase depends only on a single coordinate, say 'x', and utilize $\phi(x) \sim (1 + \tanh(x/d_{\mathrm{phase}}))$. We consider a Fermi gas in a three–dimensional box or harmonic trap characterized by the frequencies ω_x, ω_y, and ω_z. Both are separable in Cartesian coordinates. The one–particle orbitals $\varphi_k(\vec{r})$ are taken as a product $\varphi^{(1)}_{n_x}(x)\, \varphi^{(2)}_{n_y}(y)\, \varphi^{(3)}_{n_z}(z)$ of eigenvectors of the Hamiltonians of one–dimensional boxes or harmonic oscillators.
In the second stage the system undergoes the free evolution in three–dimensional space. However, because the Hamiltonian separates in coordinates 'x', 'y', and 'z', the time propagation of each orbital can be easily reduced to one–dimensional case:

$$\begin{aligned} \varphi_k(x, y, z, t) &= e^{-i\mathrm{E_{n_y}\,t}/\hbar} e^{-i\mathrm{E_{n_z}\,t}/\hbar} \\ &\quad \times \varphi^{(2)}_{n_y}(y, 0)\, \varphi^{(3)}_{n_z}(z, 0) \\ &\quad \times \varphi^{(1)}_{n_x}(x, t) \end{aligned}$$

where

$$\varphi^{(1)}_{n_x}(x, t) = e^{-i\mathrm{H_x\,t}/\hbar} \varphi^{(1)}_{n_z}(x, 0)\, e^{i\phi(x)}$$

and $\mathrm{H_x}$ is the Hamiltonian of one–dimensional box or harmonic oscillator. The diagonal part of one–particle density matrix is given then by the expression:

$$\rho(\vec{r},t) = \frac{1}{\mathrm{N}} \sum_{n_x,n_y,n_z} |\varphi^{(2)}_{n_y}(y,0)|^2 \, |\varphi^{(3)}_{n_z}(z,0)|^2 \times |\varphi^{(1)}_{n_x}(x,t)|^2 \tag{12}$$

In Figure 15 we plotted the density profiles of a uniform system of 500 atoms after imprinting the phase designed in the form $\phi(x) = \phi_0(1 + \tanh(x/d_{\mathrm{phase}}))/2$. The characteristic length (the Fermi length) is given by the formula $\lambda_F = h/p_F = 2/NL$, where p_F is the Fermi momentum and L is the size of one–dimensional box. For the case of Figure 15, the Fermi length equals $0.004\,L$ and is 2.5 times smaller than the width characterising the jump of the imprinted phase. As discussed more precisely in Paragraph 3.2, the evolution of the density after phase imprinting depends strongly on the ratio $d_{\mathrm{phase}}/\lambda_F$ between the width of the phase step and the Fermi length.

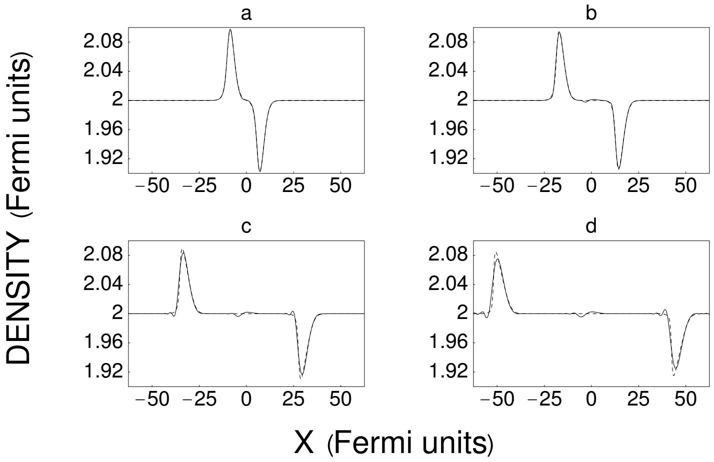

Figure 15:
Images of the fermionic density (normalized to the number of atoms) of N=500 *atoms after writing a single phase step of* $1.0\,\pi$ *and the width* $d_{\mathrm{phase}} = 2.5\,\lambda_F$ *onto a one–dimensional non–interacting Fermi gas confined in a box at different times: (a) 24.7, (b) 49.3, (c) 98.7, and (d) 148.0 in Fermi units* ($\hbar/\varepsilon_F$)*. Each graph consists of two curves: one obtained based on the many–body Schrödinger equation (solid line) and the second coming from the one–dimensional Thomas–Fermi model (dashed line).*

It is clear from Figure 15 (as well as Figure 16) that two quasisolitons (the bright and the dark one) are generated. They propagate in opposite directions with distinct velocities. We present in Table 1 the values of soliton's velocities for various widths of the phase steps. The speed of the bright quasisoliton is always higher than the speed of sound whereas dark quasisolitons move slower than the sound. However, increasing the ratio $d_{\mathrm{phase}}/\lambda_F$ both velocities are getting closer to the speed of sound (p_F/m in one–dimensional space), reaching eventually (i.e., in the limit $d_{\mathrm{phase}} \gg \lambda_F$) the value p_F/m as shown in Paragraph 3.2 and Paragraph 3.3. In Sec. Paragraph 3.3 we also analyze the $d_{\mathrm{phase}} \gg \lambda_F$ limit by decreasing λ_F (increasing the number of atoms) and solving the equations of the Thomas–Fermi model.

$\frac{d_{\text{phase}}}{\lambda_F}$	$\frac{v_b}{c}$	$\frac{v_d}{c}$
1.25	-1.061	+0.953
2.50	-1.044	+0.958
5.00	-1.033	+0.963
12.5	-1.014	+0.981

Table 1: Speeds of dark and bright quasisolitons (in units of speed of sound) generated in a one–dimensional homogeneous Fermi gas of 500 atoms after imprinting a single phase step of π and various widths d_{phase} (in units of the Fermi length).

Figure 16 shows that going deeper into the regime $d_{\text{phase}} \gg \lambda_F$ the soliton structures become less pronounced. This again is explained in terms of Wigner function in Sec. Paragraph 3.2 and based on Thomas–Fermi approach in Sec. Paragraph 3.3. The condition $d_{\text{phase}} \gg \lambda_F$ means that the height (or depth) of solitons is getting smaller in comparison with unperturbed density. Going in opposite direction (i.e., $d_{\text{phase}} <\sim \lambda_F$) results, as presented in Figure 17, in a change of shape of the structures (dispersion) on a time scale of the order of $\hbar/\varepsilon_F$.
Another aspect of Figure 15 is connected with the Thomas–Fermi approximation discussed in Sec. Paragraph 3.3. Each frame of Figure 15 shows, in fact, two curves; one of them (solid line) is obtained by solving the many–body Schrödinger equation, and the second (dashed line) is representing the Thomas–Fermi approach. Both curves match well which proves the validity of the Thomas–Fermi approximation in one–dimensional space for large enough number of atoms just as it happens in the case of a harmonic trap (see Fig. 1 in Ref. [110], where two– and three–dimensional cases are also discussed). For polarized Fermi gas the use of Thomas-Fermi approximation is in fact legitimate only in 1D or quasi-1D (elongated cigar shape traps) [112].

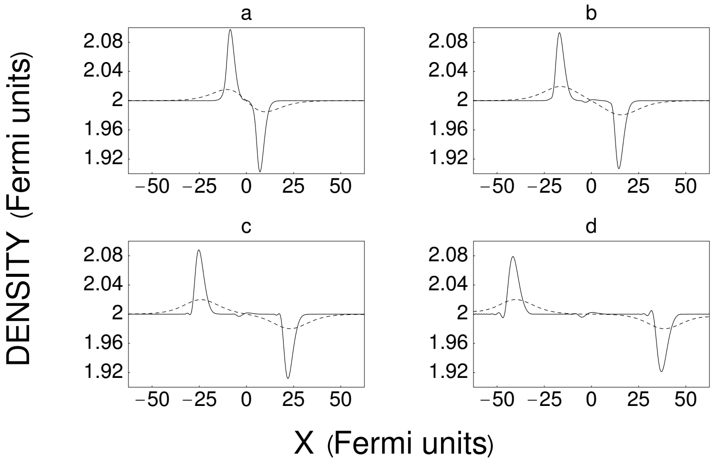

Figure 16:
Comparison of bright–dark soliton structures for various widths of imprinted phase: 2.5 λ_F (solid line) and 12.5 λ_F (dashed line). The snapshots are taken at times (a) 24.7, (b) 49.3, (c) 74.0, and (d) 123.3 in Fermi units. Other parameters are the same as in Figure 15.

3.2.2 Finite temperatures

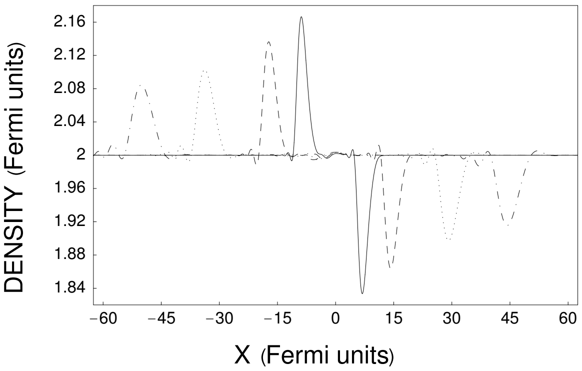

Figure 17:
Soliton–like structures in the regime where $d_{\rm phase} <\sim \lambda_F$ (here, $d_{\rm phase} = 1.25\,\lambda_F$). The snapshots are taken at times (a) 24.7 (solid line), (b) 49.3 (dashed line), (c) 98.7 (dotted line), and (d) 148.0 (dashed–dotted line) in Fermi units. Other parameters are the same as in Figure 15.

One way of including temperature effects on the soliton's generation and propagation is to allow for populating the single–particle states of higher energy than the Fermi energy. We have realized this by considering a grand canonical ensemble for a system of non–interacting fermions. We generate a number of many–particle configurations according to the Fermi–Dirac statistics, i.e., with the probability of populating a particular one–particle state φ_k given by $\exp(\beta(\varepsilon_k - \mu)) + 1)^{-1}$, where ε_k is the state energy, β determines the bath temperature (via $\beta = 1/k_BT$), and μ is the chemical potential (dependent on temperature in general). More precisely, for each one–particle state (unless the probability of populating this state is lower than 10^{-6}) we generate a random number from the interval $[0, 1]$. If the number is less than $\exp(\beta(\varepsilon_k - \mu)) + 1)^{-1}$, the one–particle state is populated, otherwise it is left empty. Here, ε_k is the energy of the state under consideration, the chemical potential

$$\mu = \varepsilon_F[1 - (\pi^2/3)(k_BT/\varepsilon_F)^2], \tag{13}$$

and ε_F equals the Fermi energy corresponding to the average number of atoms. The above formula for the chemical potential applies for the Fermi gas trapped in a harmonic potential for the temperatures up to $0.55\,T_F$ [105].

In such a way, having given the temperature and the average number of atoms, the many–particle configurations are sampled. Then, for each many–particle configuration the phase imprinting is performed followed by a free evolution. Finally, the density is calculated as an average according to a grand canonical ensemble rules. We have investigated in this way the propagation of quasisolitons for temperatures up to $0.3\,T_F$, already attainable in experiment [64, 101, 102].

In Figure 18 we plot evolution of the averaged density of the Fermi gas confined in a one–dimensional harmonic trap of frequency ω after phase imprinting of a single step of 2π and the width equal to 0.5 osc. units. $(\sqrt{\hbar/(m\omega)})$. Here, the chemical potential is given by the formula $\mu = \varepsilon_F + k_BT\log[1 - \exp(-\varepsilon_F/k_BT)]$, which is a one–dimensional counterpart of formula ((13)), the temperature equals $0.2\,T_F$, and the averaging procedure is performed over 5000 many–body configurations. Both, bright and dark solitons are still present in the system exhibiting basically the same properties as at zero temperature. For higher temperatures (already $0.3\,T_F$) the soliton structures start to get hidden within the noise originating in the averaging procedure (Figure 19). However, one has to remember that rather a particular many–body configuration is realized in a single experiment, and not an ensemble of them. Finally, Figure 20 gives an example that going from one– to three-dimensional space, predictions made based on lower dimensionality survive. Figure 20 shows density profiles of fermionic gas trapped in a spherically symmetric potential (averaged over

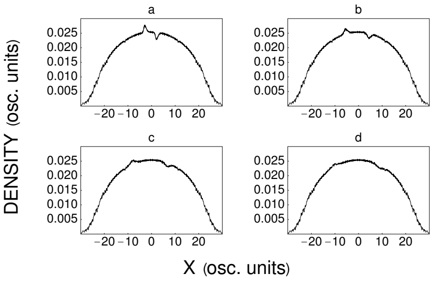

Figure 18:
Evolution of the density distribution of 300 (average number) Fermi atoms in one–dimensional harmonic trap at temperature $0.2\,T_F$ *after imprinting a single phase step of* $2.0\,\pi$ *and* $d_{\rm phase} = 0.5$ *osc. units. The successive frames correspond to moments: (a) 0.1, (b) 0.2, (c) 0.3, and (d) 0.4 in units of* $1/\omega$.

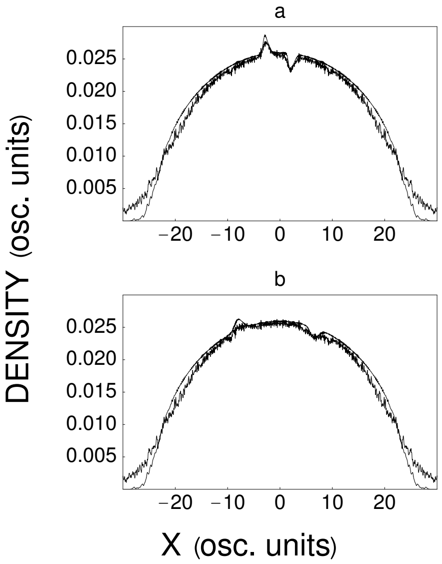

Figure 19:
Comparison of bright–dark soliton structures at different temperatures: $0.1\,T_F$ *(less rugged curve, averaged over* 1000 *configurations) and* $0.3\,T_F$ *(more rugged curve, averaged over* 10000 *configurations). Frames (a) and (b) correspond to moments* 0.1 *and* 0.3 *in units of* $1/\omega$ *respectively and other parameters are the same as in Figure 18.*

1000 configurations at $0.1\,T_F$ temperature) and can be compared with corresponding figure from Ref. [110] at zero temperature since the details of phase imprinting are the same.

3.3 Wigner function approach

The Wigner function $w(x,p,t)$ is defined as

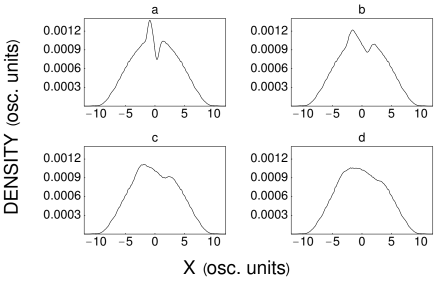

Figure 20:
Density profiles of non–interacting fermionic gas confined in three–dimensional spherically symmetric harmonic trap at different times: (a) 0.1, (b) 0.2, (c) 0.3, and (d) 0.4 in units of $1/\omega$ *after writing a single phase step of* $\phi_0 = 1.0\,\pi$ *and* $\zeta = 0.2$ *osc. units. The average number of atoms N=*10^4*, the temperature is equal to* $0.1\,T_F$*, and* 1000 *configurations were used in the averaging procedure.*

$$w(x,p,t) = \int dy \left\langle \hat{\psi}^\dagger(x+y/2,t)\hat{\psi}(x-y/2,t)\right\rangle \exp(-ipy) \;, \tag{14}$$

where $\hat{\psi}^\dagger(x,t)$ and $\hat{\psi}(x,t)$ denote atomic creation and annihilation operators in the Heisenberg picture, respectively. It obeys the equation

$$\left(\partial_t + \frac{p}{m}\partial_x - \partial_x V_{ext}(x)\partial_p\right) w(x,p,t) = 0 \;, \tag{15}$$

where $V_{ext}(x)$ is the external harmonic trap potential. It immediately follows from the definition, Eq. (14), that the density of particles at time t is

$$\rho(x,t) = \int \frac{dp}{2\pi\hbar}\, w(x,p,t). \tag{16}$$

The phase imprinting at $t = 0$ modifies the Wigner function in the following way:

$$\begin{aligned} w_0(x,p,t=0) \rightarrow w_0(x,p) = \int dy &\left\langle \hat{\psi}^\dagger(x+y/2,t=0)\hat{\psi}(x-y/2,t=0)\right\rangle \\ &\times \exp(-ipy/\hbar - i\phi(x+y/2) + i\phi(x-y/2)) \end{aligned} \tag{17}$$

where $\phi(x)$ is the imprinted phase. The function $w_0(x,p)$ provides the initial condition for the dynamical evolution according to Eq. ((15)).
Let us consider first the spatially homogeneous case ($V_{ext}(x) = 0$). Eq. ((15)) with the initial condition $w(x,p,t=0) = w_0(x,p)$ can be easily solved. The solution is

$$w(x,p,t) = w_0(x-(p/m)t,p) \;, \tag{18}$$

and reflects the ballistic motion of particles in the absence of an external potential. By using the fact that in the spatially homogeneous case the correlation function

$$\left\langle \hat{\psi}^\dagger(x+y/2,t=0)\,\hat{\psi}(x-y/2,t=0)\right\rangle = \rho_0(y),$$

i.e., it depends only on 'y', the expression for $w_0(x,p)$ can be rewritten in the form

$$w_0(x,p) = \int dy \rho_0(y) \exp(-ipy/\hbar - i\phi(x+y/2) + i\phi(x-y/2)) \;. \tag{19}$$

The above formulae have a general character, and are valid for both degenerate and non-degenerate (Boltzmann) Fermi gas. The difference between these two cases is only in the specific form of the function $\rho_0(y)$.

Usually in the experiments, the imprinted phase $\phi(x)$ is a function with transition regions of the size of the order of d_{phase} between the regions with constant values of the phase. Depending on the ratio between d_{phase} and the characteristic width of the function $\rho_0(y)$, one has completely different behavior of the solution Eq. ((18)) and, therefore, the density evolution. In the degenerate regime, the characteristic width of ρ_0 is given by the Fermi wavelength λ_F, which is inversely proportional to the Fermi momentum, $\lambda_F = h/p_F$. In the opposite case of a Boltzmann gas, the width is given by the thermal wavelength $\lambda_T = h/\sqrt{2mT}$.

We first analyze the case where $d_{\text{phase}} \gg \lambda_F,\ \lambda_T$. Under this condition, one can expand the exponent in Eq. ((19)) in powers of y, and leave only the lowest, linear in y, contribution:

$$\begin{aligned} w_0(x,p) &\approx \int dy \rho_0(y) \exp(-ipy/\hbar - i\phi'(x)y) \\ &= \widetilde{\rho}_0(p+\phi'(x)), \end{aligned} \tag{20}$$

where $\widetilde{\rho}_0(p)$ is the Fourier transform of the function $\rho_0(y)$ and ϕ' is the derivative of ϕ. The density of the particles, Eq. ((16)), can then be written as

$$\begin{aligned} \rho(x,t) &= \int \frac{dp}{2\pi\hbar} w_0(x-(p/m)t,p) \\ &\approx \int \frac{dp}{2\pi\hbar} \widetilde{\rho}_0(p+\hbar\phi'(x-(p/m)t)) \end{aligned}. \tag{21}$$

Keeping in mind that $\phi' <\sim \pi/d_{\text{phase}}$ and, therefore, is much smaller than the characteristic momenta, p_F and $p_T \sim \sqrt{mT}$ for the degenerate and Boltzmann gas, respectively, Eq. ((21)) can be simplified as:

$$\rho(x,t) \approx \rho_0 + \int \frac{dp}{2\pi} \widetilde{\rho}_0'(p)\phi'(x-(p/m)t), \tag{22}$$

where $\rho_0 = \int(dp/(2\pi\hbar))\widetilde{\rho}_0(p)$ is the initial constant density and $\widetilde{\rho}_0'$ is the derivative of $\widetilde{\rho}_0$. The function $\phi'(x)$ is only nonzero in the transition regions of the width d_{phase}. Therefore, Eq. ((22)) has a very clear meaning. It represents a superposition of bumps moving with different velocities p/m which are distributed with the weights $\widetilde{\rho}_0'(p)$.

For a degenerate Fermi gas at zero temperature one has $\widetilde{\rho}_0'(p) = \delta(p+p_F) - \delta(p-p_F)$, and, hence,

$$\rho(x,t) \approx \rho_0 + \frac{1}{2\pi}[\phi'(x+(p_F/m)t) - \phi'(x-(p_F/m)t)]. \tag{23}$$

The above formula describes a "soliton-like" motion (without broadening and interaction) of bright and dark structures in the density, described by the function $\phi'(x)$, in the opposite directions with the same velocity $v_F = p_F/m$. The physical explanation of this phenomenon is very simple. Under the condition $d_{\text{phase}} \gg \lambda_F$, the quantum state of the system after the phase imprinting contains excitations, particle-hole pairs, only in the vicinity of the Fermi surface. (The energy width of the excitation distribution is of the order of $\hbar/d_{\text{phase}} \ll p_F$.) As a result, they have the same velocity. either v_F or $-v_F$, and, therefore, the corresponding density profile moves in both directions with velocities $\pm v_F$, respectively, without any distortion. To be precise, the broadening in this case is of the second order in $d_{\text{phase}}/\lambda_F$. To determine the characteristic time scale τ_{F0}, one has to keep in mind that the width of the distribution of the excitation momenta after the phase imprinting is of the order of $\delta p \sim \hbar/d_{\text{phase}} \ll p_F$. Hence, the time τ_{F0} can be estimated as $\tau_{F0} \sim (\hbar/T_F)(d_{\text{phase}}/\lambda_F)^2 \gg \hbar/T_F$.

At temperatures $T \ll T_F$ (but $T > T_F\lambda_F/d_{\text{phase}}$, the condition when the thermal width of the excitation distribution is larger then that after the phase imprinting), the situation is very similar, and Eq. ((22)) can be written in the form

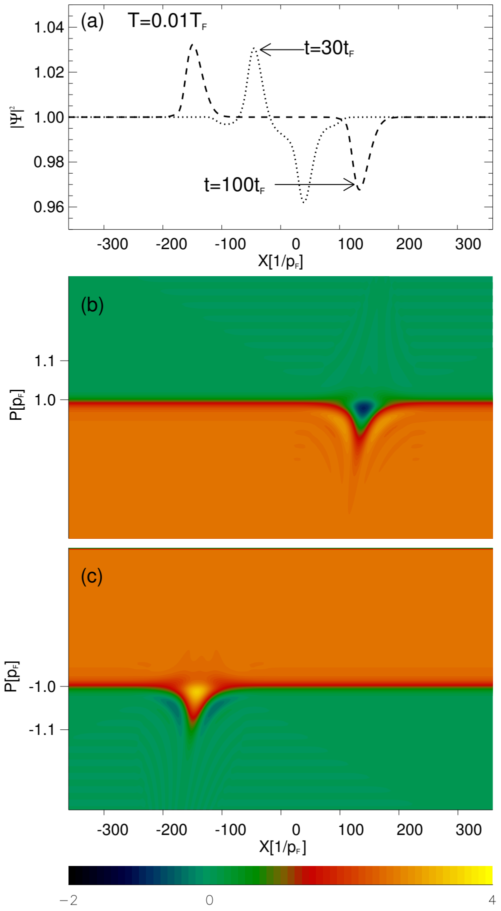

Figure 21:
The time evolution of the gas density and the Wigner function after the phase imprinting with $d_{\mathrm{phase}} = 160\lambda_F$ *at temperature* $T = 0.01T_F$*: (a) the density profile at the times* $t = 30t_F$ *(the dotted curve) and* $t = 100t_F$ *(the dashed curve), respectively, where* $t_F = \hbar/T_F$*; (b) and (c) the Wigner function for the time* $t = 100t_F$*, where* $t_F = \hbar/\varepsilon_F$*.*

$$\begin{aligned}\rho(x,t) \approx \rho_0 + \int \frac{ds}{2\pi} f_F(s,T)\,[\phi'(x + t(p_F + s)/m)) \\ -\phi'(x - t(p_F + s)/m)]\end{aligned}, \tag{24}$$

where $f_F'(s,T) = (p_F/4mT)\cosh^{-2}(sp_F/2mT)$ is related to the derivative of the Fermi-Dirac distribution and describes broadening of the δ-like peaks at $p = \pm p_F$ in the distribution $\widetilde{\rho}_0'(p)$ at finite temperatures. As a result, now one has a superposition of bright bumps and dark wells in the density profile, moving with slightly different velocities distributed with two narrow peaks at $\pm p_F/m$ with the width of the order of $mT/p_F \sim p_F T/T_F \ll p_F$. This results in spreading of bumps and wells in the density profile on a time scale $\tau_{FT} \sim (\hbar/T)(d_{\mathrm{phase}}/\lambda_F) \sim (\hbar/T_F)(T_F/T)(d_{\mathrm{phase}}/\lambda_F) \gg \hbar/T$, $\hbar/T_F$ (at $T = T_F\lambda_F/d_{\mathrm{phase}}$ one has $\tau_{FT} = \tau_{F0}$). Therefore, the time evolution of the gas density after a phase imprinting can be described in terms of a combination of several quasisolitons (bumps) and quasi–darksolitons (wells) which move through each other without any interaction and, for times $t \ll \tau$, decay (broaden) very slowly. In Figure 21 we present the results of numerical calculations of the time evolution of the density and Wigner functions for a spatially homogeneous gas at the temperature $T = 0.01T_F$ after the 2π–step phase imprinting with $d_{\text{phase}} = 160\lambda_F$. The results clearly demonstrate (see Figure 21a) that under these conditions the soliton–like structures caused by the phase imprinting behave like real solitons, i.e., they propagate without any noticeable decay (broadening) on a long time scale. The blue regions in Figure 21b and Figure 21c correspond to negative values of the Wigner function, and, therefore, indicate the quantum origin of the phenomenon. For high temperatures $T \gg T_F$ gas is in the Boltzmann regime, and Eq. ((22)) takes the form

$$\rho(x,t) \approx \rho_0 + \int \frac{dp}{2\pi} f_B(p,T)\phi'(x-(p/m)t) \ , \tag{25}$$

where $f_B(p,t) = \rho_0\sqrt{2\pi/mT}(p/mT)\exp(-p^2/2mT)$ describes the distribution with two broad peaks at $p = \pm p_T$ with $p_T \sim \sqrt{mT}$, with the width $\delta p \sim p_T$. In this case, the decay of the original density profile takes place more rapidly than in the case of a degenerate gas, on the time scale $\tau_B \sim (\hbar/T)(d_{\text{phase}}/\lambda_T) \sim \tau_F\sqrt{T_F/T} \gg \tau_F$. The corresponding numerical results for the density evolution at the temperature $T = 5T_F$ are shown in Figure 22. Although the parameters of the phase imprinting are exactly the same as for the case of Figure 21, the temperature (or, in other words, the absence of the sharp Fermi surface) cause a rapid decay of soliton-like structures.

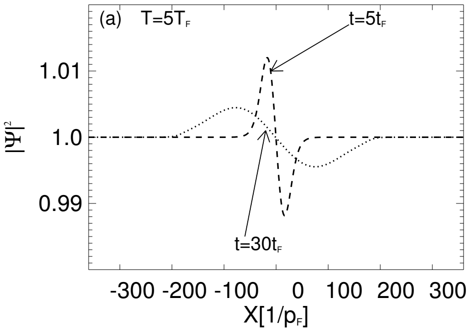

Figure 22:
The density of the gas with temperature $T = 5T_F$ at time $t = 5t_F$ (the dashed curve) and $t = 30t_F$ (the dotted curve), respectively, after the phase imprinting with $d_{\text{phase}} = 160\lambda_F$.

The same consideration is applied to the trapped gas in the harmonic potential. In this case, due to the periodicity of the motion, the essential scale for the time evolution is set by the inverse level spacing: $t \leq 2\pi/\omega$, where ω is the trap frequency. Therefore, after phase imprinting one would observe a quasisoliton behavior if $2\pi/\omega \ll \tau_{F0}$, τ_{FT}, or $2\pi/\omega \ll \tau_B$ for the degenerate or Boltzmann regime, respectively. More explicitly, in the degenerate regime one has the following requirement for the temperature T and the width d_{phase}: $[\hbar\omega/\max(T, T_F\lambda_F/d_{\text{phase}})](d_{\text{phase}}/\lambda_F) \gg 1$, or $d_{\text{phase}}/l_0 \gg \max(1, T/\hbar\omega\sqrt{N})$, where $l_0 = \sqrt{\hbar/m\omega}$ is the oscillator length and N is the number of particle. Correspondingly, in the regime of a Boltzmann gas, the requirement reads: $(\hbar\omega/T)(d_{\text{phase}}/\lambda_T) \gg 1$, or $d_{\text{phase}}/l_0 \gg \sqrt{T/\hbar\omega}$.

In the regime where $d_{\text{phase}} <\sim \lambda_F$, λ_T, the excitations created during the phase imprinting have a very broad distribution with the width $\delta p \sim \hbar/d_{\text{phase}} >\sim p_F$, p_T in a spatially homogeneous gas, and $\delta\varepsilon \sim \hbar\omega(l_0/d_{\text{phase}})^2$ in a trapped one. In this case one would expect a very rapid decay of "solitons" on a time scale $\tau \sim [\hbar/\max(T_F,T)][d_{\text{phase}}/\min(\lambda_F,\lambda_T)]^2 \ll \hbar/T_F$ for both spatially homogeneous and trapped Fermi gases. The corresponding numerical results for the density and Wigner function evolution after the 2π–step phase imprinting with $d_{\text{phase}} = 2\lambda_F$ are shown in

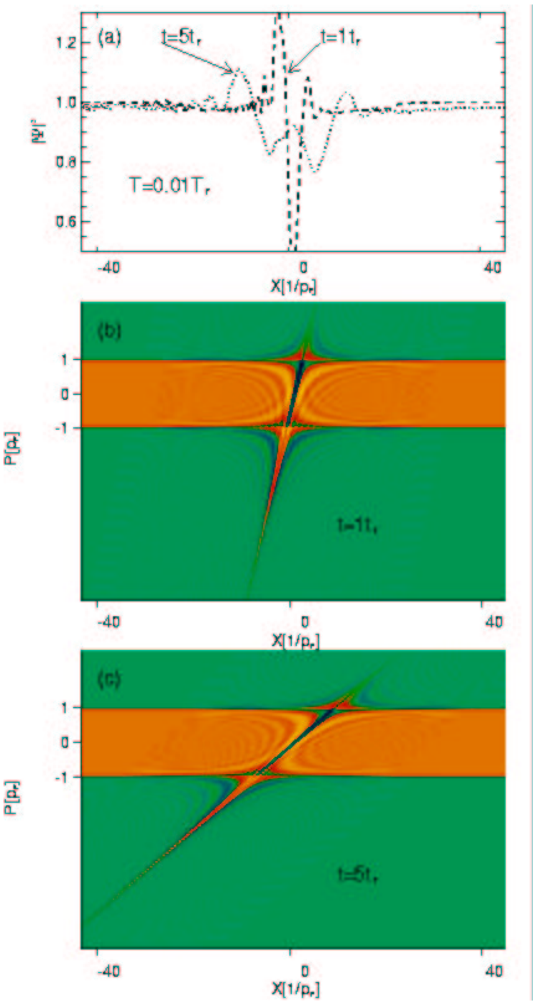

Figure 23:
The time evolution of the gas density and the Wigner function after the phase imprinting with $d_{\mathrm{phase}} = 2\lambda_F$: (a) the gas density at the times $t = t_F$ (the dashed curve) $t = 5t_F$ (the dotted curve); (b) the Wigner function at the time $t = t_F$; (c) the Wigner function at the time $t = 5t_F$. The temperature of the gas $T = 0.01T_F$.

Figure 23 (for the temperature $T = 0.01T_F$) and Figure 24 (for the temperature $T = T_F$). In the quantum degenerate case (Figure 23), the Wigner function has a well pronounced fringes structure, and the corresponding complicated structure in the density profile decays rather fast. For the non–degenerate gas (Figure 24), the Wigner function is smooth everywhere except for the narrow region subjected by the phase imprinting. In this case, the density profile has no small-scale structures, as compared to the degenerate case from Figure 23, but also relaxes very fast to the uniform density distribution.

3.4 Density matrix formalism

Another way to discuss the soliton's formation in a gas of neutral fermionic atoms is to start from a set of equations for reduced density matrices. In particular, the equation of motion for the

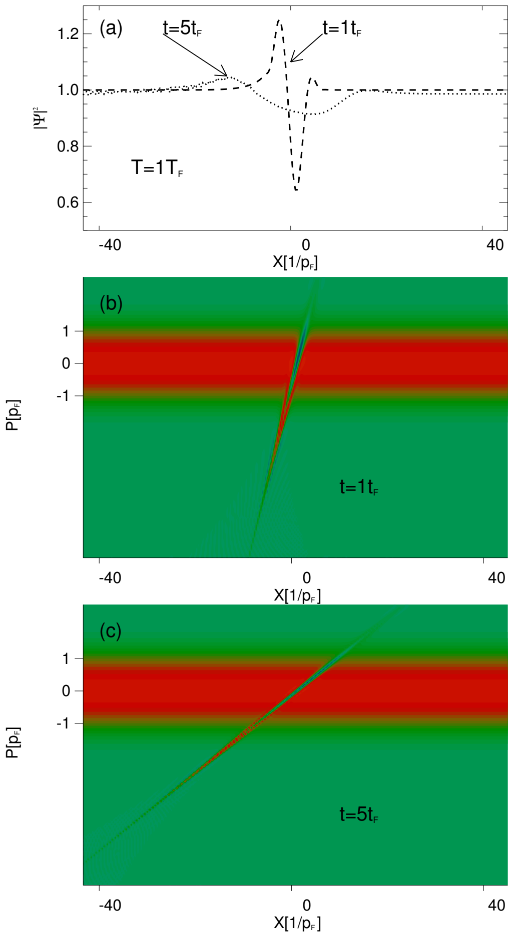

Figure 24:
The same as in Figure 21 but for the temperature $T = T_F$.

one–particle density matrix involves the two–particle density matrix ρ_2 and is given by (26)

$$\begin{aligned} i\hbar\frac{\partial}{\partial t}\rho_1(\vec{r}_1,\vec{r}_2,t) = & -\frac{\hbar^2}{2m}(\vec{\nabla}_1^2-\vec{\nabla}_2^2)\,\rho_1(\vec{r}_1,\vec{r}_2,t) \\ & + \int d^3r'\,[V(\vec{r}_1-\vec{r}\,')-V(\vec{r}_2-\vec{r}\,')]\,\rho_2(\vec{r}_1,\vec{r}\,';\vec{r}_2,\vec{r}\,',t)\,, \\ & + [V_{ext}(\vec{r}_1,t)-V_{ext}(\vec{r}_2,t)]\,\rho_1(\vec{r}_1,\vec{r}_2,t) \end{aligned} \tag{26}$$

where $V(\vec{r}_1-\vec{r}_2)$ is the two–particle interaction term and $V_{ext}(\vec{r},t)$ is the external potential. In the limit $\vec{r}_1\to\vec{r}_2$ Eq. ((26)) leads to the continuity equation

$$\frac{\partial\rho(\vec{r},t)}{\partial t}+\vec{\nabla}\cdot[\rho(\vec{r},t)\,\vec{v}(\vec{r},t)]=0, \tag{27}$$

where the density and velocity fields are defined as follows:

$$\begin{aligned} \rho(\vec{r},t) &= \lim_{\vec{r}_1\to\vec{r}_2}\rho_1(\vec{r}_1,\vec{r}_2,t) \\ \vec{v}(\vec{r},t) &= \frac{\hbar}{2m}\lim_{\vec{r}_1\to\vec{r}_2}(\vec{\nabla}_1-\vec{\nabla}_2)\,\chi_1(\vec{r}_1,\vec{r}_2,t), \end{aligned} \tag{28}$$

and $\chi_1(\vec{r}_1, \vec{r}_2, t)$ is the phase of the one–particle density matrix.
One can also rewrite Eq. ((26)) introducing the center–of–mass ($\vec{R} = (\vec{r}_1 + \vec{r}_2)/2$) and the relative position ($\vec{s} = \vec{r}_1 - \vec{r}_2$) coordinates. By taking the derivative of Eq. ((26)) with respect to the coordinate $\vec{s}$ the hydrodynamic Euler–type equation of motion is obtained in the limit $\vec{s} \to 0$

$$\begin{aligned} \frac{\partial \vec{v}(\vec{r},t)}{\partial t} &= -\frac{\vec{\nabla} \cdot \mathrm{T}}{m\,\rho(\vec{r},t)} - [\vec{v}(\vec{r},t) \cdot \vec{\nabla}]\,\vec{v}(\vec{r},t) \\ &+ \frac{\vec{F}_{int}(\vec{r},t)}{m\,\rho(\vec{r},t)} - \frac{\vec{\nabla} V_{ext}(\vec{r},t)}{m} \end{aligned} . \tag{29}$$

Here, the kinetic–energy stress tensor T, whose elements are given by

$$\mathrm{T}_{kl} = -\frac{\hbar^2}{m} \lim_{\vec{s} \to 0} \frac{\partial^2 \sigma_1(\vec{R}, \vec{s}, t)}{\partial s_k \partial s_l}, \tag{30}$$

depends on $\sigma_1(\vec{r}_1, \vec{r}_2, t)$, the amplitude of one–particle density matrix and can be calculated based on a local equilibrium assumption which is the substance of Thomas–Fermi approximation. $\vec{F}_{int}(\vec{r},t)$, on the other hand, represents the force due to fermion–fermion interaction (for spin–polarized atomic fermions the dipole–dipole interaction is a good candidate) and is defined as

$$\vec{F}_{int}(\vec{r},t) = -\int d^3r'\, \vec{\nabla}_{\vec{r}}\, V(\vec{r} - \vec{r}')\, \rho_2(\vec{r}, \vec{r}'; \vec{r}, \vec{r}', t)\ .$$

The one–particle Wigner function within the Thomas–Fermi approximation is given by

$$w(\vec{r}, \vec{p}) = \eta(\hbar^2 [6\pi^2 \rho(\vec{r})]^{2/3} - \vec{p}^{\,2})\ ,$$

where $\eta()$ is Heaviside's unit step function and hence the one–particle density matrix is calculated as

$$\rho_1(\vec{R}, \vec{s}) = \int \frac{d^3p}{(2\pi\hbar)^3} w(\vec{R}, \vec{p}) e^{i\vec{p}\vec{s}/\hbar}\ .$$

After straightforward algebra one obtains:

$$\rho_1(\vec{R}, \vec{s}) = \frac{2}{(2\pi\hbar)^2} \frac{1}{s} \left[-\frac{\hbar p_F}{s} \cos\left(\frac{p_F s}{\hbar}\right) + \frac{\hbar^2}{s^2} \sin\left(\frac{p_F s}{\hbar}\right) \right]\ .$$

The one–particle density matrix is a real function in this case and depends only on the length $s = |\vec{s}|$ of vector $\vec{s}$. In the limit $\vec{s} \to 0$ the kinetic–energy stress tensor T is getting diagonal with $(\hbar^2/m)(1/30/\pi^2)(6\pi^2\rho)^{5/3}$ term at each position. Then, assuming the case of non–interacting fermions (spin–polarized atoms at low temperature), the Eqs. ((27)) and ((29)) become a closed set of equations for the density and velocity fields:

$$\begin{aligned} &\frac{\partial \rho}{\partial t} + \vec{\nabla} \cdot (\rho \vec{v}) = 0 \\ &\frac{\partial \vec{v}}{\partial t} + (\vec{v} \cdot \vec{\nabla})\,\vec{v} + \vec{\nabla}\left(\frac{\hbar^2}{2m^2} (6\pi^2)^{3/2}\, \rho^{2/3} + \frac{V_{\mathrm{ext}}}{m} \right) = 0 \end{aligned} . \tag{31}$$

Note that the Eqs. ((27)) and ((29)) are general and could be used also for a bosonic system. For example, for the system of bosons described by the many–body wave function $\Psi(\vec{r}_1, ..., \vec{r}_N) = \varphi(\vec{r}_1) \cdot ... \cdot \varphi(\vec{r}_N)$ (as in the case of the Bose–Einstein condensate in the mean–field approximation) the one–particle density matrix is given by

$$\rho_1(\vec{R}, \vec{s}) = \varphi(\vec{R} + \frac{1}{2}\vec{s}) \varphi^*(\vec{R} - \frac{1}{2}\vec{s}).$$

Now, the kinetic–energy stress tensor possesses off–diagonal elements and leads to the so–called "quantum pressure" term in the equation of motion. Assuming contact interaction between the bosonic atoms dominates, the appropriate equations are written as

$$\begin{aligned}&\frac{\partial\rho}{\partial t}+\vec{\nabla}\cdot(\rho\vec{v})=0\\&\frac{\partial\vec{v}}{\partial t}+\vec{\nabla}\left(\frac{4\pi\hbar^2 a}{m^2}\rho+\frac{\vec{v}^2}{2}+\frac{V_{\rm ext}}{m}-\frac{\hbar^2}{2m^2}\frac{\vec{\nabla}^2\sqrt{\rho}}{\sqrt{\rho}}\right)=0\end{aligned}, \tag{32}$$

and are the hydrodynamic [113] representation of the Gross–Pitaevskii equation.

It is easy to check that for the spatially homogeneous system, the one–dimensional counterpart of Eqs. ((31)) has the following solution

$$\begin{aligned}\rho(x,t)&=\rho_0+\frac{1}{2\pi}[\phi'(x+(p_F/m)t)-\phi'(x-(p_F/m)t)]\\v(x,t)&=-\frac{\hbar}{2m}[\phi'(x+(p_F/m)t)+\phi'(x-(p_F/m)t)]\end{aligned}, \tag{33}$$

assuming the slope of the phase being imprinted is much less than the unperturbed density ($\phi' \ll \rho_0$). This assumption is equivalent to the condition $d_{\rm phase} \gg \lambda_F$ considered by us in Sec. (3.2) and the solution ((33)) coincides with expression ((23)). It also coincides with the Thomas–Fermi approximation, valid in one–dimensional space when the number of atoms is large enough (Sec. Paragraph 3.1). Again, the solution ((33)) represents two quasisolitons (a bright and a dark one) traveling in opposite directions after imprinting (at $t = 0$) the phase $\phi(x)$. The speed of quasisolitons is equal to the speed of sound. A similar solution can be found also in two– and three–dimensional case

$$\begin{aligned}\rho(t)&=\rho_0+\alpha[\phi'(x+ct)-\phi'(x-ct)]\\v_x(t)&=-\frac{\hbar}{2m}[\phi'(x+ct)+\phi'(x-ct)]\end{aligned}, \tag{34}$$

where c equals the speed of sound, $\alpha \sim \rho_0^{1/2}$ or $\alpha \sim \rho_0^{2/3}$ respectively in two– and three–dimensional space, and the phase being imprinted changes only in 'x' direction. Again, the solutions ((34)) are valid in the limit $d_{\rm phase} \gg \lambda_F$.

It is clear from Figure 17 that in the regime where $d_{\rm phase} <\sim \lambda_F$, the dynamics of fermionic system should be discussed rather in terms of soliton–like structures with dispersion leading to the fast broadening of pulses. Even at zero temperature the phase imprinting excites states with energy above Fermi level, depending on the width of the phase step $d_{\rm phase}$.The deviation of the group velocity of bright and dark wave packets from the zero–temperature sound velocity p_F/m maybe qualitatively understood by the following argument. In the spirit of the local density approximation one considers local value of the Fermi momentum determined by the local value of the density. Since the local density is lower at the center of dark quasisoliton its velocity is thus reduced. Of course, the opposite is true for the bright quasisoliton. Using Eq. ((33)) one gets local corrections to p_F of the form $\delta p_F = \mp\frac{\hbar}{2}\phi'(0)$. This correction agrees with numerical results in the order of magnitude. More precise estimation of the asymmetry of velocities requires, however, taking into account dispersion effects and systematic expansion in $\lambda_F/d_{\rm phase}$ up to higher orders.

There is an equivalent way of calculating the kinetic–energy stress tensor T ((30)), involving the one–particle Wigner function

$$\mathrm{T}_{kl}=\int\frac{p_k p_l}{m}w(\vec{r},\vec{p})\,d^3p, \tag{35}$$

which is, however, more suitable for the finite–temperature extension of the Thomas–Fermi approach. In equilibrium, the Wigner function for a uniform system is just the Fermi–Dirac distribution function $f(\varepsilon) = (\exp(\beta(\varepsilon-\mu))+1)^{-1}$ with $\varepsilon = p^2/2m$ and μ being the particle's kinetic energy and the chemical potential (constant for a homogeneous case) respectively. The Thomas–Fermi approximation assumes, as usually, that the system is locally uniform and the appropriate equations (in one–dimensional form) are written as

$$\begin{aligned} &\frac{\partial \rho}{\partial t} + \frac{\partial}{\partial x}(\rho v) = 0 \\ &\frac{\partial v}{\partial t} + v\frac{\partial v}{\partial x} + \frac{1}{m\rho}\frac{\partial}{\partial x}\frac{1}{2\pi\hbar}\int\limits_{-\infty}^{\infty}\frac{p^2/m\,dp}{\exp(\beta(\frac{p^2}{2m}-\mu))+1} = 0 \end{aligned} \cdot \tag{36}$$

Here, the chemical potential is position–dependent and is calculated from the relation

$$\rho = \frac{1}{2\pi\hbar}\int\limits_{-\infty}^{\infty}\frac{dp}{\exp(\beta(\frac{p^2}{2m}-\mu))+1}. \tag{37}$$

We consider now the case when the temperature is finite but the gas is still strongly degenerate, i.e. $T \ll T_F$. By using the Sommerfeld expansion and keeping only the first term one can easily find the expression $\mu = (2\pi\hbar)^2/(8m)\,\rho^2$. It turns out that in the regime where the imprinted phase changes slowly in comparison with unperturbed density, the finite–temperature time–dependent Thomas–Fermi model defined by the Eqs. ((36)) and ((37)) has the following solution

$$\begin{aligned} \rho &= \rho_0 + \int\limits_0^{\infty}\frac{d\varepsilon}{2\pi}\left(-\frac{\partial f}{\partial \varepsilon}\right)[\phi'(x+\sqrt{\frac{2\varepsilon}{m}}t) - \phi'(x-\sqrt{\frac{2\varepsilon}{m}}t)] \\ v &= -\frac{\hbar}{2m}\int\limits_0^{\infty}d\varepsilon\left(-\frac{\partial f}{\partial \varepsilon}\right)[\phi'(x+\sqrt{\frac{2\varepsilon}{m}}t) + \phi'(x-\sqrt{\frac{2\varepsilon}{m}}t)] \end{aligned} \tag{38}$$

For the temperature $T = 0$ one has $(-\partial f/\partial\varepsilon) = \delta(\varepsilon - \varepsilon_F)$ and the solution ((38)) reduces to the one found previously ((23), (33)). To verify the ansatz ((38)) we put it in the set of Eqs. ((36)) and keep only linear terms in ϕ' (according to $d_{\text{phase}} \gg \lambda_F$). The solvability condition has then the form

$$\int\limits_0^{\infty}d\varepsilon\left(-\frac{\partial f}{\partial \varepsilon}\right)\left[\sqrt{\frac{2\varepsilon}{m}} - \sqrt{\frac{2\varepsilon_F}{m}}\right] \times \left[\phi''\left(x+\sqrt{\frac{2\varepsilon}{m}}t\right) \pm \phi''\left(x-\sqrt{\frac{2\varepsilon}{m}}t\right)\right] = 0$$

and is true for low temperatures $T \ll T_F$ since then the derivative of the Fermi–Dirac distribution function strongly peaks at $\varepsilon = \varepsilon_F$, whereas the rest of the integrand is very small. The solution ((38)) is identical with ((24)). Unfortunately, this approach leads to the false soliton velocities in 2D and 3D, and cannot be used there [112]. It works however in quasi-1D case, i.e. in strongly elongated traps.

N	$\frac{v_b}{c}$	$\frac{v_d}{c}$
500	-1.061	+0.937
1000	-1.038	+0.965
5000	-1.010	+0.993
8000	-1.006	+0.994

Table 2 Speeds of dark and bright quasisolitons (in units of speed of sound) generated in a one–dimensional homogeneous Fermi gas of various number of atoms after imprinting a single phase step of π and the width of $2.5\,\lambda_F$

3.4.1 Numerical results

We have solved numerically the set of Eqs. ((31)). To this end, we applied the inverse Madelung transformation [114] to Eqs. ((31)) and used the Split-Operator technique. Imaginary–time propagation method was chosen to generate the ground state of a nonuniform (trapped) Fermi gas. Real–time propagation, on the other hand, allows to investigate the phase imprinting and developing instabilities after that.
First, by imprinting the phase on a one–dimensional uniform system we again investigate the regime where $d_{\mathrm{phase}} \gg \lambda_F$, however, this time by increasing the number of atoms while keeping the same the width of the phase step. Of course, larger number of atoms means smaller Fermi length. Increasing the number of atoms is easily attainable within Thomas–Fermi approach as opposed to the direct solution of the many–body Schrödinger equation. Results regarding the speeds of bright and dark quasisolitons are presented in Table 2. It is clear that reaching the above mentioned regime forces both quasisolitons to move with the same velocity equal to the speed of sound, as predicted by our theoretical analysis of Paragraph 3.2.

4 Generating Dipole condensate

In recent years considerable interest has been devoted to cold gases of the particles possessing dipole moment. If such dipole moment is sufficiently large, the resulting dipole-dipole forces may influence, or even completely change the properties of BEC in bosonic gases, the conditions for BCS transition in fermionic gases, or the phase diagram for quantum phase transitions for ultracold dipolar gases in optical lattices. In this paper we present a review of our recent results on ultracold dipolar gases. We consider here only the case of polarized dipolar gases when all dipoles are oriented in the same direction, and discuss the effects of the dipole-dipole interactions and their interplay with short range (Van der Waals) interactions. We do not consider several other important aspects of dipole-dipole interactions, e.g. the role of the dipole-dipole interactions in the spontaneous polarization of spinor condensates in optical lattices [115], or the self-bound structures in the field of a traveling wave [116]. As dipolar interactions can be quite strong (relative to the typical low-energy collisions characterized by the s-wave scattering length), the dipolar particles are considered as promising candidates for the implementation of fast and robust quantum-computing schemes [117, 118].

Lets consider a system of N bosonic particles possessing a dipole moment, and confined in a harmonic trap of cylindrical symmetry. We constraint our analysis to the case in which all dipoles are assumed to be oriented along the symmetry axis of the trap. Additionally, we assume that the particles interact via dipole-dipole forces, and that these forces either play a dominant role, or at least compete with the short-range forces.

Why are dipolar gases interesting? The answer is simple: because they are dipolar. The dipole-dipole interaction potential between two dipolar particles with parallel dipoles is given by

$$V_d(\mathbf{R}) = (d^2/R^3)(1 - 3\cos^2\theta),$$

where d characterizes the dipole moment, $\mathbf{R}$ is the vector between the dipoles ($R = |\mathbf{R}|$ being its length), and θ the angle between $\mathbf{R}$ and the dipole orientation (Fig. 1). The potential $V_d(\mathbf{R})$ has two important properties: it is anisotropic, and is of long-range character.

At low temperatures one expects the dipolar Bose gases to condense. One expects also that the condensate properties will dramatically depend on the geometry of the trap. In cigar-shape traps along the dipole direction the interactions will be mainly attractive, and the condensate will be unstable, similar to the case of a gas with attractive short-range interactions (negative s-wave scattering length) [18]. Conversely, in pancake traps the interactions will be mainly repulsive, and the gas might become stable. Therefore, the dipolar gases offer the unprecedented possibility of modifying the atom-atom interactions by turning an “easy knob”, namely the trap geometry, which is relatively easy to control and modify experimentally.

Several groups have recently studied the physics of ultracold dipolar bosonic gases. L. You and his collaborators [45, 46] have considered the question of the validity of the mean-field approach in this case. This is a non trivial question, since contrary to the case of short-range potentials, where the s-wave scattering always becomes dominant at very low temperatures, the scattering amplitude for dipole-dipole interactions has non vanishing contributions of all partial waves at low energies. Moreover, the interplay play between the dipole interactions and the short range forces might lead to shape resonances in the atom-atom scattering. Close to such resonances the effective scattering length diverges, and the mean field approach cannot be used. Away from shape resonances, however, the Gross-Pitaevskii (GP) equation, including the non-local dipole-dipole interactions, provides a good description of the condensate. Both L. You and his co-workers [45], Góral *et al.* [47] and Mackie *et al.* [119] have investigated the properties of the ground state of these systems, and the interplay between dipolar forces and the short-range interactions. In [4] authors concentrated on the case of dominant dipole-dipole interactions.

In this chapter we will concentrate on the problem of creation of BEC interacting via dipole forces. One of the possible physical realizations of a gas of dipolar particles is provided by electrically polarized gases of polar molecules. These molecules can have a large permanent electric dipole. The creation of cold clouds of polar molecules has been recently demonstrated in experiments with buffer-gas cooling [69, 120], as well as in experiments based on deceleration and cooling of polar molecules by time-dependent electric fields [121, 122, 123]. The molecular dipole moments typically range from 0.1 D (1 D= 10^{-18}charge SGS × cm) to 1 D. For bosonic molecules that should be sufficient for achieving BEC at relatively low density of the gas. For example, the dipole moment of the fermionic deuterated ammonia molecule ^{15}ND$_3$ is $d = 1.5$ D, which corresponds to an effective scattering length of $a_{\mathrm{d}} = -1450$ Å. This is even larger than the scattering length for the inter-component interaction in the widely discussed case of fermionic ^{6}Li. On the other hand, for the fermionic molecule ^{14}N^{16}O with dipole moment $d = 0.16$ D, the corresponding scattering length $a_{\mathrm{d}} = -24$ Å.

Another possibility is to use magnetic atomic dipoles [124, 125, 126, 127, 128]. Chromium atoms have a magnetic moment $\mu = 6\mu_B$, which is equivalent to an electric dipole moment of $d^* = 6 \cdot 10^{-2}$ D, and an effective scattering length $a_{\mathrm{d}} = -5$ Å. This is too small and is unlikely to result in any interesting fermionic effects, such as BCS pairing, however, this could be enough to observe the influence of dipole-dipole interactions on the elementary excitations of Chromium BEC, provided the (still unknown) s-wave scattering length is not anomalously large, and it takes a value in the range of few tens of Å.

Permanent electric dipole moments can also be created by applying a high dc electric field to an atom. This possibility was discussed in Ref. [129], and here we only mention that in order to induce the dipole moment of the order of 0.1 D (the corresponding scattering length $a_d \sim -10 \div 100$ Å) one needs an electric field of the order of 10^6 V/cm. Nevertheless, the influence of dipole forces on elementary excitation spectrum of a dipolar BEC might be in this case also perhaps observable using not as high electric fields (see also [44]).

In the next section we:

- propose the possibility of inducing a time averaged electric dipole moment of an atom by a stroboscopic laser coupling of the ground atomic state to a Rydberg state in a moderate dc electric field,
- than we analyze this method,
- to finally prove its uselessness.

In the section "Dynamically induced dipole" we will discuss the method of creation of dipole BEC using dynamical Stark effect.

4.1 Stroboscopic method

4.1.1 Method

Stroboscopic method of generating dipole proposed in [4, 44] and [5] was based on the observation that highly excited Rydberg states of atoms posses the dipolar moment,

$$d_n \sim e a_{\mathrm{B}} n^2,$$

where e is electron charge, a_B Bohr radius and n is a principal quantum number [130].
We proposed the setup, in which the stroboscopic pulses excites atoms in BEC to the Rydberg states. The duration of each pulse is T_p, and the separation between pulses is T_sep. The area of each pulse is a multiple of 2π. We assume that we tune the frequency of the laser such, that it does not couple the selected lowest sublevel to other Rydberg states.
In this case the atoms posses an average dipolar moment:

$$d_\mathrm{eff} = ea_\mathrm{B} n^2 T_p/T_\mathrm{sep} \times p,$$

where $0 < p < 1$ is a number between 0 and 1 describing the probability of finding an atom during the pulse in an excited state. For Gauss shaped pulses p is typically ≈ 0.3.

4.1.2 Analysis

The excited Rydberg states are not stable, i.e. after some time they decay into the ground state via spontaneous emission. This precesses will lead to losses and heating. The life time of the atom in the Rydberg state n is proportional to [130]:

$$T_\mathrm{loss} = T_0 n^3, \tag{39}$$

where, for instance, T_0 for Lithium is 5ns.
In order to induce the effective dipolar moment d_eff we need to make the duration of pulse equal to:

$$T_p = \frac{T_{sep}}{p}\frac{d_\mathrm{eff}}{d_\mathrm{R}},$$

where d_R is a dipole of the chosen Rydberg state. Let us say that our experiment will last for time T. During this time we will make $N_p = T/T_{sep}$ pulses. In order to prevent losses due to the spontaneous emission we have to assure that time atoms spend in excited state $N_p T_p$ is small compare to T_loss

$$\frac{d_\mathrm{eff}}{d_\mathrm{R}}\frac{T_{sep}N_p}{p} < T_0 n^3. \tag{40}$$

In our further analyses we assume that the time atoms spend in the excited state is ϵ times time T_loss i.e.

$$T_0 n^3 \epsilon = \frac{d_\mathrm{eff}}{d_\mathrm{R}}\frac{T}{p}.$$

We need to keep ϵ small because losses are proportional to exponent of epsilon.
Unfortunately it is not the only one condition we have to take into account. There is other fundamental source of losses. We can describe our system using the following set of two coupled Gross-Pitayevsky equations:

$$\begin{aligned}
i\hbar\frac{\partial\Psi(\vec{r},t)}{\partial t} &= \left(\frac{p^2}{2m} + V_{trap}(\vec{r}) + g_{11} \mid \Psi(\vec{r},t) \mid^2 + g_{12} \mid \Psi_R(\vec{r},t) \mid^2\right)\Psi(\vec{r},t) + \hbar\Omega(t)\Psi_R(\vec{r},t) \\
i\hbar\frac{\partial\Psi_R(\vec{r},t)}{\partial t} &= \left(\frac{p^2}{2m} + V_{trap}(\vec{r}) + g_{22} \mid \Psi_R(\vec{r},t) \mid^2 + g_{21} \mid \Psi(\vec{r},t) \mid^2\right. \\
&\left. +\sigma\int d^3r' V_{dd}(\vec{r}-\vec{r}')|\Psi_R(\vec{r},t)|^2\right)\Psi_R(\vec{r},t) + \hbar\Omega(t)\Psi(\vec{r},t),
\end{aligned} \tag{41}$$

where $\Omega(t)$ is Rabbi frequency of pulse, $V_{trap} = m\omega^2 r^2/2$ is a trapping potential, and $\sigma = d_\mathrm{R}^2 N/(4\pi\epsilon_0)$ is a constant characterizing a mean field dipole-dipole interaction.
If the T_p is very small in comparison to the trap time scale we can than make a rough approximation and consider these equations without the trapping and kinetic terms. We cannot really solve these

equation, but we can see that if we assume that $\Psi(r,t) = \Psi(t)$ is spatially constant, than we can rewrite these equations as:

$$\begin{aligned} \mathrm{i}\frac{\mathrm{d}\Psi(t)}{\mathrm{d}t} =& \Omega(t)\Psi_R(t); \\ \mathrm{i}\frac{\mathrm{d}\Psi_R(t)}{\mathrm{d}t} =& \Omega(t)\Psi(t) + \sigma/\hbar|\Psi_R(t)|^2\Psi(t)\int \mathrm{d}^3r' V(r'-r) \end{aligned}, \tag{42}$$

and of course, these equations have no solutions because, the RHS of the second equation depends on $\vec{r}$, while LHS not. This we can easily understand, the overall shape of condensate will change with on time scales given by the trap, and this cannot happen in the framework of the used approximation, because we have neglected the kinetic term. For a given position we can understand (42) as the dynamic equations for the two level atom with the levels coupled by the pulse $\Omega(t)$, where the Ψ_R state is interacting with all other atoms. The energy shift is proportional to σ. Due to this shift, the 2π pulse is losing its meaning, and it is impossible to prepare a pulse which will coherently move all the atoms to the excited state and back. Atoms, which will remain in the excited state are going to be lost, due to the spontaneous emission. In order to minimize the losses of this kind one has to keep the ratio of nonlinear dipole-dipole energy to the Rabi frequency small:

$$\frac{d_{\mathrm{R}}^2 N}{4\pi\epsilon_0 a_{\mathrm{HO}}^3} \ll \hbar\Omega, \tag{43}$$

where $a_{\mathrm{HO}} = \sqrt{\hbar/m\omega}$ is a harmonic oscillator characteristic length. For a square pulse $\Omega = 2\pi/T_p$. In this case we do not have a simple exponential law for losses, but we can find using numerics the dependence of losses, after a single pulse, as a function of the ratio R of nonlinear energy and Rabi frequencyFigure 25.

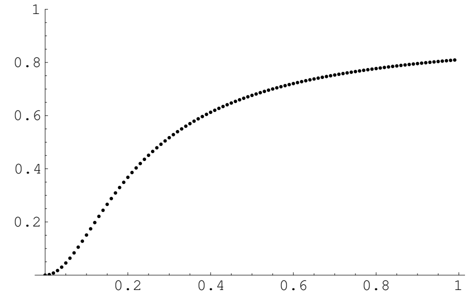

Figure 25:
Dependence of losses after the single pulse on the ratio of nonlinear energy to Rabi frequency.

Now we have everything we need to conclude. Calculating d_{R} from (40) and pluging it into (43) we got:

$$\frac{d_{\mathrm{eff}}^2 T^2 T_p}{T_0^2 n^6 \epsilon^2 p^2 4\pi\epsilon_0 a_{\mathrm{HO}}^3 \hbar} \ll 1$$

Assuming that we want our experiment to:
- last for 5 trap periods $T = 5/\omega$, and
- an effective dipole to be equal to $d_{eff} = 0.1\mathrm{Deb}$,
- trap frequency $\omega = 2\pi 50\mathrm{Hz}$ and
- use Lithium with $T_0 = 5\mathrm{ns}$, we got for $p = 0.5$ and $\epsilon = 0.5$, We obtain that

$$n \gg 265,$$

which is unfortunately unrealistic for present experiments.

4.2 Dynamically induced dipole

The other method of generating dipole condensate [116, 131, 6] is the one based on the dynamical stark effect [132]. Atoms in the oscillating electrical field posses time dependent dipolar moment $d(t)$. Two such atoms interact via time dependent dipole potential [87].
In our simulations we have studied a system shown on the Figure 26. A cigar shaped condensate is illuminated with a continuos laser beem. The polarization of the laser beem is chosen to be parallel to the long axes of the condensate. This configuration prohibits superradiance [133]. In this case atoms in the condensate exhibit the dynamic Stark effect and interact via induced potential:

$$V(\vec{r},\vec{R}) = (\frac{(E\alpha(q))^2}{4\pi\epsilon_0})\cos(qz)\frac{1}{r^3}\left[(1-3\cos^2(\theta))(\cos(qr)+qr\sin(qr))-\sin^2(\theta)q^2r^2\cos(qr)\right], \tag{44}$$

where:
- θ is the angle between the interatomic axis and z-axis,
- $\alpha(q)$ is an isotropic, dynamic polarizability of the atoms at frequency cq

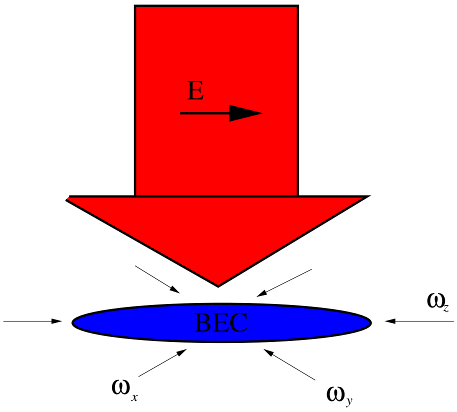

Figure 26:
Scheme of the proposed experiment. On a BEC located in a strongly elongated trap $\omega_z \gg \omega_{x,y}$ we impinge a laser beem on one of the short axes in our case y. The polarisation of the electric field, is choosen to be parallel to the long axis of the condensate, in order to avoid superradiance.

It is worth to mention that scheme proposed here has been already partially realized by Tillman Pfau in Stutgard [134]. In this experiment the incident light was very close to the resonance, hence the generated dipole is very big in this experiment of the order of 10Debyes. This destroys the condensate, but dipole-dipole interaction leads to the interesting, easily observable (during expansion) phenomena.
The experimental scheme we would like to propose is different. Strongly elongated trapped condensate is irradiated by laser beam. The wavelength is kept sufficiently far from resonance not to destroy condensate. The polarization of the beam is chosen parallel to the long axis in order to avoid super-radiance. Light is focused on a spot with a radius smaller than the long size of the condensate. It leads to the more local character of the interaction. Atoms get polarized only within this spot, and only these atoms interact. In order to describe this situation an additional factor $\exp(-(-((\vec{R}-\vec{H})/\eta)^2))$ in (44) appears, where R is the center of mass coordinate and $\vec{H}$ is the focus of the laser. We want to sweep this laser beam rapidly along the condensate in order

to induce interaction in an entire cloud. This corresponds to setting H dependent on time, and assuming sufficiently fast oscillations leads us to the average regularized potential. We write this potential in the Fourier space:

$$V(\vec{k}) = (\frac{(E\alpha(q))^2}{4\pi\epsilon_0})\left(\frac{k_z^2-q^2}{k_x^2+(k_y+q)^2+k_z^2-q^2+i/\eta}+\frac{k_z^2-q^2}{k_x^2+(k_y-q)^2+k_z^2+q^2+i/\eta}\right)$$

The regularization factor i/η comes from the finite range of the interaction caused by the finite size of the laser spot.

4.3 Results

For Rubidium the dynamic polarizability α is well described by the expression:

$$\alpha = 6\pi\epsilon_0 c^3 \frac{\Gamma/\omega_0^2}{\omega_0^2-\omega^2-\mathrm{i}(\omega^3/\omega_0^2)\Gamma},$$

where ω_0 corresponds to the center of the D doublet where $\lambda_0 = 787.5$nm, and $\Gamma = 2\pi 5.9$MHz. This formula is valid for $\lambda_0 \approx 1\mu$m $\sim 10\mu$m let us obtain the dependence of generated dipole in Debye d/Deb as a function of intensity $I/Watt$ expressed in Watts and frequency ω.

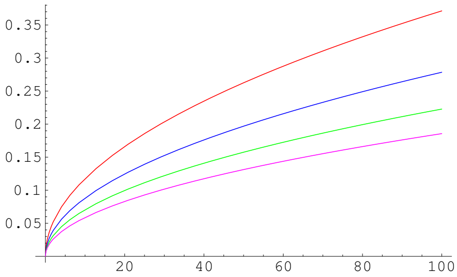

Figure 27:
Dependence of the generated dipole $d/Debyes$ on the intensity $I/Watt$ of the impinged light. Each curve corresponds to the different focus. i) Red $R = 3\lambda$, ii) Blues $R = 4\lambda$, iii) Green $R = 5\lambda$, iv) pink $R = 6\lambda$ This picture corresponds to wave length of incident light $\lambda = 1000\mu$m.

Figure 27 shows that for experimentally reachable parameters one can generate condensates with a reasonably big dipole moment. This scheme leads to the two different scenarios, characterized by geometric properties:
a) λ comparable with typical size of condensate,
b) λ smaller than that.
This two cases as it is shown on the figures Figure 28, Figure 30, exhibit completely different properties. Let us first discuss the case (a), spacial compression in the direction parallel to the dipole polarization, shown already in [131], comes from dipolar term$1/r^3$. It is the same effect, as the one described by Santos in [4]. Just that in this case the condensate is strongly deformed and decompression in ρ direction is not well visible. It is interesting to compare the shape of the density function for the ground state and for interacting one. The ground state of the BEC for $d = 0$ is well described by the paraboloid $(\mu - r^2)$, the ground state for $d \neq 0$ is well described by square root of paraboloid it is $|z|$. The condensate is getting compressed along the $Z-$axis Figure 29. This two effects may be used for the experimental detection.

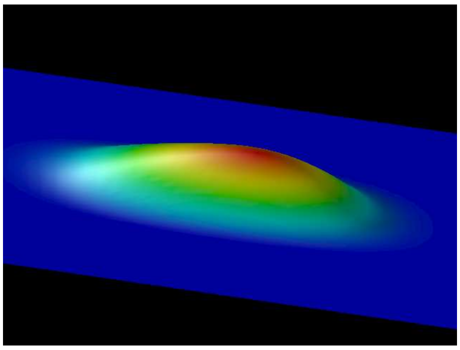

Figure 28:
Image of the density of the BEC in the rectangle $40\mu\mathrm{m}\mu\mathrm{m}$*, in plane* YZ *where the induced dipole is of the order of* $d = 0.04\mathrm{Deb}$*, the wave length of incident laser is* $\lambda = 10\mu\mathrm{m}$*,* $\omega_x = \omega_y = 300\mathrm{Hz}$ *and* $\omega_z = 60\mathrm{Hz}$*, number of atoms in condensate is equal to* 10^6*. The generated dipole moment corresponds to laser intensity equal to* $1\mathrm{KW}$

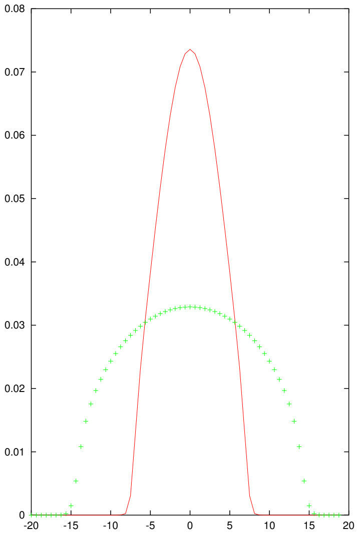

Figure 29:
Image of condensate densities in the rectangle $40\mu\mathrm{m}\mu\mathrm{m}$*,* $|\Psi(x = 0, y = 0, z)|^2$*, cut along* Z *axes. The green solid curve it is the ground state of the non-locally interacting system, while the red doted one is the characteristic inverted paraboloid, which is the ground state of the pure Gross Pitaevskii equation with contact interaction.*

Shorter wave length (in this case $\lambda = 3\mu\mathrm{m}$) brings us closer to the resonance, it means that in order to generate the same dipole one has to use lower intensities. In this case for experimentally feasible parameters $\omega_z = \omega_y = 300\mathrm{Hz}$ and $N = 10^6$ the size of the condensate is bigger than the wave length. This results in the dramatic consequences for the density profile. One can observe the hole in the middle of the trap. This are the first and shay evidences of the density modulations from [116]. This state is energetically preferable although in an obvious way it has higher kinetic energy than the smooth Tomas Fermi ground state. The $\cos(qr)$ in (44), is responsible for changing the sign of interaction on the distance $\lambda/2$ and this results in density modulation shown on Figure 30.

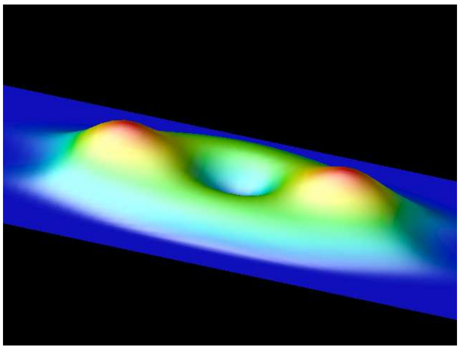

Figure 30:
Image of the BEC density, in the plane YZ where the induced dipole is of the order of $d = 0.02\mathrm{Deb}$, the wave length of incident laser is $\lambda = 3\mu\mathrm{m}$, $\omega_x = \omega_y = 300\mathrm{Hz}$ and $\omega_z = 60\mathrm{Hz}$, number of atoms in condensate is equal to 10^6. The generated dipole moment corresponds to laser intensity equal to $20\mathrm{W}$

5 Dipolar BCS

The temperature of the BCS transition in a two-component Fermi gas with the short range interaction depends drastically on the difference of concentrations of the two components, which presents a serious experimental obstacle. This problem is not relevant for polarized Fermi gas with long-range interactions, such as dipole-dipole one, and that is why there has been a considerable interest in studying the BCS transition in dipolar Fermi gases. The possibility of Cooper pairing has been predicted in [129].

Dipole-dipole interaction is not only of the long-range, but also anisotropic, i.e. partially attractive and partially repulsive. Thus for trapped gases, the nature of the interaction may be controlled be the geometry of the trap. For dipolar Bose gas in cylindrical trap the axial (radial) frequency $\omega_z(\omega_\rho)$ there exist a critical aspect ratio $\lambda = \sqrt{\omega_z/\omega_\rho}$ above which Bose-condensed gas collapses if the number of particles is too large, and below which the condensate is a subject to roton-maxon instability. The effects of a trap geometry are expected to dominate also the physics of trapped dipolar Fermi gases. So far, we have only been able to derive analytic corrections to T_c in "loose" traps, and to consider the case of an infinite "slab" ($\omega_\rho = 0$, ω_z is finite). In the latter case there exists a critical frequency above which the dipole interaction is predominantly repulsive, and the superfluid phase ceases to exists. In the chapter we present the ultimate results concerning the effect of a trap geometry on the BCS transition in trapped dipolar Fermi gases. We calculate the phase diagram in the plane $\Gamma - \lambda$, where $\Gamma \sim nd^2/\mu$ is the dipole-dipole interaction energy per particle in units of chemical potential μ. Below the critical value $\Gamma < \Gamma_c$, the BCS transition does not take place. We determine dependence of Γ_c on λ, and calculate the order parameter at the criticality. The order parameter exhibits a novel oscillatory behavior in strongly elongated cylindrical traps.

We consider a dipolar single-component Fermi gas in trap described by the Hamiltonian:

$$\begin{aligned}\mathcal{H} = &\int d\vec{r}\hat{\Psi}^\dagger(\vec{r})\left[-\frac{\hbar^2\nabla^2}{2m} + V_{\text{trap}}(\vec{r}) - \mu\right]\Psi\hat{(}\vec{r})\\ &+ \frac{1}{2}\int d\vec{r}d\vec{r}'\,\hat{\Psi}^\dagger(\vec{r})\hat{\Psi}^\dagger(\vec{r}')V_{\text{dip}}(\vec{r}-\vec{r}')\hat{\Psi}(\vec{r})\hat{\Psi}(\vec{r}),\end{aligned} \tag{45}$$

where m is the atoms mass, $V_{\text{trap}} = m[\omega_\rho^2(x^2+y^2)+\omega_z z^2]$ the trapping potential, μ the chemical potential, and $V_{\text{dip}} = (d^2/r^2)(1-3z^2/r^2)$. The dipoles are assume to be polarized along the z-direction, $\hat{\Psi}^\dagger(\vec{r})$ and $\hat{\Psi}(\vec{r})$ are atomic creation and annihilation operators that fulfill the canonical anticommutation relation. Our aim is to apply the BCS theory to the system described by (45), calculate the critical temperature and the superfluid order parameter $\Delta(\vec{r},\vec{r}') = V_{\text{dip}}(\vec{r}-\vec{r}')\langle\hat{\Psi}(\vec{r})\hat{\Psi}(\vec{r}')\rangle$. In particular we are interested in the critical value of the aspect ratio λ below which the BCS paring does not take place for a given strength of the dipole interaction. The BCS theory leads to the gap equation that has the form of a linear integral equation for $\Delta(\vec{r},\vec{r}')$(a function of 6 variables) with kernel that depends on 12 coordinates. Numerical solution of this equation is practically impossible without further analytical simplifications.

As it was shown in [68], the leading contribution to the BCS pairing comes from the p-wave scattering. Therefore, to simplify the calculations, we model the dipole-dipole interaction between particles of the gas by the short-range p-wave scattering (off-shell) amplitude of the form

$$\Gamma_1(\mathbf{p},\mathbf{p}',E)=p_z p'_z \widetilde{\gamma}_1(E), \tag{46}$$

where p is the incoming momentum, p' the outgoing one, and $\gamma_1(E)$ some function of the energy E. This form of the scattering amplitude implies that the scattering takes place only in the state of the relative motion with $m=0$. The function $\gamma_1(E)$ obeys the equation

$$\widetilde{\gamma}_1(E)-\widetilde{\gamma}_1(E')=\int^{\Lambda}\frac{d\mathbf{p}}{(2\pi)^3}\widetilde{\gamma}_1(E)\left\{\frac{p_z^2}{p^2-E+i0}-\frac{p_z^2}{p^2-E'+i0}\right\}\widetilde{\gamma}_1(E'), \tag{47}$$

and is assumed to be negative, $\widetilde{\gamma}_1(E)<0$, in order to guarantee the BCS pairing in the p-wave state. The cut-off parameter Λ ensures the convergence of the integral and, in fact, can be expressed in terms of the observable (on-shell: $p=p'$ and $E=p^2/m$) scattering data. As it follows from the above equation, the function $\widetilde{\gamma}_1(E)$ is inversely proportional to E, $\widetilde{\gamma}_1(E)=\gamma_1\,(2mE)^{-1}$, with some coefficient γ_1. Therefore, the on-shell amplitude is energy independent, as it should be in the case of scattering with odd angular momenta on the dipole-dipole potential (see Ref. [129]).
The coefficient γ_1 determines the value of the critical temperature of the BCS transition in the spatially homogeneous gas. In this case, the order parameter has the form $\Delta(\mathbf{p})=p_z\Delta_0$ with some constant Δ_0, and the corresponding equation for the critical temperature T_c reads

$$\frac{1}{\widetilde{\gamma}_1(\mu)}=-\int\frac{d\mathbf{p}}{(2\pi)^3}\frac{p_z^2}{2(p^2/2m-\mu)}\left[\tanh\frac{p^2/2m-\mu}{2T_c}-1\right], \tag{48}$$

where we renormalized the (unknown) bare interaction potential in terms of the scattering amplitude $\widetilde{\gamma}_1(\mu)=\gamma_1/p_F^2$ at the Fermi energy $\varepsilon_F=\mu=p_F^2/2m$ along the lines of Gorkov–Melik-Barkhudarov paper [135]. Integration over p is straightforward and results in the following equation for T_c:

$$1=\frac{1}{3}\left|\gamma_1\right|\nu_F\left[\ln\frac{2\mu}{T_c}-\frac{8}{3}-\ln\frac{\pi}{4}+C\right], \tag{49}$$

where $\nu_F=mp_F/2\pi^2$ is the density of states at the Fermi energy and $C=0.5772$ the Euler constant. After the Fourier transformation to ordinary space, the scattering amplitude (46) reads

$$\Gamma_1(\mathbf{r},\mathbf{r}',E)=\partial_z\delta(\mathbf{r})\partial_{z'}\delta(\mathbf{r}')\widetilde{\gamma}_1(E), \tag{50}$$

where $\mathbf{r}$ and $\mathbf{r}'$ have the meaning of the relative distances between the incoming and outgoing particles, respectively. Therefore, the order parameter $\Delta(\mathbf{r}_1,\mathbf{r}_2)\sim\langle\psi(\mathbf{r}_1)\psi(\mathbf{r}_2)\rangle$ has the form

$$\Delta(\mathbf{r}_1,\mathbf{r}_2)=\partial_z\delta(\mathbf{r})\Delta_0(\mathbf{R}), \tag{51}$$

where $\mathbf{r}=\mathbf{r}_1-\mathbf{r}_2$ and $\mathbf{R}=(\mathbf{r}_1+\mathbf{r}_2)/2$. With anzatz for the order parameter, the equation for the critical temperature can be written as

$$\begin{aligned}\frac{\Delta_0(\mathbf{R})}{\widetilde{\gamma}_1(\mu)}=-\int d\mathbf{R}'\Bigg[&\sum_{\mathbf{n}_1,\mathbf{n}_2}M_{\mathbf{n}_1\mathbf{n}_2}(\mathbf{R})\frac{\tanh\left(\xi(\mathbf{n}_1)/2T\right)+\tanh\left(\xi(\mathbf{n}_2)/2T\right)}{2(\xi(\mathbf{n}_1)+\xi(\mathbf{n}_2))}M_{\mathbf{n}_1\mathbf{n}_2}(\mathbf{R}')\\&-\int\frac{d\mathbf{p}}{(2\pi)^3}\int\frac{d\mathbf{q}}{(2\pi)^3}\frac{p_z^2}{2(p^2/2m-\mu)+q^2/4m}\exp(i\mathbf{q}(\mathbf{R}-\mathbf{R}'))\Bigg]\Delta_0(\mathbf{R}'),\end{aligned} \tag{52}$$

where $\mathbf{n}=(n_x,n_z,n_z)$ are the oscillatory quantum numbers,

$$\xi(\mathbf{n})=\hbar\left[\omega_z(n_z+1/2)+\omega_\rho(n_x+n_y+1)\right]-\mu,$$

and the function $M_{n_1n_2}(z)$ is defined as

$$M_{\mathbf{n}_1\mathbf{n}_2}(\mathbf{R}) = M^{(z)}_{n_{1z}n_{2z}}(z)M^{(\rho)}_{n_{1x}n_{2x}}(x)M^{(\rho)}_{n_{1y}n_{2y}}(y) \tag{53}$$

with

$$M^{(z)}_{n_1n_2}(z) = \frac{1}{2}\left[\varphi_{n_1}(z)\partial_z\varphi_{n_2}(z) - \varphi_{n_2}(z)\partial_z\varphi_{n_1}(z)\right], \quad M^{(\rho)}_{n_1n_2}(x) = \varphi_{n_1}(x)\varphi_{n_2}(y), \tag{54}$$

$\varphi_n(z)$ being the harmonic oscillator wave functions.
We will assume that the chemical potential μ is much large that the trap frequencies, $\mu \gg \omega_z, \omega_\rho$. Then, keeping in mind that the most important contribution in the BCS pairing comes from the states near the Fermi energy $\varepsilon_F = \mu$, we can use the WKB approximation for the wave functions φ_n in calculating the functions $M_{\mathbf{n}_1\mathbf{n}_2}(\mathbf{R})$. Another simplification is due to the fact the BCS order parameter $\Delta_0(\mathbf{R})$ is a smooth function on a scale of interparticle distance $n^{-1/3} \sim \hbar/p_F$, where $p_F = \sqrt{2m\mu}$ is the Fermi momentum in the center of the trap in the Thomas-Fermi approximation. This corresponds to a simple physical picture that the pairing correlations take place only between close in energy states. Therefore, one can neglect $q^2/4m$ in the denominator of the second term in (52) as well as rapidly oscillating contributions in the functions $M_{\mathbf{n}_1\mathbf{n}_2}(\mathbf{R})$. Under these assumptions, it is straightforward to see that

$$M^{(z)}_{n_1n_2}(z) \equiv M^{(z)}_{Nn}(z) \approx (-1)^n \frac{m\omega_z}{\pi}\sqrt{1-(z/l_{zN})^2}\,\mathrm{U}_{n-1}(z/l_{zN}) \tag{55}$$

and

$$M^{(\rho)}_{n_1n_2}(x) \equiv M^{(\rho)}_{Nn}(x) \approx (-1)^n \frac{1}{\pi l_{\rho N}}\frac{1}{\sqrt{1-(x/l_{\rho N})^2}}\mathrm{T}_n(x/l_{\rho N}), \tag{56}$$

where $n \equiv |n_1 - n_2| \ll N \equiv (n_1+n_2)/2$, $l_{iN} = \sqrt{2N\hbar/n\omega_i} = l_{0i}\sqrt{2N}$, $\mathrm{U}_n(z) = \sin((n+1)\arccos z)/\sin(\arccos z)$ and $\mathrm{T}_n(x) = \cos(n\arccos x)$ are the Tchebyshev polynomials. The functions $M^{(z)}_{n_1n_2}(z)$ and $M^{(\rho)}_{n_1n_2}(x)$ fulfill the following conditions

$$\begin{aligned}
\sum_{n\geq 1} M^{(z)}_{Nn}(z)M^{(z)}_{Nn}(z') &= \frac{(n\omega_z)^2}{2\pi}\sqrt{l^2_{zN}-z^2}\,\delta(z-z'),\\
\sum_{n\geq 0} \delta_n M^{(\rho)}_{Nn}(x)M^{(\rho)}_{Nn}(x') &= \frac{1}{\pi}\frac{1}{\sqrt{l^2_{\rho N}-x^2}}\delta(x-x'),
\end{aligned} \tag{57}$$

with $\delta_0 = 1$ and $\delta_{n>0} = 2$, that result from the completeness of the Tchebyshev polynomials.
It is convenient to rewrite (52) in the following way

$$\begin{aligned}
-\frac{\Delta_0(\mathbf{R})}{\widetilde{\gamma}_1(\mu)} \approx \int d\mathbf{R}' \Bigg[\sum_{\mathbf{n}_1,\mathbf{n}_2} M_{\mathbf{n}_1\mathbf{n}_2}(\mathbf{R})\Bigg\{&\frac{\tanh\left(\xi(\mathbf{n}_1)/2T\right) + \tanh\left(\xi(\mathbf{n}_2)/2T\right)}{2(\xi(\mathbf{n}_1)+\xi(\mathbf{n}_2))}\\
&-\frac{\tanh((\xi(\mathbf{n}_1)+\xi(\mathbf{n}_2))4T)}{\xi(\mathbf{n}_1)+\xi(\mathbf{n}_2)}\Bigg\} M_{\mathbf{n}_1\mathbf{n}_2}(\mathbf{R}')\\
+\sum_{\mathbf{n}_1,\mathbf{n}_2} M_{\mathbf{n}_1\mathbf{n}_2}(\mathbf{R})&\left\{\frac{\tanh((\xi(\mathbf{n}_1)+\xi(\mathbf{n}_2))4T)}{2(\xi(\mathbf{n}_1)+\xi(\mathbf{n}_2))} - \frac{1}{\xi(\mathbf{n}_1)+\xi(\mathbf{n}_2)}\right\} M_{\mathbf{n}_1\mathbf{n}_2}(\mathbf{R}')\\
\times\sum_{\mathbf{n}_1,\mathbf{n}_2} M_{\mathbf{n}_1\mathbf{n}_2}(\mathbf{R})&\frac{1}{\xi(\mathbf{n}_1)+\xi(\mathbf{n}_2)} M_{\mathbf{n}_1\mathbf{n}_2}(\mathbf{R}')\\
-\int \frac{d\mathbf{p}}{(2\pi)^3}\int &\frac{d\mathbf{q}}{(2\pi)^3}\frac{p_z^2}{2(p^2/2m-\mu)}\exp(i\mathbf{q}(\mathbf{R}-\mathbf{R}'))\Bigg]\Delta_0(\mathbf{R}')\\
= \int d\mathbf{R}' &\left[K_1(\mathbf{R},\mathbf{R}') + K_2(\mathbf{R},\mathbf{R}') + K_3(\mathbf{R},\mathbf{R}')\right]\Delta_0(\mathbf{R}').
\end{aligned} \tag{58}$$

The advantage of thes decomposition is that that the sum $\xi(\mathbf{n}_1)+\xi(\mathbf{n}_2)$ does not depend on $n_1 - n_2$ and, therefore, the summation over n in kernels K_2 and K_3 can easily be performed with the help of formulae (57). On the other hand, the contribution to the kernel K_1 comes only from the states near the Fermi energy.

We begin with the calculation of the discrete sum in the kernel $K_3(\mathbf{R},\mathbf{R}')$:

$$\begin{aligned}
\sum_{\mathbf{n}_1,\mathbf{n}_2} M_{\mathbf{n}_1\mathbf{n}_2}(\mathbf{R})\frac{1}{\xi(\mathbf{n}_1)+\xi(\mathbf{n}_2)}M_{\mathbf{n}_1\mathbf{n}_2}(\mathbf{R}') &= \sum_{\mathbf{N}}\sum_{\mathbf{n}_1-\mathbf{n}_2} M_{\mathbf{N}\mathbf{n}}(\mathbf{R})\frac{1}{2\xi(\mathbf{N})}M_{\mathbf{N}\mathbf{n}}(\mathbf{R}') \\
&= \delta(\mathbf{R}-\mathbf{R}') \sum_{N_i \geq R_i^2/2l_{0i}^2} \frac{1}{2\xi(\mathbf{N})}\frac{(n\omega_z)^2}{\pi^3}\sqrt{\frac{l_{zN}^2 - z^2}{(l_{\rho N}^2 - x^2)(l_{\rho N}^2 - y^2)}} \\
&= \delta(\mathbf{R}-\mathbf{R}') \sum_{N_i\geq 0} \frac{1}{2\xi(\mathbf{N})}\frac{(n\omega_z)^2}{\pi^3}\frac{l_{zN}}{l_{\rho N}l_{\rho N}} \\
&= \delta(\mathbf{R}-\mathbf{R}') \int_0 \prod_i \frac{dp_i}{\pi}\frac{p_z^2}{2(p^2/2m-\mu(\mathbf{R}))},
\end{aligned}$$

where $\mu(\mathbf{R}) = \mu - \sum_i m\omega_i^2 R_i^2/2$ and, to obtain the last result, we replaced the discrete sums with the integrals over variables $p_i = \sqrt{2m\omega_i N_i}$.Finally, for the kernel $K_3(\mathbf{R},\mathbf{R}')$ we have

$$K_3(\mathbf{R},\mathbf{R}') \approx \int \frac{d\mathbf{p}}{(2\pi)^3}\left[\frac{p_z^2}{2(p^2/2m-\mu(\mathbf{R}))} - \frac{p_z^2}{2(p^2/2m-\mu)}\right]\delta(\mathbf{R}-\mathbf{R}'). \qquad (59)$$

This expression shows (see (47)) that the only result of the kernel K_3 is the replacement $\mu \to \mu(\mathbf{R})$ in the scattering amplitude $\tilde{\gamma}_1(\mu)$ in the left-hand-side of the gap (58).

The kernels K_1 and K_2 we calculate in the limit of small temperatures $T \ll \omega_i$ suitable for finding the critical aspect ratio. Indeed, when the aspect ratio approaches its critical value, the critical temperature of the BCS transition tends to zero. In this limit, the summation over $\xi(\mathbf{N}) = (\xi(\mathbf{n}_1)+\xi(\mathbf{n}_2))/2$ in the kernel K_2 is within the limits $-\mu \leq \xi(\mathbf{N}) \leq -\omega_z/2$, where $-\omega_z/2$ appears as an upper limit for the summation due to the fact that the function $M_{n_1n_2}^{(z)}$ is nonzero only when $|n_{1z} - n_{2z}| \geq 1$. The calculations are similar to those of the Kernel K_1 and give

$$K_2(\mathbf{R},\mathbf{R}') \approx \frac{1}{3}p_F^2(\mathbf{R})\nu_F(\mathbf{R})\left\{\ln\frac{2\mu(\mathbf{R})}{\omega_z} - \frac{2}{3}(4-2\ln 2)\right\}\delta(\mathbf{R}-\mathbf{R}'), \qquad (60)$$

where $p_F(\mathbf{R}) = \sqrt{2m\mu(\mathbf{R})}$ is the local Fermi momentum in the Thomas-Fermi approximation.

In the considered limt $T \ll \omega_i$, the expression under summation in the kernel K_1 equals $-2\mathrm{sign}(\xi(\mathbf{N}))$ when $\omega_z/2 \leq |\xi(\mathbf{N})| \leq \varepsilon(\mathbf{n})/2$, where, as before, $n_i = |n_{1i} - n_{2i}|$ and $\varepsilon(\mathbf{n}) = \hbar\sum_i \omega_i n_1$, and zero otherwise. Therefore, the kernel $K_1(\mathbf{R},\mathbf{R}')$ can be written as

$$\begin{aligned}
K_1(\mathbf{R},\mathbf{R}') &= -\sum_{n_z>0;n_x,n_y\geq 0}\delta_{n_x}\delta_{n_y}\sum_{\omega_z/2\leq\xi(\mathbf{N})\leq\varepsilon(\mathbf{n})/2}\frac{1}{\xi(\mathbf{N})}M_{\mathbf{N}\mathbf{n}}(\mathbf{R})M_{\mathbf{N}\mathbf{n}}(\mathbf{R}') \\
&= -\sum_{n_z>0;n_x,n_y\geq 0}\delta_{n_x}\delta_{n_y}\int_{\omega_z/2}^{\varepsilon(\mathbf{n})/2}\frac{d\xi}{\xi}\sum_{\mathbf{N}}\delta(\xi-\xi(\mathbf{N}))M_{\mathbf{N}\mathbf{n}}(\mathbf{R})M_{\mathbf{N}\mathbf{n}}(\mathbf{R}').
\end{aligned}$$

In a generic case, the function $f(\xi) = \sum_{\mathbf{N}}\delta(\xi-\xi(\mathbf{N}))M_{\mathbf{N}\mathbf{n}}(\mathbf{R})M_{\mathbf{N}\mathbf{n}}(\mathbf{R}')$ is a smooth function of $\mathbf{N}$ and, keeping in mind that only $\varepsilon(\mathbf{n}) \ll \mu$ contributes, therefore, can be taken at $\xi = 0$. We now replace the summation over N_i with the integration over $\alpha = \omega_\rho N_x/\mu$, $\beta = \omega_\rho N_y/\mu$, and $\zeta = \omega_z N_z/\mu$. This results in

$$\begin{aligned} K_1(\mathbf{R},\mathbf{R}') &\approx -\sum_{n_z>0;n_x,n_y\geq 0} \delta_{n_x}\delta_{n_y} \ln\frac{\varepsilon(\mathbf{n})}{\omega_z} \sum_{\mathbf{N}} \delta(\xi(\mathbf{N})) M_{\mathbf{Nn}}(\mathbf{R}) M_{\mathbf{Nn}}(\mathbf{R}') \\ &\approx -\sum_{n_z>0;n_x,n_y\geq 0} \delta_{n_x}\delta_{n_y} \frac{\mu^2}{\omega_\rho^2\omega_z} \ln\frac{\varepsilon(\mathbf{n})}{\omega_z} \int_0^1 d\alpha d\beta d\zeta \delta(1-\alpha-\beta-\zeta) M_{\mathbf{Nn}}(\mathbf{R}) M_{\mathbf{Nn}}(\mathbf{R}'), \end{aligned} \tag{61}$$

where now $N_x = \alpha\mu/\omega_\rho$, $N_y = \beta\mu/\omega_\rho$, and $N_z = \zeta\mu/\omega_z$.
If we write the order parameter in the form $\Delta_0(\mathbf{R}) = \Delta_0(zR_{TF}^{(z)}, xR_{TF}^{(\rho)}, yR_{TF}^{(\rho)})$, where $R_{TF}^{(i)}$ is the Thomas-Fermi radius of the gas cloud in the i-direction and $|x|, |y|, |z| \leq 1$, and combine together (58), (61), (60), and (59), then the gap equation in the dimensional variables $\mathbf{r} = (x, y, z)$ reads

$$\begin{aligned} \frac{3}{\Gamma}(1-r^2)\Delta_0(\mathbf{r}) = (1-r^2)^{3/2} &\left\{ \ln\frac{2\mu(\mathbf{r})}{\omega_z} - \frac{2}{3}(4 - 2\ln 2) \right\} \Delta_0(\mathbf{r}) \\ &- \frac{3\pi^2}{2} \int d\mathbf{r}' K(\mathbf{r},\mathbf{r}') \Delta_0(\mathbf{r}'), \end{aligned} \tag{62}$$

where $\Gamma = |\gamma_1| \nu_F$ and

$$\begin{aligned} K(\mathbf{r},\mathbf{r}') = &\sum_{n_z>0;n_x,n_y\geq 0} \delta_{n_x}\delta_{n_y} \ln[n_z + \frac{\omega_\rho}{\omega_z}(n_x+n_y)] \\ &* \int_{\max(z^2,z'^2)}^1 d\zeta \int_{\max(x^2,x'^2)}^1 d\alpha \int_{\max(y^2,y'^2)}^1 d\beta \; \delta(1-\zeta-\alpha-\beta) \\ &* \frac{4}{\pi^2} \frac{\sqrt{(\zeta-z^2)(\zeta-z'^2)}}{\zeta} \mathrm{U}_{n_z-1}(z/\sqrt{\zeta}) \mathrm{U}_{n_z-1}(z'/\sqrt{\zeta}) \\ &* \frac{4}{\pi^2} \frac{1}{\sqrt{(\alpha-x^2)(\alpha-x'^2)}} \mathrm{T}_{n_x}(x/\sqrt{\alpha}) \mathrm{T}_{n_x}(x'/\sqrt{\alpha}) \\ &* \frac{4}{\pi^2} \frac{1}{\sqrt{(\beta-y^2)(\beta-y'^2)}} \mathrm{T}_{n_y}(y/\sqrt{\beta}) \mathrm{T}_{n_y}(y'/\sqrt{\beta}). \end{aligned} \tag{63}$$

Before describing the numerical procedure of solving the above equation, we present the analysis of the behavior of the solution near the edge of the gas sample $r \to 1$. In this region $\max(x^2, x'^2) = x^2$, etc. and it is convenient to introduce new variables in the integral for $K(\mathbf{r},\mathbf{r}')$, $a = \alpha - x^2$, $b = \beta - y^2$ and $c = \zeta - z^2$. Then the delta function in (63) reads as $\delta(1 - r^2 - a - b - c)$ and therefore, only small $a, b, c \leq 1 - r^2 \to 0$ contribute to the integral. This allow as to write the last term in (62) in the form

$$\begin{aligned} &-\frac{3\pi^2}{2} \int R_{TF}^{(z)} R_{TF}^{(\rho)2} d\mathbf{r}' K(\mathbf{r},\mathbf{r}') \Delta_0(\mathbf{r}') \\ &\approx -(1-r^2)^{3/2} \frac{256}{\pi^3} \sum_{n_z>0;n_x,n_y\geq 0} \delta_{n_x}\delta_{n_y} \ln[n_z + \frac{\omega_\rho}{\omega_z}(n_x+n_y)] \mathrm{U}_{n_z-1}(1) \mathrm{T}_{n_x}(1) \mathrm{T}_{n_y}(1) \\ &* \int d\mathbf{r}' \frac{\mathrm{U}_{n_z-1}(z') \mathrm{T}_{n_x}(x') \mathrm{T}_{n_y}(y')}{\sqrt{(1-x'^2)(1-y'^2)(1-z'^2)}} \Delta_0(xx', yy', zz'), \end{aligned} \tag{64}$$

and, as it can be easily seen, this term determines the asymptotic of $\Delta_0(\mathbf{r}) \sim (1-r^2)^{3/2}$ for $r \to 1$. This result can be used as a test for numerically found solutions of (62).
Our numerical procedure of solving (62) is based on the observation that the linear equation of the form

$$\Delta_0(\mathbf{R}) = \int d\mathbf{R}' K(\mathbf{R},\mathbf{R}') \Delta_0(\mathbf{R}')$$

with a symmetric kernel $K(\mathbf{R},\mathbf{R}')$ can be viewed as the equation on the extremum of the quadratic functional

$$F[\Delta_0]=\frac{1}{2}\int d\mathbf{R}d\mathbf{R}'\Delta_0(\mathbf{R})[\delta(\mathbf{R}-\mathbf{R}')-K(\mathbf{R},\mathbf{R}')]\Delta_0(\mathbf{R}').$$

Another simplification can be achieved by using the following ansatz

$$\Delta_0(\mathbf{R})\to\Delta_0(\mathbf{r})=\Delta_0[(zR_{TF}^{(z)})^2,(x^2+y^2)(R_{TF}^{(\rho)})^2]=(1-r^2)^{3/2}\sum_{m_z,m_\rho\geq 0}c_{m_z m_\rho}\mathrm{U}_{m_z}(z^2)\mathrm{T}_{m_\rho}(x^2+y^2) \tag{65}$$

that takes into account the cylindrical symmetry of the problem. The functional F now becomes a quadratic form of the unknown coefficients $c_{m_z m_\rho}$ that have to determined from the equation on the extremum of this form. The latter problem reduces to the search for a zero eigenvalue of the matrix of the quadratic form and, therefore, has a solution only when the interaction Γ and the trap frequencies ω_i are related to each other. For a given Γ, this relation sets the critical aspect ration λ_c.
The functional $F[\Delta_0]$ in our case can be written in the form

$$\begin{aligned}F[\Delta_0]/p_F^2\nu_F R_{TF}^{(z)}R_{TF}^{(\rho)2}=&\frac{1}{2}\int d\mathbf{r}\left\{\frac{3(1-r^2)}{\Gamma}-(1-r^2)^{3/2}\left[\ln\frac{2\mu}{\omega_z}(1-r^2)-\frac{2}{3}(4-2\ln 2)\right]\right\}\Delta_0^2(\mathbf{r})\\&-\frac{3\pi^2}{2}\sum_{n_z>0;n_x,n_y\geq 0}\delta_{n_x}\delta_{n_y}\ln[n_z+\frac{\omega_\rho}{\omega_z}(n_x+n_y)]\\&\times\int_0^1 d\alpha d\beta d\zeta\ \delta(1-\alpha-\beta-\zeta)\zeta V_{\mathbf{n}}(\alpha,\beta,\zeta)^2,\end{aligned} \tag{66}$$

where

$$V_{\mathbf{n}}(\alpha,\beta,\zeta)=\int_{-1}^{1}\frac{dx}{\pi}\frac{\mathrm{T}_{n_x}(x)}{\sqrt{1-x^2}}\int_{-1}^{1}\frac{dy}{\pi}\frac{\mathrm{T}_{n_y}(y)}{\sqrt{1-y^2}}\int_{-1}^{1}\frac{dz}{\pi}\sqrt{1-z^2}\mathrm{U}_{n_z-1}(z)\Delta_0(z^2\zeta,x^2\alpha+y^2\beta) \tag{67}$$

and, during the numerical procedure, the upper limits in the summations over m_i and n_i in (65) and (66) have to be chosen during the in such a way that the solution Δ_0 does not depend on them. In the harmonic trap, the chemical potential μ and the total number of particles N are related as

$$3N=\mu^3/\omega_z\omega_\rho^2.$$

On the other hand, the parameter $\Gamma=36n(0)d^2/\pi\mu$, where $n(0)=(2m\mu)^{3/2}/6\pi^2\hbar^3$ is the gas density in the center of the trap, is the ratio of the mean interaction energy per particle $n(0)d^2$ to the chemical potential μ. Therefore, in order to study the effects of the trap geometry on the BCS pairing we have to fix the number of particles N and the parameter Γ. For a given type of particles, this corresponds to the fixing the chemical potential μ, and, hence, the product $\omega_z\omega_\rho^2$. Then $\mu/\omega_z=(3N)^{1/3}\lambda^{-4/3}$ and the aspect ratio λ remains the only free parameter, which critical value has to determined through the solution of the above problem.

5.1 Numerical results

In principle the solution of the problem can be expressed in the following way: we have to find such a set of coefficients $c_{m_z m_\rho}$, that for given Γ and aspect ratio λ the lowest eigenvalue of the matrix, which defines the functional (66), is zero. This is a symmetric matrix hence this task is relatively simple. The difficulty of this problem from the numerical point of view lies in the procedure of calculating the elements of this matrix. Each element of the matrix $M_{m_z,m_\rho,n_z,n_\rho}$ is defined as:

$$\begin{aligned}
M_{m_z,m_\rho,n_z,n_\rho} =& \frac{1}{2}\int d\mathbf{r}\left\{\frac{3(1-r^2)}{\Gamma} - (1-r^2)^{3/2}\left[\ln\frac{2\mu}{\omega_z}(1-r^2) - \frac{2}{3}(4-2\ln 2)\right]\right\} \\
& \times U_{m_z}(z^2)T_{m_\rho}(x^2+y^2)U_{n_z}(z^2)T_{n_\rho}(x^2+y^2) \\
& - \frac{3\pi^2}{2}\sum_{p_z>0;p_x,p_y\geq 0}\delta_{p_x}\delta_{p_y}\ln[p_z + \frac{\omega_\rho}{\omega_z}(p_x+p_y)] \qquad (68) \\
& \times \int_0^1 d\alpha d\beta d\zeta\ \delta(1-\alpha-\beta-\zeta)\zeta V_{\mathbf{p}}^{m_z,m_\rho}(\alpha,\beta,\zeta)^2, V_{\mathbf{p}}^{n_z,n_\rho}(\alpha,\beta,\zeta),
\end{aligned}$$

where the function V is defined as:

$$V_{\mathbf{p}}^{n_z,n_\rho}(\alpha,\beta,\zeta) = \int_{-1}^{1}\frac{dx}{\pi}\frac{\mathrm{T}_{p_x}(x)}{\sqrt{1-x^2}}\int_{-1}^{1}\frac{dy}{\pi}\frac{\mathrm{T}_{p_y}(y)}{\sqrt{1-y^2}}\int_{-1}^{1}\frac{dz}{\pi}\sqrt{1-z^2}\mathrm{U}_{p_z-1}(z)U_{p_z}(z^2)T_{p_\rho}(x^2\alpha+y^2\beta) \qquad (69)$$

These are rather complicated expressions. The matrix M is naturally divided into two parts. First of them is just the 3 dimensional integral of functions, that can be compute fast. The numerical method we choose to approach this problem was based on the Monte Carlo integration. We used, the so called, VEGAS algorithm. This algorithm was design in the following way: first it splits the space over which we integrate into some smaller parts and tries to detect possible difficulties. Than it performs the final run, but concentrates more on the so called difficult regions. These are the regions were the function oscillates faster, or has singularities. Using this method we were able to compute the first part of the matrix in the relatively short time. The used algorithm was based on the excellent implementation from (GSL) Gnu Scientific Library [136].

The second part of the problem was much more difficult. The matrix element is defined as a triple sum over the 8 dimensional integral. Simple approach based on using the same numerical method as described above failed, since it was too time consuming. Hence, we have decided to use another method. The simplest approach is to try the find a fast computable approximation to the V function, so that the integral becomes than 2 dimensional. It can be than computed very fast, so than we can perform the sum. Unfortunately, it was not possible, because the V integral depends on the indices of the sum. We were therefore approximating this function for every element of the sum, using the 2 dimensional spline method. As the result of this procedure we obtained the function $V_{\mathbf{n}}^{n_z,n_\rho}(\alpha,\beta)$ which was depended only on two variables α,β and parametrically on three indices $\mathbf{n}$. The values used to find the interpolating function were computed using the described above VEGAS algorithm. In this way the time required to compute the matrix (68) was reduced to about 72h. We have performed many sanity test, in order to check if the result of the computation did not depend on these approximations. We have checked if results did not depend on the number of shots in Monte Carlo algorithms, or on the number of points chosen for interpolation, and we find the values for which the result of computation converged.

The results of this computations are presented in the four figures. Figure 31 presents the dependence of the critical Γ on the aspect ratio. The two curves correspond to two different numbers of particles. As it can be expected for the bigger number of particles the critical aspect ratio is smaller because the effective interaction is bigger. Also for $\lambda^{-1}\to 0$ (pancake trap), since the interactions are predominantly repulsive, higher values of Γ for fixed λ are required to reach the region where BCS transition occurs at finite T, conversely, for λ^{-1} large (cigar trap) the interactions are predominantly attractive and the occurrence of the BCS transition requires much modest values of Γ.

The following three pictures Figure 32, Figure 33, Figure 34 show the order parameter and precisely its center of mass part. Amazingly the order parameter is not monotonic function of the distance from the trap center which is the case for BCS order parameter in a two component gas with short

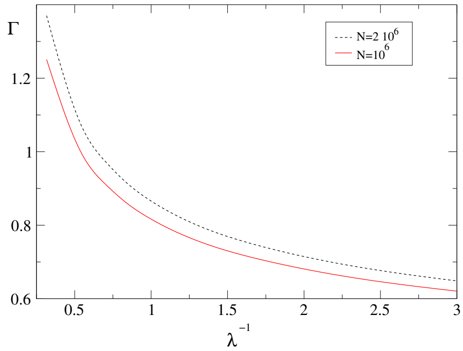

Figure 31:
Critical Γ *as a function of the aspect ratio* λ^-1 *above this curve BCS takes place at finite* T*. There are two curves each corresponding to different number of particles: the upper one corresponds to* 10^6 *particles, while the lower one to* 2×10^6.

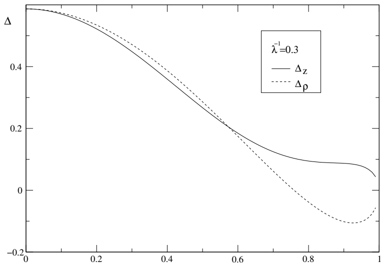

Figure 32:
Order parameter of the aspect ratio $\lambda^{-1} = 0.3$ *(corresponding to pancake geometry). The solid line shows the function* $\Delta_0(z, \rho = 0)$ *and the dashed line corresponds to* $\Delta_0(z = 0, \rho)$ *Unite distance corresponds to Tomas Fermi radious in* z *or* ρ *direction*

range interactions [137]. Here as we go towards more and more cigar shaped traps, $\Delta(z, \rho = 0)$ develops a minimum at $\rho < 1$, whereas $\Delta(z = 0, \rho)$ becomes negative in the outer parts of the cloud. This is a completely new behavior, which can have profound consequences for the spectrum of the elementary excitations. This problem however, goes beyond the scope of this Thesis.

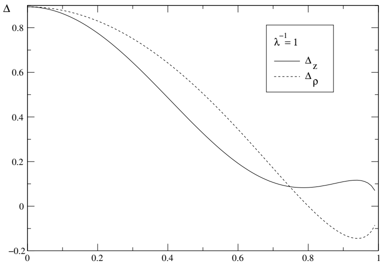

Figure 33:
Order parameter for aspect ration Same in Fig 32. but for the $\lambda^{-1} = 1$ *(corresponding to spherical geometry).*

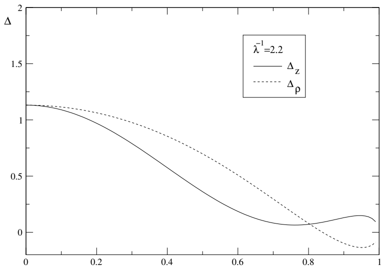

Figure 34:
Same as in Fig 32 but for the $\lambda^{-1} = 2.2$ *(corresponding to cigar shape geometry).*

6 Conclusions

In the Chapter 2 we have addressed theoretically the problem of generation of vortices by phase imprinting in trapped Bose-Einstein condensates. Phase imprinting is achieved by passing a short off-resonance laser pulse through an appropriately designed absorption plate, and impinging it on a condensate. Apart from answering the fundamental question of how the circulation and the vortex are introduced into the system, we have concentrated on practical questions concerning the controlled generation of vortices and vortex arrays, their dynamics and their detection. Although so far phase imprinting method in the version discussed in this paper has only been used to generate dark solitons in BEC, we hope that in the next future some experimental groups will apply the phase imprinting method to study the vortex generation and dynamics, and superfluidity in trapped BEC. The theory presented in this thesis should help to plan and design such experiments.

In the Chapter 3 we have studied in detail the generation of soliton–like structures in ultracold Fermi gases using the phase imprinting method. The generation of such structures is feasible in existing experimental setups. The soliton–like structures are generated because in the process of phase imprinting, in the limit in which the characteristic length of the imprint $d_{\text{phase}} \ll \lambda_F$, only a narrow band of states with momenta close to $\pm p_F$ are excited. The life time of the soliton–like structures can be quite long, even at not extremely low temperatures, allowing for observations. We have presented both numerical and analytical results explaining the mechanism of generation and evolution of the soliton–like structures, both in homogeneous quasi 1D cylinders and in quasi 1D harmonic traps.

In Chapter 4 we studied the laser-induced generation of dipole-dipole interactions in BEC. The stroboscopical excitation of Rydberg states was shown to be very difficult to realized experimentally. On the contrary, the laser-induced polarization, and subsequently induced dipole-dipole interaction, should provide a relatively simple way to study the very rich properties of dipolar ultracold gases. Although in this chapter we were mainly concentrated on Bose Einstein condensation, the developed ideas can be also applied to ultra cold fermionic gases. The dipolar ultracold fermionic gases were studied in Chapter 5. It was shown that the critical dipole strength above which BCS occurs, is a function of the trap geometry. This function has been found and unusual properties of the order parameter have been discovered.

7 Appendixes

7.1 Bibliography

[1] Ł Dobrek, M. Gajda, M. Lewenstein, K. Sengstock, G. Birkl, and W. Ertmer. Optical generation of vortices in trapped Bose-Einstein condensates. *Phys. Rev. A*, 60(5):R3381–R3384, 1999.

[2] G. Andrelczyk, M. Brewczyk, Ł Dobrek, M. Gajda, and M. Lewenstein. Optical generation of vortices in trapped Bose-Einstein condensates. *Phys. Rev. A*, 64(4), 2001.

[3] T. Karpiuk, M. Brewczyk, Ł. Dobrek, M. A. Baranov, M. Lewenstein, and K. Rzążewski. Optical generation of solitonlike pulses in a single-component gas of neutral fermionic atoms. *Phys. Rev. A*, 66(023612), 2002.

[4] L. Santos, G. V. Shlyapnikov, P. Zoller, and M. Lewenstein. Bose-Einstein condensation in trapped dipolar gases. *Phys. Rev. Lett.*, 85(9):1791–1794, 2000.

[5] Baranov M., Ł Dobrek, K. Góral, L. Santos, and M. Lewenstein. Ultracold dipolar gases - a challenge for experiments and theory. *Physica Scripta*, T102:74–81, 2002.

[6] S. Giovanazzi, G. Kurizki, I. E. Mazets, and S. Stringari. Collective excitations of a "gravitationally" self-bound Bose gas. *Europhys. Lett.*, 56(1):1–7, 2001.

[7] Satyendra Nath Bose. Planck's law and the hypothesis of light quanta. *Zeitschrift für Physik*, 26(178), 1924.

[8] A. Einstein. *Sitzungsber. Kgl. Preuss. Akad. Wiss.*, 3, 1925.

[9] A. Einstein. *Sitzungsber. Kgl. Preuss. Akad. Wiss.*, 261, 1924.

[10] Kerson Huang. *Statistical Mechanics.* John Wiley and Sons, 1987.

[11] F. London. *Nature*, 163(4148):694–696, 1949.

[12] M. H. Anderson, J. R. Ensher, M. R. Matthews, C. E. Wieman, and E. A. Cornell. Observation of Bose-Einstein condensation in a dilute atomic vapor. *Science*, 269(5221):198–201, 1995.

[13] S. Burger, K. Bongs, S. Dettmer, W. Ertmer, K. Sengstock, A. Sanpera, G. V. Shlyapnikov, and M. Lewenstein. Dark solitons in Bose-Einstein condensates. *Phys. Rev. Lett.*, 83(25):5198–5201, 2000.

[14] J. Denschlag, J. E. Simsarian, D. L. Feder, C. W. Clark, L. A. Collins, J. Cubizolles, L. Deng, E. W. Hagley, K. Helmerson, W. P. Reinhardt, S. L. Rolston, B. I. Schneider, and W. D. Phillips. Generating solitons by phase engineering of a Bose-Einstein condensate. *Science*, 287(5450):97–101, 2000.

[15] L. N. Cooper. *Phys. Rev.*, 104:1198, 1956.

[16] J. Bardeen, L. N. Cooper, and J. R. Schrieffe. Theory of Superconductivity. *Phys. Rev.*, 108(5):1957, 1175-1204.

[17] K. B. Davis, M. O. Mewes, M. R. Andrews, N. J. Vandruten, D. S. Durfee, D. M. Kurn, and W. Ketterle. Bose-Einstein condensation in a gas of sodium atoms. *Phys. Rev. Lett.*, 75(22):3969–3973, 1995.

[18] C. C. Bradley, C. A. Sackett, J. J. Tollett, and R. G. Hulet. Evidence of Bose-Einstein condensation in an atomic gas with attractive interactions. *Phys. Rev. Lett.*, 75(9):1687–1690, 1995.

[19] E. J. Mueller and G. Baym. Finite-temperature collapse of a Bose gas with attractive interactions. *Phys. Rev. A*, 62(5):art. no. 053605, 2000.

[20] Y. Kagan, A. E. Muryshev, and G. V. Shlyapnikov. Collapse and Bose-Einstein condensation in a trapped Bose gas with negative scattering length. *Phys. Rev. Lett.*, 81(5):933–937, 1998.

[21] Y. Kagan, E. L. Surkov, and G. V. Shlyapnikov. Evolution and global collapse of trapped bose condensates under variations of the scattering length. *Phys. Rev. Lett.*, 79(14):2604–2607, 1997.

[22] N. P. Proukakis, K. Burnett, and H. T. C. Stoff. Microscopic treatment of binary interactions in the nonequilibrium dynamics of partially Bose-condensed trapped gases. *Phys. Rev. A*, 57(2):1230–1247, 1998.

[23] C.A. Sackett C.C. Bradley and R.G. Hulet. Bose-einstein condensation of lithium: Observation of limited condensate number. *Phys. Rev. Lett.*, 78:985, 1997.

[24] D. Guery-Odelin and S. Stringari. Scissors mode and superfluidity of a trapped Bose-Einstein condensed gas. *Phys. Rev. Lett.*, 83(22):4452–4455, 1999.

[25] Y. Castin and . Dum. Instability and depletion of an excited bose-einstein condensates in a trap. *Phys. Rev. Lett.*, 1997:762.

[26] D. A. W. Hutchinson, K. Burnett, R. J. Dodd, S. A. Morgan, M. Rusch, E. Zaremba, N. P. Proukakis, M. Edwards, and C. W. Clark. Gapless mean-field theory of Bose-Einstein condensates. *Journal of Physics B-Atomic Molecular and Optical Physics*, 33(19):3825–3846, 2000.

[27] F. Dalfovo and S. Stringari. Shape deformations and angular-momentum transfer in trapped Bose-Einstein condensates. *Phys. Rev. A*, 63(1):art. no. 011601, 2001.

[28] P. Rosenbusch, D. S. Petrov, S. Sinha, F. Chevy, V. Bretin, Y. Castin, G. V. Shlyapnikov, and J. Dalibard. Critical rotation of a harmonically trapped Bose gas. *Phys. Rev. Lett.*, 88(25):art. no. 250403, 2002.

[29] P. O. Fedichev and G. V. Shlyapnikov. Dissipative dynamics of a vortex state in a trapped Bose-condensed gas. *Phys. Rev. A*, 60(3):R1779–R1782, 1999.

[30] A. L. Fetter and A. A. Svidzinsky. Vortices in a trapped dilute Bose-Einstein condensate. *Journal of Physics - Condensed Matter*, 13(12):R135–R194, 2001.

[31] J. E. Williams and M. J. Holland. Preparing topological states of a Bose-Einstein condensate. *Nature*, 401(6753):568–572, 1999.

[32] M. G. Moore, O. Zobay, and P. Meystre. Quantum optics of a Bose-Einstein condensate coupled to a quantized light field. *Phys. Rev. A*, 60(2):1491–1506, 1999.

[33] M. G. Moore and P. Meystre. Optical control and entanglement of atomic Schrödinger fields. *Phys. Rev. A*, 59(3):R1754–R1757, 1999.

[34] M. G. Moore and P. Meystre. Effects of atomic diffraction on the collective atomic recoil laser. *Phys. Rev. A*, 58(4):3248–3258, 1998.

[35] A. Muryshev, G. V. Shlyapnikov, W. Ertmer, K. Sengstock, and M. Lewenstein. Dynamics of dark solitons in elongated Bose-Einstein condensates. *Phys. Rev. Lett.*, 89(11):art. no. 110401, 2002.

[36] L. Khaykovich, F. Schreck, G. Ferrari, T. Bourdel, J. Cubizolles, L. D. Carr, and Y. Castinand C. Salomon. *Science*, 269:1290–1293, 2002.

[37] J. Dziarmaga, A. Smerzi, W. H. Zurek, and A. R. Bishop. Dynamics of quantum phase transition in an array of Josephson junctions. *Phys. Rev. Lett.*, 88(16):2002, art. no. 167001.

[38] F. Meier and W. Zwerger. Josephson tunneling between weakly interacting Bose-Einstein condensates. *Phys. Rev. A*, 64(3):2001, art. no. 033610.

[39] M. Y. Kagan, M. A. Baranov, Y. Kagan, and D. S. Petrov. On the possibility of a superfluid transition in a Fermi-gas of neutral particles at ultra-low temperatures. *Physica B*, 284(1):2000, 5-6.

[40] D. Hellweg, S. Dettmer, P. Ryytty, J. J. Arlt, W. Ertmer, K. Sengstock, D. S. Petrov, G. V. Shlyapnikov, H. Kreutzmann, L. Santos, and M. Lewenstein. Phase fluctuations in Bose-Einstein condensates. *APPLIED PHYSICS B-LASERS AND OPTICS*, 73(8):781–789.

[41] C. W. Gardiner and P. Zoller. Quantum kinetic theory: A quantum kinetic master equation for condensation of a weakly interacting Bose gas without a trapping potential. *Phys. Rev. A*, 55(4):2902–2921, 1997.

[42] T. L. Ho and V. B. Shenoy. Local spin-gauge symmetry of the Bose-Einstein condensates in atomic gases. *Phys. Rev. Lett.*, 77(13):2595–2599, 1996.

[43] H. Pu, W. P. Zhang, and P. Meystre. Ferromagnetism in a lattice of Bose-Einstein condensates. *Phys. Rev. Lett.*, 87(4):art. no. 140405, 2001.

[44] K. Góral and L. Santos. Ground state and elementary excitations of single and binary Bose-Einstein condensates of trapped dipolar gases. *Phys. Rev. A*, 66(2):art. no. 023613, 2002.

[45] S. Yi and L. You. Trapped atomic condensates with anisotropic interactions. *Phys. Rev. A*, 61(4):art. no. 041604, 2000.

[46] S. Yi and L. You. Trapped condensates of atoms with dipole interactions. *Phys. Rev. A*, 63(5):art. no. 053607, 2001.

[47] K. Góral, K. Rzążewski, and T. Pfau. Bose-Einstein condensation with magnetic dipole-dipole forces. *Phys. Rev. A*, 61(5):art. no. 051601, 2000.

[48] E. Zaremba, T. Nikuni, and A. Griffin. Dynamics of trapped Bose gases at finite temperatures. *Journal of Low Temperature Physics*, 116(3-4):277–345, 1999.

[49] M. Kostrun, M. Mackie, R. Cote, and J. Javanainen. Theory of coherent photoassociation of a Bose-Einstein condensate. *Phys. Rev. A*, 62(6):art. no. 063616, 2000.

[50] S. J. J. M. F. Kokkelmans, H. M. J. Vissers, and B. J. Verhaar. Formation of a Bose condensate of stable molecules via a Feshbach resonance. *Phys. Rev. A*, 63(3):art. no. 031601, 2001.

[51] G. Baym, J. P. Blaizot, and Zinn-Justin J. The transition temperature of the dilute interacting Bose gas for N internal states. *Europhys. Lett.*, 49(2):150–155, 2000.

[52] G. Baym, J. P. Blaizot, M. Holzmann, F. Laloe, and D. Vautherin. Bose-Einstein transition in a dilute interacting gas. *European Phys. Journal B*, 24(1):107–124, 2001.

[53] Z. Idziaszek, M. Gajda, P. Navez, M. Wilkens, and K. Rzążewski. Fluctuations of the weakly interacting Bose-Einstein condensate. *Phys. Rev. Lett.*, 1999(82):4376–4379, 22.

[54] P. O. Fedichev, M. W. Reynolds, U. M. Rahmanov, and G. V. Shlyapnikov. Inelastic decay processes in a gas of spin-polarized triplet helium. *Phys. Rev. A*, 53(3):1447–1453, 1996.

[55] M. Girardeau. Relationship between systems of impenetrable bosons and fermions in one dimension. *Journal of Math. Phys.*, 1(6):516–523, 1960.

[56] V. Dunjko, V. Lorent, and M. Olshanii. Bosons in cigar-shaped traps: Thomas-Fermi Tonks-Girardean regime, and in between. *Phys. Rev. Lett.*, 86(24):5413–5416, 2001.

[57] A Recati, P. O. Fedichev, W. Zwerger, and P. Zoller. *Phys. Rev. Lett.*, 90(2):atr. no. 020401, 2003.

[58] D Jaksch, Cirac J. I., P. Zoller, Rolston S. L., R. Cote, and M. D. Lukin. Fast quantum gates for neutral atoms. *Phys. Rev. Lett.*, 85(10):2208–2211, 2000.

[59] D. Jaksch, C. Bruder, J. I. Cirac, C. W. Gardiner, and P. Zoller. Cold bosonic atoms in optical lattices. *Phys. Rev. Lett.*, 81(15):3108–3111, 1998.

[60] K. Góral, L. Santos, and M. Lewenstein. Quantum phases of dipolar bosons in optical lattices. *Phys. Rev. Lett.*, 88(17):art. no. 170406, 2002.

[61] S. Rapsch, U. Schollwock, and W. Zwerger. Density matrix renormalization group for disordered bosons in one dimension. *Europhys. lett.*, 46(5):559–564, 1999.

[62] M. Greiner, O. Mandel, T. Esslinger, T. W. Hansch, and I. Bloch. *Nature*, 415(6867):39–44, 2002.

[63] B. DeMarco and D. S. Jin. Onset of Fermi degeneracy in a trapped atomic gas. *Science*, 285(5434):1703–1706, 1999.

[64] B. DeMarco, S. B. Papp, and D. S. Jin. Pauli blocking of collisions in a quantum degenerate atomic Fermi gas. *Phys. Rev. Lett.*, 86(24):5409–5412, 2001.

[65] L. Vichi and S. Stringari. Collective oscillations of an interacting trapped Fermi gas. *Phys. Rev. A*, 60(6):4734–4737, 1999.

[66] T. Busch, J. R. Anglin, J. I. Cirac, and P. Zoller. Inhibition of spontaneous emission in Fermi gases. *Europhys. Lett.*, 44(1):1–6, 1998.

[67] M. Holland, S. J. J. M. F. Kokkelmans, M. L. Chiofalo, and R. Walser. Resonance superfluidity in a quantum degenerate Fermi gas. *Phys. Rev. Lett.*, 87(12):art. no. 120406, 2001.

[68] M. A. Baranov, M. S. Marenko, V. S. Rychkov, and G. V. Shlyapnikov. Superfluid pairing in a polarized dipolar Fermi gas. *Phys. Rev. A*, 66(1):art. no. 013606, 2002.

[69] J. D. Weinstein, R. deCarvalho, T. Guillet, B. Friedrich, and J. M. Doyle. Magnetic trapping of calcium monohydride molecules at millikelvin temperatures. *Nature*, 395(6698):148–150, 1998.

[70] M. A. Baranov. Single-particle excitations and the order parameter for a trapped superfluid Fermi gas. *JETP Lett.*, 70(6):396–402, 1999.

[71] F. Zambelli and S. Stringari. Moment of inertia and quadrupole response function of a trapped superfluid. *Moment of inertia and quadrupole response function of a trapped superfluid*, 63(3):art. no. 033602, 2001.

[72] J. Ruostekoski. Optical response of a superfluid state in dilute atomic Fermi-Dirac gases. *Phys. Rev. A*, 60(3):R1775–R1778, 1999.

[73] C. Raman, Köhl M., R. Onofrio, D. S. Durfee, C. E. Kuklewicz, Z. Hadzibabic, and W. Ketterle. Evidence for a critical velocity in a Bose-Einstein condensed gas. *Phys. Rev. Lett.*, 83(13):2502–2505, 1999.

[74] R. Onofrio, C. Raman, J. M. Vogels, J. R. Abo-Shaeer, A. P. Chikkatur, and W. Ketterle. Observation of superfluid flow in a Bose-Einstein condensed gas. *Phys. Rev. Lett.*, 85(11):2228–2231, 2000.

[75] P. O. Fedichev, G. V. Shlyapnikov, and J. T. M. Walraven. Damping of low-energy excitations of a trapped Bose-Einstein condensate at finite temperatures. *Phys. Rev. Lett.*, 80(11):2269–2272, 1998.

[76] K. W. Madison, F. Chevy, W. Wohlleben, and J. Dalibard. Vortex formation in a stirred Bose-Einstein condensate. *Phys. Rev. Lett.*, 84(5):806–809, 2000.

[77] F. Chevy, K. W. Madison, and J. Dalibard. Measurement of the angular momentum of a rotating Bose-Einstein condensate. *Phys. Rev. Lett.*, 85(11):2223–2227, 2000.

[78] M. R. Matthews, B. P. Anderson, P. C. Haljan, D. S. Hall, C. E. Wieman, and E. A. Cornell. Vortices in a Bose-Einstein condensate. *Phys. Rev. Lett.*, 83(13):2498–2501, 1999.

[79] O. M. Marago, S. A. Hopkins, J. Arlt, E. Hodby, G. Hechenblaikner, and C. J. Foot. Observation of the scissors mode and evidence for superfluidity of a trapped Bose-Einstein condensed gas. *Phys. Rev. Lett.*, 84(10):2056–2059, 2000.

[80] D. Guery-Odelin and S. Stringari. Scissors mode and superfluidity of a trapped Bose-Einstein condensed gas. *Phys. Rev. Lett.*, 83(22):4452–4455, 1999.

[81] R. J. Marshall, G. H. C. New, K. Burnett, and S. Choi. Exciting, cooling, and vortex trapping in a Bose-condensed gas. *Phys. Rev. A*, 59(3):2085–2093, 1999.

[82] F. Dalfovo and S. Stringari. Bosons in anisotropic traps: Ground state and vortices. *Phys. Rev. A*, 53(4):2477–2485, 1996.

[83] D. A. Butts and D. S. Rokhsar. Predicted signatures of rotating Bose-Einstein condensates. *Nature*, 397(6717):327–329, 1999.

[84] D. L. Feder, C. W. Clark, and B. I. Schneider. Vortex stability of interacting Bose-Einstein condensates confined in anisotropic harmonic traps. *Phys. Rev. Lett.*, 82(25):4956–4959, 1999.

[85] J. E. Williams and M. J. Holland. Preparing topological states of a Bose-Einstein condensate. *Nature*, 401(6753):568–572, 1999.

[86] J. R. Abo-Shaeer, C. Raman, and W. Ketterle. Formation and decay of vortex lattices in Bose-Einstein condensates at finite temperatures. *Phys. Rev. Lett.*, 88(7):art. no. 070409, 2002.

[87] B. Jackson, J. F. McCann, and C. S. Adams. Vortex formation in dilute inhomogeneous Bose-Einstein condensates. *Phys. Rev. Lett.*, 80(18):3903–3906, 1998.

[88] B. M. Caradoc-Davies, R. J. Ballagh, and K. Burnett. Coherent dynamics of vortex formation in trapped Bose-Einstein condensates. *Phys. Rev. Lett.*, 83(5):895–898, 1999.

[89] K. P. Marzlin and W. P. Zhang. Laser-induced rotation of a trapped Bose-Einstein condensate. *Phys. Rev. A*, 57(5):3801–3804, 1998.

[90] R. Dum, J. I. Cirac, M. Lewenstein, and P. Zoller. Creation of dark solitons and vortices in Bose-Einstein condensates. *Phys. Rev. Lett.*, 80(14):2972–2975, 1998.

[91] K. P. Marzlin, W. P. Zhang, and E. M. Wright. Vortex coupler for atomic Bose-Einstein condensates. *Phys. Rev. Lett.*, 79(24):4728–4731, 1997.

[92] K. Staliunas. Vortex creation in Bose-Einstein condensates by laser-beam vortex guiding. *App. Phys. B - Lasers and Optics*, 71(4):555–559, 2000.

[93] C. O. Weiss, M. Vaupel, K. Staliunas, G. Slekys, and V. B. Taranenko. Solitons and vortices in lasers. *App. Phys. B - Lasers and Optics*, 68(2):151–168, 1999.

[94] E. L. Bolda and D. F. Walls. Detection of vorticity in Bose-Einstein condensed gases by matter-wave interference. *Phys. Rev. Lett.*, 81(25):5477–5480, 1998.

[95] Y. S. Kivshar and B. Luther-Davies. Dark optical solitons: physics and applications. *Physics Reports-Review section of Physics Lett.*, 298(2-3):81–197, 1998.

[96] D. S. Rokhsar. Condensates in a twist. *Nature*, 401(6753):533–534, 1999.

[97] F. Dalfovo, S. Giorgini, L. P. Pitaevskii, and S. Stringari. Theory of Bose-Einstein condensation in trapped gases. *Rev. of Modern Physics*, 71(3):463–512, 1999.

[98] M. Kozuma, L. Deng, E. W. Hagley, J. Wen, R. Lutwak, K. Helmerson, S. L. Rolston, and W. D. Phillips. Coherent splitting of Bose-Einstein condensed atoms with optically induced Bragg diffraction. *Phys. Rev. Lett.*, 82(5):871–875, 1999.

[99] M. R. Andrews, C. G. Townsend, H. J. Miesner, D. S. Durfee, D. M. Kurn, and W. Ketterle. Observation of interference between two Bose condensates. *Science*, 275(5300):637–641, 1997.

[100] L. Deng, E. W. Hagley, J. Wen, M. Trippenbach, Y. Band, P. S. Julienne, J. E. Simsarian, K. Helmerson, S. L. Rolston, and W. D. Phillips. Four-wave mixing with matter waves. *Nature*, 1999(6724):218–220, 398.

[101] A. G. Truscott, K. E. Strecker, W. I. McAlexander, G. B. Partridge, and R. G. Hulet. Observation of Fermi pressure in a gas of trapped atoms. *Science*, 291(5513)):2570–2572, 2001.

[102] F. Schreck, L. Khaykovich, K. L. Corwin, G. Ferrari, T. Bourdel, J. Cubizolles, and C. Salomon. Quasipure Bose-Einstein condensate immersed in a Fermi. *Phys. Rev. Lett.*, 87(8):art. no. 080403, 2001.

[103] K. M. O'Hara, S. L. Hemmer, M. E. Gehm, S. R. Granade, and J. E. Thomas. Observation of a strongly-interacting degenerate Fermi gas of atoms. *Science*, pages 2179–2182, 2002.

[104] J. Goldwin, S. B. Papp, B. DeMarco, and D. S. Jin. Two-species magneto-optical trap with 40K and 87Rb. *accepted to Phys. Rev. A*, page 1, 2003.

[105] D. A. Butts and D. S. Rokhsar. Trapped Fermi gases. *Phys. Rev. A*, 55(6):4346–4350, 1997.

[106] G. M. Bruun and K. Burnett. Interacting Fermi gas in a harmonic trap. *Phys. Rev. A*, 58(3):2427–2434, 1998.

[107] R. Roth and H. Feldmeier. Phase diagram of trapped degenerate Fermi gases including effective s- and p-wave interactions. *J. Phys. B*, 34:4629, 2001.

[108] G. M. Bruun and C. W. Clark. Hydrodynamic excitations of trapped Fermi gases. *Phys. Rev. Lett.*, 83(26):5415–5418, 1999.

[109] K. Góral, B. G. Englert, and K. Rzążewski. Semiclassical theory of trapped fermionic dipoles. *Phys. Rev. A*, 63(3):art. no. 033606, 2001.

[110] T. Karpiuk, M. Brewczyk, and K. Rzążewski. Solitons and vortices in ultracold fermionic gases. *Journal of Physics B-Atomic Molecular and Optical Physics*, 35(14):L315–L321, 2002.

[111] B. Damski, L. Santos, E. Tiemann, M. Lewenstein, S. Kotochigova, P. Julienne, and P. Zoller. Creation of a dipolar superfluid in optical lattices. *Phys. Rev. Lett.*, 90(110401), 2003.

[112] A. Shirani. Private communication.

[113] E. Madelung. *Z. Phys*, 40:1926, 322.

[114] B. K. Dey. Femtosecond quantum fluid dynamics of helium atom under an intense laser field. *International Journal of Quantum Chemistry*, 70(3):441–474, 1998.

[115] H. Pu, W. P. Zhang, and P. Meystre. Ferromagnetism in a lattice of Bose-Einstein condensates. *Phys. Rev. Lett.*, 87(14):art. no. 140405, 2001.

[116] S. Giovanazzi, D. O'Dell, and G. Kurizki. Density modulations of Bose-Einstein condensates via laser-induced interactions. *Phys. Rev. Lett.*, 88(13):2002, art. no. 130402.

[117] D. Jaksch, J. I. Cirac, P. Zoller, S. L. Rolston, R. Cote, and M. D. Lukin. Fast quantum gates for neutral atoms. *Phys. Rev. Lett.*, 85(10):2208–2211, 2000.

[118] G. K. Brennen, C. M. Caves, F. S. Jessen, and I. H. Deutsch. Quantum logic gates in optical lattices. *Phys. Rev. Lett.*, 82(5):1060–1063, 1999.

[119] J. P. Martikainen, M. Mackie, and K. A. Suominen. Comment on "Bose-Einstein condensation with magnetic dipole-dipole forces". *Phys. Rev. A*, 64(3), 2001.

[120] J. M. Doyle and B. Friedrich. Chemical physics - Molecules are cool. *Nature*, 401(6755):749–+, 1999.

[121] H. L. Bethlem, G. Berden, van Roij A. J. A., F. M. H. Crompvoets, and G. Meijer. Trapping neutral molecules in a traveling potential well. *Phys. Rev. Lett.*, 84(25):5744–5747, 2000.

[122] H. L. Bethlem, G. Berden, and G. Meijer. Decelerating neutral dipolar molecules. *Phys. Rev. Lett.*, 83(8):1558–1561, 1999.

[123] H. L. Bethlem, G. Berden, F. M. H. Crompvoets, R. T. Jongma, van Roij A. J. A., and G. Meijer. Electrostatic trapping of ammonia molecules. *Nature*, 406(6795):491–494, 2000.

[124] J. D. Weinstein, R. deCarvalho, J. Kim, D. Patterson, B. Friedrich, and J. M. Doyle. Magnetic trapping of atomic chromium. *Phys. Rev. A*, 57(5):R3173–R3175, 1998.

[125] A. S. Bell, J. Stuhler, S. Locher, S. Hensler, J. Mlynek, and T. Pfau. A magneto-optical trap for chromium with population repumping via intercombination lines. *Europhys. Lett.*, 45(2):156–161, 1999.

[126] C. C. Bradley, J. J. McClelland, W. R. Anderson, and R. J. Celotta. Magneto-optical trapping of chromium atoms. *Phys. Rev. A*, 61(5):art. no. 053407, 2000.

[127] J. Stuhler, P. O. Schmidt, S. Hensler, J. Werner, J. Mlynek, and T. Pfau. Continuous loading of a magnetic trap. *Phys. Rev. A*, 64(3):art. no. 031405, 2001.

[128] J. H. Kim, B. Friedrich, D. P. Katz, D. Patterson, J. D. Weinstein, R. DeCarvalho, and J. M. Doyle. Buffer-gas loading and magnetic trapping of atomic europium. *Phys. Rev. Lett.*, 78(19):3665–3668, 1997.

[129] M. Marinescu and L. You. Controlling atom-atom interaction at ultralow temperatures by dc electric fields. *Phys. Rev. Lett.*, 81(21):4596–4599, 1998.

[130] T. F. Gallagher. *Rydberg Atoms.* Cambridge University Press, New York, 1994.

[131] S. Giovanazzi, D. O'Dell, and G. Kurizki. One-dimensional compression of Bose-Einstein condensates by laser-induced dipole-dipole interactions. *Journal of Physics B - Atomic Molecular and Optical Physics*, 34(23):4757–4762, 2001.

[132] Albert Messiah. *Quantum Mechanics.* Dover Publications, 2000.

[133] W. Ketterle and S. Inouye. Collective enhancement and suppression in Bose-Einstein condensates. *Comptes Rendus de l Academie des Sciences serie IV Physique Astrophysique*, 2(3):2001, 339-380.

[134] T. Pfau. Private communication, 2003.

[135] L. P. Gorkov and T. K. Melik-Burkhudarov. *Sov. Phys. JETP*, 13:1018, 1961.

[136] Mark Galassi, Jim Davies, James Theiler, Brian Gough, Gerard Jungman, Michael Booth, and Fabrice Rossi. *GNU Scientific Library Reference Manual.* , 2003.

[137] G. Bruun, Y. Castin, R. Dum, and K. Burnett. BCS theory for trapped ultracold fermions. *Europ. Phys. Jour. D*, 7(3):433–439, 1999.

7.2 Wigner Function

Wigner function in quantum optics is often derived from general concept of quantum mechanical phase space description of a system. Imagine that the $\hat{O}$ operator is a function of a and $a^\dagger$, $\hat{O} = f(a, a^\dagger)$. Lets ρ be a density matrix, it is an operator that describes the state. Then the average value of $\hat{O}$ is given by:

$$\langle \hat{O} \rangle = \mathrm{Tr}\left[\rho f(a, a^\dagger)\right]. \tag{70}$$

To perform this trace we choose a complete set of quantum states. We choose the coherent states as basis states $a|\alpha\rangle = \alpha|\alpha\rangle$. In this basis one can expand density matrix as:

$$\rho = \frac{1}{\pi^2}\int d^2\alpha \int d^2\beta \rho(\alpha,\beta)|\alpha\rangle\langle\beta|,$$

where $\rho(\alpha,\beta)=\langle\alpha|\rho|\beta\rangle$. Inserting this equation into (70) we get:

$$\langle\hat{O}\rangle=\langle f(a,a^\dagger)\rangle=\frac{1}{\pi^2}\int d^2\alpha\int d^2\beta\rho(\alpha,\beta)\langle\alpha|f(a,a^\dagger)|\beta\rangle. \tag{71}$$

It is worth to note, that substitution $a,a^\dagger\to\alpha,\alpha^*$ gives the classical statistics.
Let us denote $f(\alpha)$ be a diagonal element of $f(a,a^\dagger)$ in coherent state representation, $f(\alpha)=\langle\alpha|f(a,a^\dagger)|\alpha\rangle$. Using definition of the Dirac delta we can write:

$$f(\alpha)=\int d^2\beta\delta(\alpha-\beta)f(\beta),$$

where $\delta(\alpha)$ is i a usual two dimensional object defined as follows:

$$\delta(\alpha)=\frac{1}{\pi^2}\int d^2\gamma\exp(\alpha\gamma^*-\alpha^*\gamma).$$

coming back from c-number to operators we can write the operator valued delta function:

$$\delta(a-\alpha)=\frac{1}{\pi^2}\int d^2\beta\exp\left[(a^\dagger-\alpha^*)\beta-(a-\alpha)\beta^*\right].$$

Comparing above equation with (71) we can see that we can identify the average value of $\langle\delta(a-\alpha)\rangle$ with the density distribution defined on the phase space. This definition is ambiguous. Delta function must be expanded to be computed, and the ordering in which we express this expansion defines different (quasi distribution) functions.
There are three most common way of ordering operators:

- **normal:** that is all annihilation operators are right to all creation operators; this one leads to the, so called, $P-$function, or Glauber Sudrshern representation
- **antinormal:** when all creation operators are right to all anihilation operators; this one defines the $Q-$function,
- **symmetric:** when operators are positioned symmetrically; this finally defines the Wigner function W.

7.3 Gap Equation

The method of deriving the gap equation, which is the basic equation for BCS theory, and the starting point of our considerations in the Chapter 5, is presented in the language of the effective field theory.
We assume we are working in the zero temperature, and all external fields vanish. All the forces are spin independent hence Lagrangian has the $SU(2)$ symmetry. It is convenient to work in the coordinate space, Gauge symmetry tells us that Lagrangian has the form:

$$\begin{aligned}L=&-\sum_s\int d^3x\Psi_s^\dagger(\mathbf{x},t)\left[-i\frac{\partial}{\partial t}-A_0(\mathbf{x},t)+E(-i\nabla+\mathbf{A}(\mathbf{x},t))\right]\Psi_s(\mathbf{x},t)\\&+\sum_{s_1s_2s_3s_4}\int d^3x_1d^3x_2d^3x_3d^3x_4V_{s_1s_2s_3s_4}(\mathbf{x}_1,\mathbf{x}_2,\mathbf{x}_3,\mathbf{x}_4)\Psi_{s_1}^\dagger(\mathbf{x}_1,t)\Psi_{s_1}^\dagger(\mathbf{x}_2,t)\Psi_{s_1}(\mathbf{x}_1,t)\Psi_{s_1}(\mathbf{x}_2,t),\end{aligned}$$

where $\Psi_s(\mathbf{x},t)$ is defined in the usual way:

$$\Psi_s('bx,t)=(2\Pi)^{-3/2}\int d^3p\exp(i\mathbf{p}\mathbf{x})a(\mathbf{p},s,t)$$

To this Lagrangian we add the term

$$\begin{aligned}\Delta L =&1/4\int d^3x_1d^3x_2d^3x_3d^3x_4 \sum_{s_1s_2s_3s_4} V_{s_1s_2s_3s_4}(\mathbf{x}_1,\mathbf{x}_2,\mathbf{x}_3,\mathbf{x}_4)\\ &\times\left[\Psi^\dagger_{s_2s_1}(\mathbf{x}_2,\mathbf{x}_1,t)-\Psi^\dagger_{s_1}(\mathbf{x}_1,t)\Psi^\dagger_{s_2}(\mathbf{x}_2,t)\right]\\ &\times\left[\Psi_{s_3s_4}(\mathbf{x}_3,\mathbf{x}_4,t)-\Psi^\dagger_{s_3}(\mathbf{x}_3,t)\Psi^\dagger_{s_4}(\mathbf{x}_4,t)\right]\end{aligned},$$

and perform functional integrals over new field of pair $\Psi_{ss'}(\mathbf{x},\mathbf{x}',t)$. It is possible because ΔL is quadratic in pair field. Performing this integral is simple, since it is enough to put $\Psi_{ss'}(\mathbf{x},\mathbf{x}',t)=\Psi_{s_1}(\mathbf{x}_1)\Psi_{s_2}(\mathbf{x}_2)$, while it is the saddle point of the action where $\Delta L=0$. The terms in ΔL are chosen in such a way that the term with $\Psi_{s_1}(\mathbf{x},t)$ in forth power cancel. Only quadratic terms in $L+\Delta L$ remain:

$$\begin{aligned}L+\Delta L=&-\sum_s\int d^3x\Psi^\dagger_s(\mathbf{x},t)\left\{-i\frac{\partial}{\partial t}-A_0(\mathbf{x},t)+E\left(-i\nabla+A(\mathbf{x},t)\right)\right\}\Psi_s(\mathbf{x},t)\\ &-\frac{1}{4}\sum_{s_1s_2s_3s_4}\int d^3x_1d^3x_2d^3x_3d^3x_4V_{s_1s_2s_3s_4}(\mathbf{x}_1,\mathbf{x}_2,\mathbf{x}_3,\mathbf{x}_4)\\ &\times\left[\Psi^\dagger_{s_1}(\mathbf{x}_1,t)\Psi^\dagger_{s_2}(\mathbf{x}_2,t)\Psi_{s_3s_4}(\mathbf{x}_3,\mathbf{x}_4,t)+\Psi^\dagger_{s_1s_2}(\mathbf{x}_1,\mathbf{x}_2,t)\Psi_{s_3}(\mathbf{x}_3,t)\Psi_{s_4}(\mathbf{x}_4,t)\right.\\ &\left.-\Psi^\dagger_{s_1s_2}(\mathbf{x}_1,\mathbf{x}_2,t)\Psi_{s_3s_4}(\mathbf{x}_3,\mathbf{x}_4,t)\right].\end{aligned}\tag{72}$$

It can be shown that the only diagrams which survive when we calculate quantum effective action $\Gamma[\Psi]$ is diagram constructed from the vertex of the last term of (72) and diagram with one loop. To further simplify we assume that the pair field $\Psi_{s_1s_2}=\Psi_{+-}(\mathbf{x}',\mathbf{x},t)=-\Psi_{-+}(\mathbf{x},\mathbf{x}')=\Psi(\mathbf{x}',\mathbf{x},t)$ is a spin singlet. In this case one can calculate the quantum effective action $\Gamma[\Psi]$:

$$\begin{aligned}\Gamma[\Psi]=&\int dt\int d^3x_1d^3x_2d^3x_3d^3x_4V(\mathbf{x}_1,\mathbf{x}_2,\mathbf{x}_3,\mathbf{x}_4)\\ &\times\Psi^\dagger(\mathbf{x}_1,\mathbf{x}_2,t)\Psi(\mathbf{x}_3,\mathbf{x}_4,t)\\ &-i\ln\det\begin{pmatrix}A & B\\ B^\dagger & -A^T\end{pmatrix}+const,\end{aligned}$$

where $2V(\mathbf{x}_1,\mathbf{x}_2,\mathbf{x}_3,\mathbf{x}_4)=V_{+-+-}(\mathbf{x}_1,\mathbf{x}_2,\mathbf{x}_3,\mathbf{x}_4)-V_{+--+}(\mathbf{x}_1,\mathbf{x}_2,\mathbf{x}_3,\mathbf{x}_4)$, A and B are "matrices":

$$\begin{aligned}A_{\mathbf{x}'t',\mathbf{x}t}&=\left\{-i\frac{\partial}{\partial t}-A_0(\mathbf{x},t)+E\left(-i\nabla+A(\mathbf{x},t)\right)\right\}\delta^3(\mathbf{x}'-\mathbf{x})\delta(t'-t)\\ B_{\mathbf{x}'t',\mathbf{x}t}&=-\Delta(\mathbf{x}'.\mathbf{x},t)\delta(t'-t),\end{aligned}$$

where Δ is the famous Gap function:

$$\Delta(\mathbf{x}',\mathbf{x},t)=\int d^3y'd^3yV(\mathbf{x}',\mathbf{x},\mathbf{y}'\mathbf{y})\Psi(\mathbf{y}',\mathbf{y},t).$$

Performing Fourier transforms on Δ, V and Ψ, and defining the effective potential $V[\Phi]$ as effective action divided by the volume of the space we obtain:

$$\begin{aligned}V[\Psi]=&\Gamma[\Psi]/\mathcal{V}_4=\\ &-\int d^3pd^3p\Psi^\dagger(\mathbf{p}')V(\mathbf{p},\mathbf{p}')\Psi(\mathbf{p})\\ &+\frac{i}{(2\pi)^4}\int d\omega d^3p\ln\left(1-\frac{|\Delta(\mathbf{p})|^2}{\omega^2-E^2(\mathbf{p})+i\epsilon}\right),\end{aligned}$$

where in this case $\Delta(\mathbf{p})$ is given by:

$$\Delta(\mathbf{p}) = -\int d^3p V(\mathbf{p}', \mathbf{p})\Psi(\mathbf{p}).$$

Performing the Wick rotation, integrating over ω and expressing Ψ as a function of Δ, we can write effective potential as:

$$\begin{aligned} V[\Psi] = &-\int d^3p d^3p' \Delta^*(\mathbf{p}')V^{-1}(\mathbf{p}', \mathbf{p})\Delta(\mathbf{p}) \\ &- \frac{1}{(2\pi)^3}\int d^3p \left[\sqrt{E^2(\mathbf{p}) + |\Delta(\mathbf{p})|^2} - E(\mathbf{p})\right]. \end{aligned}$$

The field equation are the stationary condition for effective action. In this case we finally obtain the famous gap equation for Δ_0:

$$\begin{aligned} 0 = \left.\frac{\delta V[\Delta]}{\delta \Delta^*(\mathbf{p})}\right|_{\Delta=\Delta_0} = & \\ &-\int d^3p V^{-1}(\mathbf{p}', \mathbf{p})\Delta_0(\mathbf{p}') - \frac{1}{2(2\pi)^3}\frac{\Delta_0(\mathbf{p})}{\sqrt{E^2(\mathbf{p}) + |\Delta(\mathbf{p})|^2}}, \end{aligned}$$

which can be written in the more familiar form as:

$$\Delta_0(\mathbf{p}) = \frac{1}{2(2\pi)^3}\int d^3p' \frac{V(\mathbf{p}, \mathbf{p}')\Delta_0(\mathbf{p}')}{\sqrt{E^2(\mathbf{p}') + |\Delta(\mathbf{p}')|^2}}.$$

CURRICULUM VITAE

PERSONAL INFORMATION

Name:	Łukasz Dobrek
Date and place of birth:	10 Nov 1976, Warsaw
Address	Pfartstr 65 Hannover
Nationality:	polish
Marital status:	single, no children
E-mail:	dobrek@pld.org.pl

DEGREE

1998	BS degree in mathematical modeling, **College of Science**, Warsaw, Poland
2000	MS degree in theoretical Physics, **College of Science**, Warsaw, Poland

EDUCATION

2000 2003	PHD studies in theoretical physics, **Graduate College**, University Hanover, Germany
1998 2000	MS studies in theoretical physics, **College of Science**, Warsaw, Poland
1995 1998	BS studies (math + physics + chemistry), **College of Science**, Warsaw, Poland.
1994 1995	High school nr. LXI in Warsaw.
1991 1994	High school nr. XVII in Warsaw.
1983 1991	Primary school nr. 309 in Warsaw.

ADDITIONAL INFORMATION

Scientific experience:	During last 3 years – resarch on properties of ultra cold gases, and possibillities of manipulating them. Two short-term visits at University of Hanover – theoretical studies on creation of vortices in the BEC (1999). Research on problems related to quantum information (1998).
Foreign languages:	**English** fluent, **Russian** basic. **German** basic
Computer knowledge:	Programming in C, C++, Fortran, perl, python, Unix shell, Pascal. Administrator of local area networks of Unix computers in College of Science later at Hannover University.
Other activities	I am one of the developers of Polish Linux Distribution
Hobby:	Programming, literature, climbing, music